EL NIÑO SOUTHERN OSCILLATION VARIABILITY FROM 1871-2008

A Dissertation

by

SULAGNA RAY

Submitted to the Office of Graduate Studies of
Texas A&M University
in partial fulfillment of the requirements for the degree of

DOCTOR OF PHILOSOPHY

December 2011

Major Subject: Oceanography

El Niño Southern Oscillation Variability from 1871-2008

EL NIÑO SOUTHERN OSCILLATION VARIABILITY FROM 1871-2008

A Dissertation

by

SULAGNA RAY

Submitted to the Office of Graduate Studies of
Texas A&M University
in partial fulfillment of the requirements for the degree of

DOCTOR OF PHILOSOPHY

Approved by:

Chair of Committee,	Benjamin Giese
Committee Members,	Ping Chang
	Achim Stoessel
	Ramalingam Saravanan
Head of Department,	Piers Chapman

December 2011

Major Subject: Oceanography

ABSTRACT

El Niño Southern Oscillation Variability from 1871-2008. (December 2011)

Sulagna Ray, B.S.; M.S., University of Calcutta

Chair of Advisory Committee: Dr. Benjamin Giese

The variation of El Niño Southern Oscillation (ENSO) events from the mid-nineteenth century until the beginning of the twenty-first century is explored using an ocean reanalysis. Decadal variability and trends in the strength, frequency, duration, and propagation direction of ENSO events is investigated. The hypothesis that there are different types of ENSO and that the location of ENSO is shifting to the west Pacific is also studied.

The study uses the latest version of an ocean reanalysis, called SODA 2.2.4 (Simple Ocean Data Assimilation), which covers the period from 1871 through 2008. The reanalysis uses an eddy-permitting resolution model of the ocean forced with boundary conditions available from an atmospheric reanalysis that covers the same period. SODA 2.2.4 assimilates all available hydrographic and surface marine observations of temperature and salinity to produce a "best estimate" of the ocean state in terms of temperature, current, salinity, and sea surface height.

A new index based on the first moment of anomalous sea surface temperature over the equatorial Pacific is used to describe the location and strength of warm and cold events. The results show strong decadal variability in the strength of El Niño events but

little trend during the period of 1871-2008. The strength of La Niña events has neither prominent decadal variation nor a trend. The index also documents changes in frequency, duration, and location of ENSO events. The study shows that the frequency of El Niño varies considerably over the record. Given the large variance in the period of ENSO it is difficult to reliably determine if there has been a change in the period of El Niño events. The location of warming during El Niño can be described by a normal distribution centered at about 140°W. The strength and frequency of ENSO events have very little trend indicating negligible impact from global warming.

DEDICATION

Dedicated to my parents

ACKNOWLEDGEMENTS

I am grateful to my advisor Benjamin Giese in providing guidance and financial aid towards completing my doctoral dissertation. Without his precise guidance this dissertation could not have been completed. I appreciate his encouraging me to attend different workshops, conferences and summer school around the world, which helped me to broaden my perspective on the subject. His strong motivation and advises has been one of the principle force guiding me towards improving my scientific as well as writing skills. Working with him was a pleasure and inspirational as well. I enjoyed the dinners at his house with his wife Rachel and family, which provided the much-needed home feeling that students like me are deprived while studying abroad. I would specially thank Rachel for her kindness that was so very relaxing and I enjoyed every moment that I spent in her company.

I would like to express my gratitude towards Ping Chang, Ramalingam Saravanan and Achim Stoessel for being in my advisory committee. Their valuable inputs contributed towards shaping this dissertation. I would cherish the days when Dr. Chang treated us with real Chinese food and Dr. Saravanan made us feel cozy at his house with homemade food. Particular suggestions and corrections by Dr. Stoessel was helpful for the dissertation.

I would like to appreciate Hank Seidel for providing support in handling the model and data. I would not forget the day when he taught us to eat a crab.

I would like to express my appreciation for the Department of Oceanography faculty and staff and my friends in the department for their support and company.

I also acknowledge my friends Anshu, Rashmi, Reshu, Anthony and Rajneesh for being there for me, their friendship encourages me all the time.

No words of gratitude are sufficient for my parents who have been a pillar of my strength throughout my career. It is their immense faith in me that kept me surviving in pursuit of higher studies. The constant support from my brother and sister gave me the will that was needed to complete this dissertation.

TABLE OF CONTENTS

LIST OF FIGURES

FIGURE Page

FIGURE Page

FIGURE Page

FIGURE Page

FIGURE Page

FIGURE Page

LIST OF TABLES

CHAPTER I

INTRODUCTION

Climate change is of prime concern to climate scientists currently studying climate prediction and predictability. Irrespective of whether the changing climate is being forced naturally or anthropogenically, global warming is an ongoing concern and is reported to change patterns of extreme weather events as well as normal weather conditions in different regions of the globe. This necessitates adequate disaster management policies in dealing with the consequences in different aspects, such as economic, agriculture, water resources sectors to name a few. Studies of climate variability on decadal to centennial scale would shed light on sources of predictability, thus studying different components of climate variability is a necessary move towards efficient climate prediction schemes. In my doctoral dissertation I study El Niño, the dominant mode of global interannual climate variability, which is linked to regional weather perturbations worldwide. The study sheds light on the changes in the interannual variability originating in the tropical Pacific and records its changes through periods of global warming.

El Niño and La Niña

El Niño Southern Oscillation (ENSO), the dominant interannual mode of global climate variability occurs irregularly at an interval of about 2-7 years and is

---

This dissertation follows the style of the *Journal of Geophysical Research.*

accompanied by warming of the seasonal cold waters in the eastern Pacific and weakening of the usually strong easterly trade winds over the equatorial Pacific. The phenomena involves not only local air-sea interaction in the equatorial Pacific but perturbs the large-scale atmospheric circulation that affects the weather conditions of not only the tropical Pacific but also other tropical oceans and the mid-latitudes primarily through wave dynamics. The ocean component of the phenomenon is called El Niño, which means the 'Christ child' in Spanish, since it often warms the waters along the South American coast during December. The atmospheric component of the phenomenon includes a weakening of the Walker circulation with weakened surface easterly winds, and an eastward shift in the rising branch of the circulation from the western Pacific thereby moving the convection region over the central Pacific, an eastward shift of the descending branch that brings dry, high pressure over the eastern Pacific region.

The easterly winds over the equatorial Pacific maintain a sharp thermal and pressure gradient resulting in warm waters and a deep thermocline in the western Pacific and cold waters and a shallow thermocline in the eastern Pacific. Beneath the easterlies the surface currents flow away from the equator following Ekman dynamics. These diverging surface currents induce upwelling along the equator, which pulls cold water from below the thermocline into the mixed layer so that the thermocline is close to the surface. This maintains cold sea surface temperature (SST) of the eastern Pacific and strengthens the easterly winds above in a positive feedback loop [*Bjerknes,* 1969]. This pool of cold water is referred to as the Cold Tongue. There is a prominent seasonal cycle

with the Cold Tongue expanding during July-September (boreal summer) due to strengthened easterlies, which drives vigorous upwelling thus maintaining the coldest annual SST, and retreating during February-April (boreal winter) due to weakened easterlies and a warmer annual SST. During El Niño, the eastern Pacific warms and the easterly winds weaken, which inhibits the upwelling of cold waters from below the thermocline into the mixed layer thereby further warming the eastern Pacific. At the same time the relaxation of the easterly wind is accompanied by irregular episodes of westerly wind events around the Dateline triggering Kelvin waves that propagate eastward along the equatorial thermocline. The low order Kelvin waves, with greater speeds are able to reach the eastern Pacific pushing the thermocline down and enhancing the subsurface warming thus leading to maturation of the El Niño. The warming of the surface and subsurface in the eastern Pacific reduces the east-west temperature gradient. The rising branch of warm moist air in the western Pacific convection region now shifts eastward to the central Pacific leading to an anomalous positive precipitation over this region. The descending branch of the Walker circulation, which brings high pressure and low precipitation over the region where it subsides, is now pushed towards the western tropical Atlantic. The large-scale atmospheric circulation above the tropical Pacific adjusts to the changes of the ocean below. The atmospheric pressure also shows oscillations over the Indo-Pacific region. Under normal conditions the surface pressure is high at Tahiti in the central Pacific and low at Darwin in Australia. During El Niño, the pressure levels alter in these two locations with high surface pressure anomaly over Darwin and low pressure anomaly over Tahiti. This seesaw of high and low pressures

across the Indo-Pacific region was first identified by *Walker* [1923, 1924] and *Walker and Bliss* [1932] and is referred to as the Southern Oscillation.

Generally, El Niños have been observed to be phase locked to the seasonal cycle [*Rasmusson and Carpenter*, 1982; *Rasmusson et al.,* 1990; *Mitchell and Wallace*, 1996] with the strongest anomaly coinciding with the warmest months of the seasonal cycle. Although the solar cycle is semi-annual at the equator, SST maintains a prominent annual cycle because of upwelling, vertical entrainment [*Chang*, 1994], and cloudiness [*Kessler et al.,* 1998] over the Cold Tongue region in the eastern Pacific. Seasonal maxima occur during January-May when the winds and vertical entrainment are strong, and seasonal minima occur during June-November when the winds are weak, and the surface warms directly under the influence of solar radiation. An intermediate coupled model study [*Chang et al.,* 1995], where the total surface winds and SST fields were coupled instead of the anomalies, showed the El Niño cycle was always phase-locked to the seasonal cycle, which in turn made it regular, irrespective of whether the coupled system was in a periodic or chaotic state. By increasing the seasonal forcing *Chang et al.* [1995] showed that their coupled model went through phases from periodic state to chaotic state and ultimately gave up its intrinsic ENSO mode to acquire the frequency of the seasonal cycle. The phenomenon through which the interannual oscillation frequency of the model is completely entrained by the strong external frequency (here seasonal forcing) is called frequency entrainment. The nonlinear mechanism in frequency entrainment has been proposed to be a reason for ENSO suppression in the mid-Holocene period [*Pan et al*., 2005]. But the reasons for the irregularity in the El Niño

cycle are yet to be deciphered. *Chang et al.,* [1995], *Jin et al.,* [1994], and *Tziperman et al.*, [1994] suggested that the El Niño cycle is chaotic and the irregularity is driven by the seasonal cycle, whereas *Graham and White* [1988], *Battisti and Hirst* [1989], and *Penland and Sardeshmukh* [1995] proposed that the El Niño cycle is driven by stochastic processes of the coupled system. A few theories explain the mechanism of El Niño dynamics and its occurrences such as the delayed oscillator theory [*Schopf and Suarez*, 1988; *Battisti and Hirst*, 1989], the recharge oscillator theory [*Jin*, 1997], the advective-reflective oscillator theory [*Picaut et al.,* 1997], and the western Pacific oscillator theory [*Weisberg and Wang*, 1997]. The delayed oscillator theory could explain the delayed response of the ocean due to a change in the wind forcing, but it failed to explain the irregular occurrence of El Niño, rather none of the theories could answer that question. *Jin* [1997] suggested that the El Niño occurs in response to recharge and discharge of warm western Pacific waters to the eastern Pacific.

Teleconnections

The impact of the ocean-atmosphere interaction during El Niño and La Niña impacts the weather conditions of various regions around the globe through teleconnections. The nearest teleconnection is in the western Pacific, where the usually strong convection of moist air brings abundant rainfall but below normal rain during El Niño and above normal rain during La Niña. The surface pressure over the adjacent Indian subcontinent increases as the subsiding branch of Walker circulation shifts in the Indian subcontinent region, which results in failure of the monsoons and a negative precipitation anomaly. The negative correlation between the Indian monsoon and El

Niño had long been investigated [*Rasmusson and Carpenter*, 1983; *Torrence and Webster*, 1999; *Kumar et al*., 1999; *Krishnamurthy and Goswami*, 2000; *Kumar et al.,* 2006] for their changing relationship over decades. Monsoon could influence a developing El Niño [*Kirtman and Shukla*, 2000]. The variation in the amplitude of ENSO may vary with the amplitude of the Asian Monsoon [*Liu et al.,* 2000; *Pan et al.,* 2005]. El Niño also plays a role in maintaining SST anomalies in tropical oceans [*Enfield and Mayer*, 1997; *Trenberth et al.,* 1998; *Alexander et al*., 2002; *Wang et al*., 2004; *Liu and Alexander*, 2007] through what is termed an "atmospheric bridge". The tropical convection undergoes changes during El Niño that excites planetary waves, which in turn affect the climate anomalies around the world through this atmospheric bridge. The atmospheric bridge extends to the extra tropics through the Pacific North American (PNA) pattern [*Wallace and Gutzler*, 1981; *Horel and Wallace*, 1981]. In the PNA pattern alternate positive and negative geopotential height anomalies propagate through the North Pacific, then eastward through northwestern America then turn equatorward to southeastern America and the Gulf of Mexico [*Wang et al.*, 2004]. The sea level pressure (SLP) anomalies follow the geopotential anomalies in the middle and upper troposphere, which results in deepening of the Aleutian low during El Niño. Hence during El Niño winters the Aleutian low in the North Pacific is intensified accompanied by cooling of the central North Pacific and warming along coast of Alaska and Canada. The southwestern parts of North America experiences excessive rain during El Niño years and below-average rainfall (some leading to severe droughts) during La Niña. The atmospheric bridge extends to the tropical Atlantic where it acts either

through weakened tradewinds or through changes in extratropical circulation [*Bronnimann,* 2007]. In the western tropical Atlantic, tropical cyclones are reduced during El Niño summer and fall mainly through the continent-ocean thermal contrast [*Moron and Gouirand*, 2003], which further contributes to the weakening of the Icelandic low [*Bronnimann*, 2007]. The teleconnection further stretches over different parts of Europe mainly during the following spring either through the tropical Pacific - Atlantic coupling or through downward propagation of stratospheric anomalies [*Bronnimann*, 2007]. El Niño has a strong remote influence on tropical Atlantic SST variability. For example, the dipole mode of Atlantic SST variability is weakened by the remote forcing of El Niño [*Saravanan and Chang,* 2000]. The zonal mode of tropical Atlantic SST variability is considered to be the Atlantic counterpart of El Niño [*Brandt et al.,* 2011] and is referred as the Atlantic Niño [*Chang et al.,* 2006]. The zonal mode generally peaks in the boreal summer following El Niño. Besides the remote influence of El Niño in the Pacific through atmospheric response, the ocean-atmosphere interaction in the equatorial Atlantic acts negatively towards the Atlantic Niño. The warming produced in the equatorial Atlantic due to the remote influence of El Niño through the 'tropospheric temperature mechanism' is countered by the cooling produced by the Bjerknes feedback in the equatorial Atlantic that contributes toward a 'fragile relationship' between the El Niño and Atlantic Niño [*Chang et al.,* 2006]. Also *Brandt et al*. [2011] suggests that the interannual variability in the tropical Atlantic is strongly influenced by equatorial deep-jets, through which the energy propagates to the surface and affects the sea surface conditions. Generally Europe experiences low temperatures

in northeastern regions, decreased precipitation over northern regions and increased precipitation over the Mediterranean. During La Niña, the winters are warm in most regions of Europe. Some of most intense recent climate anomalies in Europe were during the 1939-1942 El Niño. The period between 1940-1942 had the coldest temperatures over Europe in the 20th century [*Luterbacher et al*., 2004]. The atmospheric pressure anomaly created in the Pacific during El Niño has been suggested as a reason for the northward and southward displacement of icebergs of the Pacific sector of the Antarctic regions [*Koshlyakov et al*., 1998]. *Romanov et al.* [2008] further analyzed the concentration of icebergs in the Atlantic and Indian Ocean sectors of the Antarctic region over 1970-2005 to conclude that El Niño has a strong effect in increasing the concentration of icebergs in the region east of the Drake Passage that connects the Pacific Ocean to the Atlantic Ocean. Thus El Niño/La Niña events are accompanied by major worldwide teleconnections far away from the local air-sea interactions that occur in the equatorial Pacific.

There are comprehensive theories on the timing, duration and seasonality of El Niño events [*Cane and Zebiak*, 1985; *Schneider et al.,* 1995; *Goddard and Philander*, 2000; *Meinen and McPhaden*, 2000; *Cane,* 2005]. However, the long-term variations of El Niño and La Niña are not yet well understood. Understanding the long-term variability of El Niño could help us predict probable future changes in this largest mode of climate variability, which could be immensely useful for prediction studies. Thus, a hind cast study of past El Niño and La Niña events is necessary to document the changes in theses events over a long period of time.

Types of El Niño

Recent studies suggest the existence of a different type of El Niño with the warm anomaly located in the central equatorial Pacific. Studies also suggest an increase in the occurrence of this different type of El Niño in future. Different studies used different terminology and methods in defining the warm anomaly in the central Pacific. New indices are proposed to quantify different types of El Niño. *Trenberth and Stepaniak* [2001] introduced Trans Niño Index (TNI) in addition to the well-known Niño 3.4 Index to describe ENSO evolution and the differences between events. Niño 3.4 Index is the averaged SST anomaly over the region Niño 3.4 (170°W: 120°W; 5°S: 5°N). TNI is the difference in the normalized SST anomalies averaged over the Niño 1+2 region (90°W - 80°W; 5°S - 5°N) and Niño 4 region (160°E - 150°W; 5°S - 5°N), which gives the gradient of SST anomalies across equatorial Pacific. They indicated a change in ENSO flavor using a change in the lead-lag correlation between Niño 3.4 Index and TNI.

Larkin and Harrison [2005] introduced the term "Dateline El Niño" for the El Niño that has warming primarily in the Niño 3.4 region and do not extend to the South American coast. This El Niño is associated with different seasonal anomalies than a "conventional El Niño". In the "Dateline El Niño", SST anomalies are confined to the central equatorial Pacific, whereas in a "conventional El Niño" the central equatorial warming spreads toward the South American coast.

A completely different kind of El Niño was proposed by *Ashok et al.* [2007] and referred as "El Niño Modoki". They performed an empirical orthogonal function (EOF) analysis on the SST anomaly from Hadley Center Sea Ice and Sea Surface Temperature

(HadISST) data set for the period 1958-2005 and characterized the second dominant EOF mode to be the "El Niño Modoki", which warms the central Pacific similar to dateline El Niño. El Niño Modoki has a different teleconnection pattern than a conventional El Niño [*Weng et al*., 2007].

Kao and Yu [2009] proposed two types of El Niño, the Eastern Pacific El Niño (EP-El Niño) and the Central Pacific El Niño (CP-El Niño). They defined the CP-El Niño as a combination of the first two EOF modes of SST anomaly. To separate the EP-El Niño structure, the SST anomalies regressed onto the Niño 4 index were first subtracted from the original SST anomalies and the EOF analysis was applied on it. Similarly to separate the CP-El Niño structure, the SST anomalies regressed onto the Niño 1+2 index were first subtracted from the original SST anomalies and the EOF analysis was applied on it. This method of separating the CP-El Niño resulted in a warming in the central equatorial Pacific that extended toward the northeastern subtropics off Mexico and North America. They suggested EP-El Niño involved thermocline variation and variation in surface winds in its evolution, whereas CP-El Niño was not sensitive to thermocline variations and more related to atmospheric forcings.

Kug et al. [2009] proposed the two types of El Niño, Warm-Pool El Niño (WP-El Niño) and the Cold Tongue El Niño (CT-El Niño). They devised a method using only the Niño 3 and Niño 4 indices. The method involved identifying the years when the boreal winter Niño 3 and Niño 4 indices were above 0.5°C. The CT-El Niño year are identified when the winter Niño 3 index is greater than the winter Niño 4 index.

Similarly the WP-El Niño is identified when the winter Niño 3 index is smaller than the Niño 4 index. They then made composite maps of the variables using this classification. Their study suggested that different dynamical processes are involved in the evolution of WP-El Niño.

Takahashi et al. [2011] contradicted *Ashok et al.* [2007] and suggested that the first two EOF modes of tropical Pacific SST anomalies does not describe two completely different El Niño and proposed two new indices "C-index" and the "E-index" to categorize El Niños of different types. The C-index and the E-index are linear combinations of the principal components of EOF1 and EOF2.

Ren and Jin [2011] countered *Kug et al.* [2009] and showed the strong correlation between Niño 3 and Niño 4 SST indices. They proposed two new indices through linear combinations of Niño 3 and Niño 4 indices in defining two different kind of El Niño.

But EOFs are statistical techniques to reproduce the dominant physical structure and might not produce modes that explain the dynamics of climate variability [*Saravanan and Chang*, 2000]. Hence one needs to be cautious in using them to detect changes in ENSO variability.

Record from Past

Various long-term reconstructions of SST are available based on past observations. Observations in the past were not as abundant as now and the quality of these reconstructions depends on the techniques employed in constructing a global dataset. Only since the recent introduction of satellite data has global gridded coverage

of SST, sea surface height, surface winds and various other meteorological parameters become available. Observations of sea surface and the subsurface before the satellite era were mostly through in-situ observations with bathythermographs and buoys, whose spatial and temporal coverage was dependent on time, as the density of coverage increased over decades. Observations were only available where the in-situ measurements were recorded, and thus they were unevenly distributed over space and time. However, global coverage of SST is required to force climate models in order to construct a hind cast study to understand climate variability of the past. This problem was addressed using statistical interpolation techniques to reconstruct a spatially and temporally complete global dataset. Various datasets had been produced using such methods. Some examples are: the HadISST1 developed at the Met Office Hadley Center for Climate Prediction and Research [*Rayner et al.,* 2003], the Kaplan extended sea surface temperature version 2 (Kaplan SST v2) [*Kaplan et al.,* 1998], and the Extended Reconstructed Sea Surface Temperature version 3 and version 3b (ERSST.v3 and ERSST v.3b) developed by National Oceanic and Atmospheric Administration (NOAA) [*Smith and Reynolds*, 2005; *Smith et al.,* 2008]. HadISST1 is a complete field of globally gridded (1°×1°) monthly data of SST and sea-ice concentration from 1871 to the present. A two-stage reduced space optimal interpolation (RSOI) procedure was used to reconstruct the SST field with the EOFs used to define the spatial structure of the SST. Through RSOI the reconstruction was performed in two stages, first the long-term climate variability was constructed followed by the interannual variability. Kaplan SST v2 is a global analysis of monthly SST anomaly field produced using three statistic-

based methods: optimal smoothing, Kalman filter and optimal interpolation. Significantly, Kaplan v2 also applied the RSOI but they did the reconstruction in one stage only. ERSST is a merged sea surface and land-near-surface dataset of temperature anomalies. ERSST is a monthly and globally complete gridded SST dataset generated using improved statistical methods allowing stable reconstruction using sparse data. The ERSST reconstructed the low frequency component and the high frequency component separately before merging them as the total reconstruction. ERSST.v3 uses satellite data in its reconstruction of SST, which introduced a small residual cold bias. Thus, ERSST.v3b was generated using the same statistical method, as ERSST.v3 but used no satellite data. Studies of El Niño have used all the mentioned datasets to analyze trends and decadal variability during the twentieth century. Due to sparse observations before 1950, the reconstructed SST was considered less reliable during this period and usually the period post 1950 was analyzed instead. The reconstructed SST has the disadvantage of using predetermined geographical patterns while interpolating observations in data sparse periods, and thus it does not preserve the spatial structure of SST during these periods (early twentieth and late nineteenth century).

Another method for analyzing the El Niño variability across timescales of a century to a millennium is through paleo-proxy records. Various paleoclimate records such as the tree-ring records of North America, the coral and fossil coral records from the equatorial Pacific, and ice-core records from Greenland serve as a proxy of El Niño variation. Equatorial Pacific and North America are regions that are directly or remotely affected by El Niño. The annual average oxygen isotopic ($\delta^{18}O$) record from corals

found in Tarawa Atoll in Indonesia produced an excellent record of El Niño variations over 96-years [*Cole et al.,* 1993]. Tarawa Atoll is located in a region of intense rainfall in the western Pacific warm pool. The salinity of the underlying surface is altered by rainfall, and as the $\delta^{18}O$ varies linearly with the salinity in the region, it could record the variation in rainfall over the western Pacific as a proxy of the strength of the El Niño. The $\delta^{18}O$ record was collected from shallow growing coral skeletons and analyzed for past El Niño changes. Similar analysis was done with coral records from Kirimati Island in the central equatorial Pacific [*Evans et al.*, 1999] and Maiana Atoll in the central western equatorial Pacific [*Urban et al.,* 2000] for 155 years. The second kind of proxies are the fossil corals which are colonies that were not living at the time of collection and thus contain records of climate variability on a millennium scale. Fossil coral-based climate records are spread over several centuries and represents tropical Pacific climate before 1600 A.D. [*Cobb et al.,* 2003]. Such records facilitate studying El Niño under a different mean climate state [*Cobb et al.,* 2003*; Tudhope et al.,* 2001]. The annually banded fossil corals from Papua New Guinea [*Tudhope et al.,* 2001] showed that El Niño variability existed for the past 130,000 years through glacial and inter-glacial periods. Tree-ring records from the southwestern part of North America were used to reconstruct the December-February averaged Niño 3 SST for El Niño variability in the period from 1408-1978 A.D. [*D'Arrigo et al.*, 2005]. A total of 835 tree-ring chronologies for the past 2005 years were used to reconstruct a history of drought in North America, called the North American Drought Atlas (NADA) [*Cook and Krusic,* 2004]. North America is remotely affected by El Niño and La Niña teleconnections, with

La Niña sometimes accompanied by severe drought (as during 2010-2011), NADA records have been useful to study the modulation in El Niño amplitude over the past millennium [*Li et al.,* 2011].

Ocean Reanalysis

The SST data reconstructed from an unevenly spaced distribution of spatial and temporal observations in more recent times (HadISST, ERSST) or from proxy records distributed over past centuries, have either instrumental errors or errors in the methods of their construction. Reanalysis provides an alternate method for studying past climate variability employing both a dynamical model and quality-checked observations. Reanalysis is the result of assimilation of observations in a geophysical model to produce the best estimate of the ocean state. The reanalysis used in this study is the first ever effort in developing a reanalysis field for the period 1871-2008.

Global Warming

Global average surface temperature has increased by 0.6°C according to the Intergovernmental Panel on Climate Change-Fourth Assessment Report (IPCC) [*Houghton et al.,* 1995], although there are conflicting reports between what is reported by observations and estimates from coupled GCMs [*Cane et al.,* 1997] over the twentieth century. During the period 1990-2100 the global average temperature is projected to increase by 1.4°C-5.8°C [*Houghton et al.,* 1995]. The cause of such an increase in global temperature is considered to be both due to natural variability and anthropogenic causes such as the greenhouse gas effect. It has been suggested that global climate will undergo rapid changes [*Xie et al.*, 2010] due to global warming

accompanied by an increase in extreme weather conditions worldwide. Currently all global climate models (GCMs) with an added external forcing of enhanced concentration of carbon-dioxide (greenhouse gas) predict warmer future temperatures.

The tropics are at the forefront in the impact of global warming [*Collins,* 2005; *Collins et al*., 2010; *Liu et al.,* 2005; *DiNezio et al.,* 2009; *Karnauskas et al.,* 2009; *Zhang and Song,* 2006; *Vecchi and Soden*, 2007; *Vecchi et al.,* 2008; *Held and Soden*, 2006]. The tropical ocean-atmosphere circulation has been reported to weaken over the last few decades [*Zhang and Song*, 2006; *Vecchi et al.,* 2006; *Vecchi and Soden,* 2007], although an earlier study using satellite observation shows a strengthened tropical circulation in the 1990s [*Chen et al.,* 2002]. As the surface warms, evaporation from the surface and water vapor concentration in the atmosphere both increase. An increase in temperature and low-level moisture contributes to an increase in the dry stability above the tropics following the Clausius-Clapeyron scaling [*Held and Soden*, 2006]. The atmospheric circulation weakens as radiative cooling of the troposphere increases slowly compared to an increase in the dry stability. This leads to weakening of the atmospheric overturning circulation (Walker circulation) [*Vecchi et al.*, 2006; *Power and Smith*, 2007; *Vecchi and Soden*, 2007; *Zhang and Song*, 2006; *Gastineau et al*., 2009]. *Vecchi et al.* [2006] used the Kaplan sea level pressure (SLP) dataset version 1 and Hadley Centre SLP reconstruction version 1 spanning over mid nineteenth century through the 1990s, and showed that the zonal surface pressure gradient over the equatorial Pacific has decreased over the years. Further using a global climate model of the NOAA-GFDL, CM2.1, that used both natural and anthropogenic forcing, *Vecchi et al.* [2006] claimed

that weakening of the surface pressure gradient in the Tropical Pacific is due to anthropogenic global warming rather than being part of a natural variability. *Zhang and Song* [2006] also explored the weakening of the surface pressure gradient of the tropical Pacific by analyzing the extended reconstructed sea level pressure (ERSLP) analysis of the NOAA National Climate Data Center (NCDC), monthly SLP from the NCEP-NCAR and from ECMWF ERA-40 reanalyses. Other effects of global warming on the tropics include the strengthening of east-west temperature gradient [*Karnauskas et al*., 2009], intensification of the annual cycle [*Timmermann et al*., 2004] and persistent "El Niño-like" or "La Niña-like" climate conditions [*Vecchi et al*., 2008; *Collins*, 2005]. The cause of such differences in the tropical Pacific response to enhanced carbon-dioxide (CO_2) in global climate models is mainly due to the configuration of the models used [*Vecchi et al.,* 2008]. The "La Niña-like" like response is due to the simplified atmospheric process implemented in climate models such as the Cane–Zebiak model as described by *Clement et al*. [1996]. In such models the atmospheric circulation does not weaken but the zonal temperature gradient increases through an ocean thermostat mechanism. On the other hand, keeping the dynamics of the ocean fixed by simplified representation of the mixed layer in ocean models makes the resulting response of the tropical Pacific more "El Niño-like" in doubled CO_2 climate models. The differing trends of tropical Pacific climate in instrumental records contribute to more complex situations. The reconstructed SST from HadISST [*Rayner et al.,* 2003] shows a "La Niña-like" pattern with an increase in the zonal SST gradient consistent with *Cane et al*. [1997], whereas ERSST [*Smith and Reynolds*, 2005] shows an "El Niño-like" pattern consistent with the recent

analysis of the weakening of the Walker circulation [*Vecchi et al.,* 2006; *Zhang and Song*, 2006]. Proxy records reconstructed using coral skeletons from the tropical Pacific suggest a trend toward warmer and wetter climatic conditions in the central Pacific [*Cobb et al*., 2003; *Urban et al.,* 2000; *Nurhati et al.,* 2009] akin to "El Niño-like" conditions [*Vecchi et al.*, 2008].

Suggested Changes in ENSO

Current climate models predict a change in El Niño and La Niña under enhanced greenhouse gas concentration [*Zhang et al.,* 2008; *An et al.,* 2008; *Yang and Zhang*, 2008; *Philip and van Oldenborgh, 2006*; *Merryfield,* 2006; *Ye and Hseih*, 2008]. However there is yet no consensus on the characteristics of the change in the interannual signal. There are numerous published articles that describe trends and decadal variations in El Niño including changes in El Niño frequency [*Trenberth and Hoar*, 1996; *An and Wang*, 2000; *Timmermann et al.,* 1999], strength [*Zhang et al*., 2008; *Vecchi and Wittenberg*, 2010] and the location of the warming in the equatorial Pacific [*Yeh et al*., 2009]. The cause of such changes includes both the inherent characteristic of the El Niño to undergo variation on decadal to centennial scales and also because of changing external forcing, like increased concentration of CO_2 and volcanic eruptions. Though it is difficult to distinguish between the two causes, a long record of El Niño variability may be able to shed light on the issue.

Wang [1995] is one of the first to note the changes in the onset of El Niño during the late 1970s and characterized these as part of an interdecadal change in the background state of the Pacific, which occurred by altering the onset of cyclones and the

equatorial westerly anomalies prior to an El Niño. *An and Wang* [2000] and *Fedorov and Philander* [2000] show that weakening of easterlies to the west of the dateline and a change in the periodicity of El Niño from 3-5 years occurred coincident with a deepening of the thermocline from the 1960s to the 1990s. *Trenberth and Hoar* [1996, 1997] argued that there has been an increase in the occurrence of El Niños since 1976, such as the prolonged warm event of 1990-1995 and suggest the change is due to global warming. *Harrison and Larkin* [1997] show that such periods of prolonged El Niño conditions could be expected to occur every 150-200 years as an aspect of the natural variability of the tropical Pacific. The extratropical influence is argued as a possible cause for the pronounced warming of tropical Pacific during the 1990s [*Gu and Philander*, 1995] but these changes are suggested to be part of an interdecadal climate fluctuation, which changed the properties of the equatorial thermocline and winds. The activity and characteristics of El Niño, which are linked to the state of the tropical Pacific climate system, is proposed to change in response to changes in greenhouse gases along with internal climate variations [*Vecchi and Wittenberg*, 2010]. *Lee and McPhaden* [2010] showed through satellite observations an increase in intensity and occurrence of El Niño events in the central equatorial Pacific since the 1990s, which they suggest increased the temperature of the warm pool region in western Pacific. A change in the direction of anomalous warming during El Niño from an eastward propagating direction before the 1970s to a westward propagating direction after the 1970s has been highlighted in many studies [*Fedorov and Philander*, 2000; *Wang and An*, 2002; *Trenberth et al.*, 2002]. During westward propagation the warm anomaly

occurs initially along the South American coast and then proceeds toward the central equatorial Pacific while during an eastward propagating direction the central Pacific warming occurs first followed by the coastal warming. A similar change in propagation was not reported for La Niña events [*McPhaden and Zhang*, 2009] leading to suggestions of asymmetry in zonal phase propagation between El Niño and La Niña SST anomalies since 1980.

The teleconnections of El Niño and La Niña have been documented to change as a result of global warming. *Kug et al.* [2010] analyzed composites of eight member ensembles from the Intergovernmental Panel on Climate Change-Fourth Assessment Report (IPCC-AR4) coupled general circulation models (CGCMs). The study showed that future greenhouse warming would cause the main convection centers in the equatorial Pacific associated with both El Niño and La Niña to shift east, which would move the atmospheric teleconnection patterns over North America eastward, irrespective of whether the mean tropical climate response is "El Niño like" or "La Niña like". *Meehl and Teng* [2007] and *Kug et al.* [2010] agree on the teleconnections over North America but disagree on the intensification [*Kug et al*., 2010] or the weakening [*Meehl and Teng*, 2007] of the Aleutian low as a result of global warming, possibly because of differences in the multimodel ensembles. The eastward shift of the Walker circulation anomalies during El Niño events has been cited as a possible reason for the weakening of the relationship between the Indian Monsoon and El Niño after the 1970s [*Kumar et al.,* 1999]. The eastward shift of the Walker circulation leads to reduce subsidence over the Indian subcontinent favoring normal monsoon conditions during El Niño. Besides the

interdecadal variability in the relationship between El Niño and the Indian Monsoon could also be influenced by a weakened Atlantic thermohaline circulation [*Lu et al.,* 2008] and a shift in surface warming during El Niño in the equatorial Pacific [*Kumar et al*., 2006]. The tropical South Atlantic SST anomaly is suggested to be responsible for the weakened relationship between the El Niño and the Indian Monsoon [*Kucharski et al*., 2007]. An increasing trend in the number of tropical cyclone associated with El Niño was observed during 1981-2006 [*Kuleshov et al*., 2008].

There are some contrasting studies showing no significant change in variability of El Niño amplitude [*van Oldenborgh et al.,* 2005] as a result of global warming. A few observational studies also suggest no change in El Niño with global warming [*Nicholls,* 2008].

Formulation of the Problem

The central question of this dissertation is: Is El Niño changing? A best estimate of the ocean state reproduced over the past 138 years (1871-2008) through an ocean reanalysis is used to address this question. This long record includes El Niño in periods of global warming (1970s onward) and periods of little global warming (early twentieth century). There are several detailed questions that this dissertation addresses, specifically whether the strength of El Niño shows a trend due to global warming and if so whether the trend is unprecedented during earlier periods of no global warming.

In addition this dissertation addresses the issue whether El Niño is occurring more frequently in recent years, whether there is a trend in the length of the period between successive El Niño events in recent years and if the location of warming is

significantly different than what it was in the late nineteenth and early twentieth centuries. El Niño is the largest fluctuation of global climate on interannual timescale. It persists for an average 1-2 years in the tropical Pacific; repeated occurrence of such phenomena has the potential to alter the mean conditions of the ocean and atmosphere of the tropics not only locally but also in remote regions through teleconnections. Addressing this issue could assist in estimating the future frequency of El Niño.

Studies report changes in the atmospheric circulation over the tropical Pacific under global warming and the westward shifting of the location of El Niño warming in the eastern Pacific towards the central Pacific. This dissertation addresses the following question: Has the position of warm anomaly in the equatorial Pacific during El Niño changed over the last 138 years? A shift in the location of the warming over equatorial Pacific would also shift the position of convection during El Niño thus affecting the atmospheric circulation above. This might impact the extreme weather events associated with its teleconnection patterns.

Recent studies suggest changes in the direction of propagation of El Niño after the 1976/77-climate shift. This dissertation analyzes a record of 138 years to determine whether such variations are evident in El Niño variability.

This dissertation also analyzes if there are different types of El Niños based on location in the equatorial Pacific. Studies using shorter records (1950 onwards) propose that El Niño has changed in this recent years and the new flavor of El Niño is projected to continue in the global warming period. Using a long record of ocean reanalysis we

question the existence of such different types of El Niño being a result of global warming.

CHAPTER II

METHODS

To explore changes in El Niño and La Niña an ocean reanalysis incorporating the Simple Ocean Data Assimilation (SODA) methodology [*Carton and Giese*, 2008] with an ocean general circulation model (OGCM) is used. This model was used in earlier versions of SODA ocean reanalyses [*Carton et al.,* 2000a, 2000b; *Carton and Giese,* 2008; *Giese and Ray*, 2011]. The ocean general circulation model is based on the Parallel Ocean Model (POP) [*Smith et al*. 1992] version 2.0.2 numeric with an average horizontal resolution of 0.25°×0.4° with 40 vertical levels at 10-m spacing in the upper 100m. The domain of the model is global, and the grid is distorted in northern latitudes to allow for a displaced North Pole in order to resolve the Arctic Ocean. The meridional resolution increases poleward and reduces the grid anisotropy that comes about in Mercator co-ordinate grids due to convergence of meridians at high latitudes. The bottom topography is obtained from *Smith and Sandwell* [1997]. The K-profile parameterization (KPP) scheme is used in the vertical mixing and lateral subgrid-scale processes are modeled using a biharmonic-mixing scheme. Rivers are included with climatological seasonal discharge. There is no explicit sea ice model but surface heat flux is modified when the sea surface temperature reaches the freezing point of seawater.

Carton et al. [2000a] and *Carton and Giese* [2008] describes in detail the assimilation cycle; hence only a brief description is provided here. The assimilation is carried out in a 10-day cycle with corrections introduced incrementally at every time step. The corrections are updated following *Bloom et al.* [1996] to suppress excitation of

spurious variability. The methodology includes an analysis at time *t* followed by a 5-day simulation. On *t+5* day the assimilation scheme is performed to produce estimates of temperature and salinity. The data window span for the assimilation is ± 45 days. Observations further away in time have less influence on the estimates, leading to single observations influencing multiple estimates. The simulation is continued for 10 days, from day *t* to *t+10*, with temperature and salinity corrections added incrementally at every time step, producing the final analysis for the 10-day period. This process acts as a filter to suppress spurious gravity waves and maintains a nearly geostrophic relationship between pressure and velocity fields. This procedure significantly reduces bias produced in the model. The model output variables (temperature, salinity, velocity) are averaged and stored at 5-day intervals. The output is remapped onto a uniform global 0.5°×0.5° horizontal grid (720×330×40 points) using the horizontal grid spherical co-ordinate remapping and an interpolation package with second-order conservative remapping [*Jones* 1999]. Monthly averages are computed and used for analysis.

The surface boundary conditions are obtained from the latest available atmospheric reanalysis, The 20th Century Reanalysis Project, 20CRv2 [*Whitaker et al*., 2004; *Compo et al*., 2006, 2008]. Various atmospheric reanalysis are available till date to analyze climate variability. The National Center for Environmental Prediction/National Center for Atmospheric Research (NCEP/NCAR) under the NOAA developed NCEP/NCAR Reanalysis 1 project [*Kalnay et al.*, 1996] using past data from 1948 to the present. *Chelliah and Bell* [2004], *Garreaud and Battisti* [1999], and *Rao et al.* [2002] studied El Niño and the related climate variability using the NCEP/NCAR

reanalysis data. The European Center of Medium range Weather Forecast (ECMWF) also developed their own ambitious ECMWF-reanalysis project in which they constructed a 15 years reanalysis (1978-1994) called ERA-15 and a 40-year reanalysis (1957-2002) ERA-40. The ECMWF is currently developing a new reanalysis called the ERA-Interim for the period 1989 to present. Modern Era Retrospective Analysis for Research and Applications (MERRA) is a National Aeronautical and Space Administration (NASA) reanalysis for the satellite era (1979-2009) using a new version of the Goddard Earth Observing System Data Assimilation System Version 5 (GEOS-5). None of these reanalyses cover as long a period as the 20CRv2.

20CRv2 is a first attempt towards a reanalysis of global troposphere that extends back to the middle of the nineteenth century and also provides uncertainty in the analysis fields at each analysis time step. 20CRv2 output is used as boundary conditions for the ocean reanalysis, SODA 2.2.4. *Compo et al.* [2011] provides a detailed explanation of the 20th Century Reanalysis Project, 20CRv2, hence only a brief description of 20CRv2 is given here. The experimental version of NCEP Global Forecast System (GFS) is used as the coupled atmosphere-land model at a horizontal resolution of T62 and vertical resolution of 28 vertical hybrid sigma-pressure levels to generate output every 6 hours. The boundary conditions of SST and sea ice distribution are specified by the UK Met Office HadISST 1.1 data set [*Rayner et al.,* 2003]. The monthly mean SST and sea ice reconstructed data are interpolated to daily resolution. 20CRv2 assimilates surface pressure observations obtained from the International Surface Pressure Databank (ISPD) version 2. The ISPDv2 collects data from stations, marine observations and tropical

cyclone ‘best track’ pressure observations. The sea level pressure (SLP) observations are obtained from ICOADS 2.4 for the period 1952-2008 and from ICOADS 2.5 for 1871-1951 [*Woodruff et al.,* 2010]. The tropical cyclone data is obtained from International Best Track Archive for Climate Stewardship (IBTrACS; *Knapp et al.,* 2010). After passing the quality check procedures the surface pressure observations are assimilated at the elevation provided by the ISPDv2, but SLP are assimilated at zero meters. The surface pressure observations are given preference when both are available at the same location. An Ensemble Kalman Filter algorithm is used based on the Ensemble square root filter algorithm of *Whitaker and Hamill* [2002] to generate an analysis every 6 hour through an ensemble of 56 members. The 56 member of the analysis ensemble becomes the new first guess ensemble to assimilate subsequent observations. A new 56-member set of analysis is created and is used as initial condition to generate a 9-hour forecast and an analysis every 6 hours. Filter divergence is checked through covariance inflation and distance-dependent covariance localization. Covariance inflation corrects the sampling and model error, whereas covariance localization limits the radius of influence of data. The localization limit is 4000 km in the horizontal and 18 hPa in vertical for surface pressure observations at 1000 hPa. Parallel production streams are used to generate output in 27 streams, with the last stream updated to present on regular basis. Production for each stream is started after fourteen months of spin-up and continues for five years. Although the ensemble analyses are discontinuous due to the five-year stream boundaries, but the ensemble mean analysis is continuous across stream boundaries.

The surface wind stress from the atmospheric reanalysis is used for the surface momentum flux in the ocean reanalysis. Solar radiation, 2m air temperature, specific humidity, cloud cover, 10m wind speed, and precipitation are used to calculate the bulk formula for the heat flux and fresh water flux used by SODA 2.2.4.

The temperature and salinity observations used by SODA are obtained from the recent release of the World Ocean Database 2009 (WOD09) [*Boyer et al*., 2009]. WOD09 includes all available hydrographic observations collected from buoys, ships using expendable bathythermograph (XBT) and mechanical bathythermograph (MBT). The drop rate corrections [*Levitus et al.,* 2009] introduced due to fall rate errors of XBTs and MBTs significantly reduces the decadal variability in an ocean reanalysis [*Giese et al.,* 2011], particularly in the North Pacific Ocean. There were very few hydrographic observations available over the tropical Pacific during the 1920s but increases gradually with more observations being collected over time (Figure 1). The reduced hydrographic observations in the early twentieth century are compensated by the comparatively larger spread of SST observations (Figure 1) in ICOADS release 2.5 [*Woodruff et al.,* 2010]. *Carton et al*. [2011] discuss the impact of changing density of observations on ocean climate variability.

Two experiments are performed for this study. SODA 2.2.4 assimilates all available hydrographic and surface marine observations mentioned above using the SODA methodology. SODA 2.2.0 is same but without the assimilation of observations. Both experiments are forced with identical boundary conditions from 20CRv2. The purpose of these experiments is to compare the results of the simulation with the

assimilation to quantify the bias in the results due to model error. Many ocean models have a well-known bias in simulating El Niño far too west. Assimilation can correct this model bias through observations. Comparison of SODA 2.2.4 to SODA 2.2.0 indicates the impact of model bias on measuring El Niño events during periods of sparse data coverage, when too few data were available to correct for the model bias.

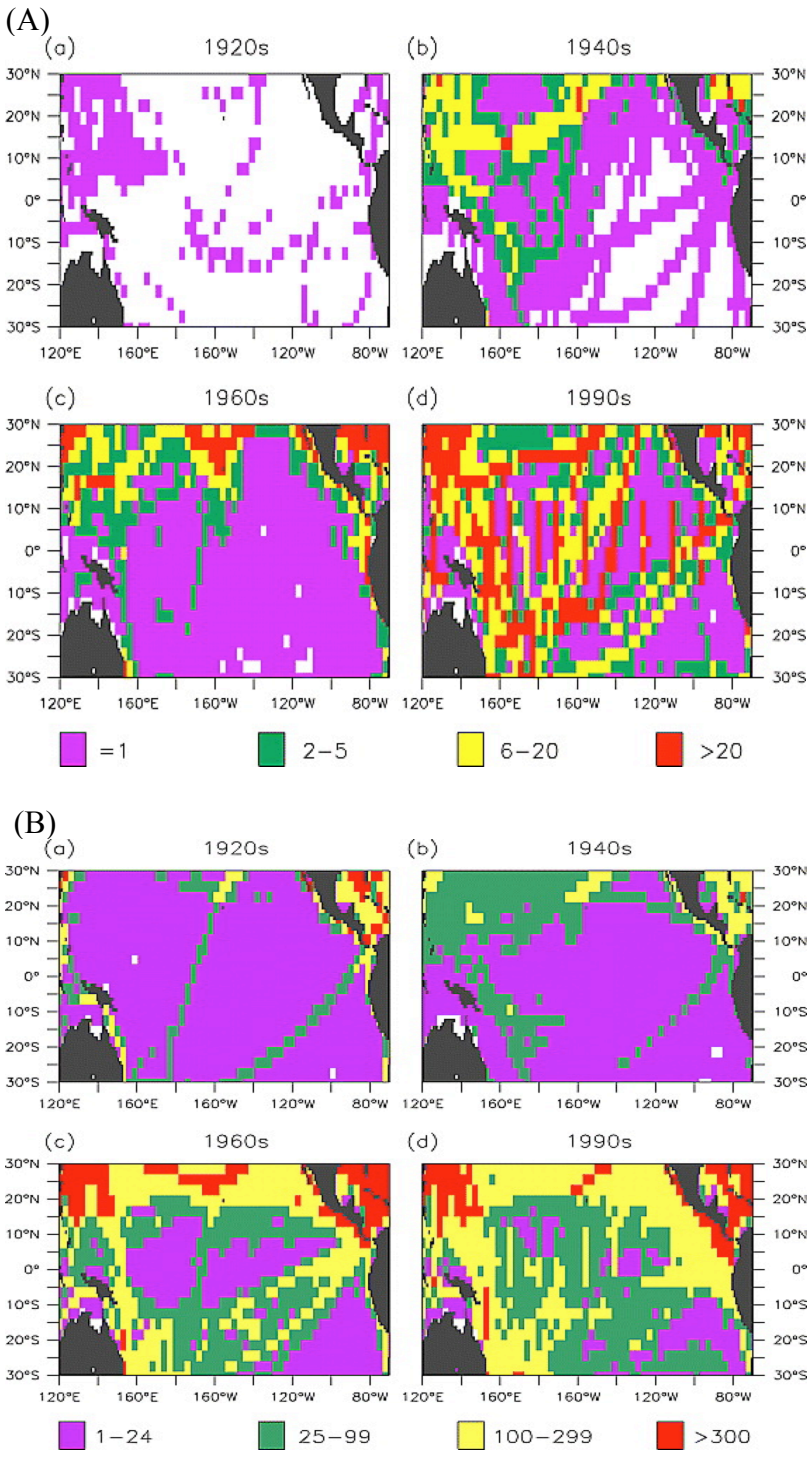

Figure 1. The number of WOD09 hydrographic temperature observations used in SODA 2.2.4 by decade (A). The number of ICOADS 2.5 SST observations used in SODA 2.2.4 by decade (B).

CHAPTER III

RESULTS *

Mean Conditions

Sea surface temperature (SST), sea surface height (SSH), zonal wind, and surface velocity from SODA 2.2.4 were explored for interannual climate variability in the tropical Pacific. The mean conditions of the equatorial Pacific consists of warm surface and subsurface waters in the western Pacific with strong westerly winds, referred as the Warm Pool region; while cold waters with strong easterly winds dominate the eastern Pacific, referred to as the Cold Tongue region. The equatorial thermocline has a noticeable gradient, deep in the western Pacific (about 170m) and shallow in the eastern Pacific (about 40m).

A warmer Warm Pool in the late nineteenth century and early twenty-first century, the relaxed east-west zonal SST gradient after the 1920s are few of the distinct features of the changing mean conditions of the equatorial Pacific. The Warm Pool was warmest in the late 19th century and early 21st century with surface temperatures rising to 30°C (Figure 2a). Between 1900-1940 the surface waters, which was normally around 29°C between 120°E-140°E throughout the record cooled to 28.5°C. The surface temperatures in the western Pacific are strongly affected by surface heat fluxes, westerly

* Reprinted with permission from "El Niño variability in simple ocean data assimilation (SODA), 1871-2008" by Benjamin S. Giese and Sulagna Ray, 2011, *Journal of Geophysical Research,* Vol. 116, C02024, Copyright 2011 by the American Geophysical Union.

wind bursts, and the intra-seasonal Madden Julian Oscillation [*McPhaden* 2002; *Chou et al.,* 2000]. The Cold Tongue was coldest during the 1910s through 1920s and during the 1960s (Figure 2a), which were periods of strengthened easterlies (Figure 2b) in the east Pacific.

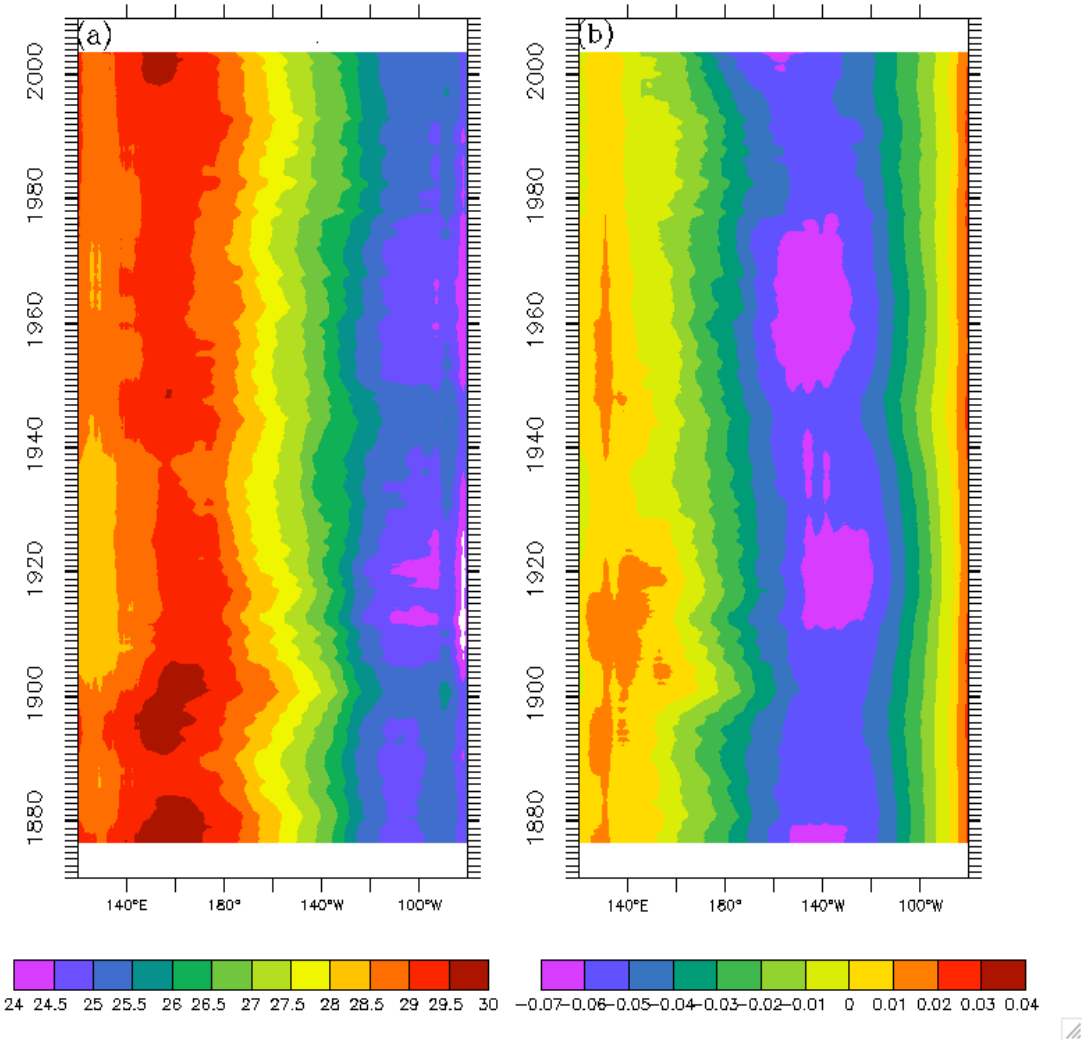

Figure 2. Time evolution of (a) SST averaged over 5°S: 5°N and (b) Taux on equator over equatorial Pacific [120°E: 80°W] from SODA 2.2.4 after applying a boxcar filter of 11 years.

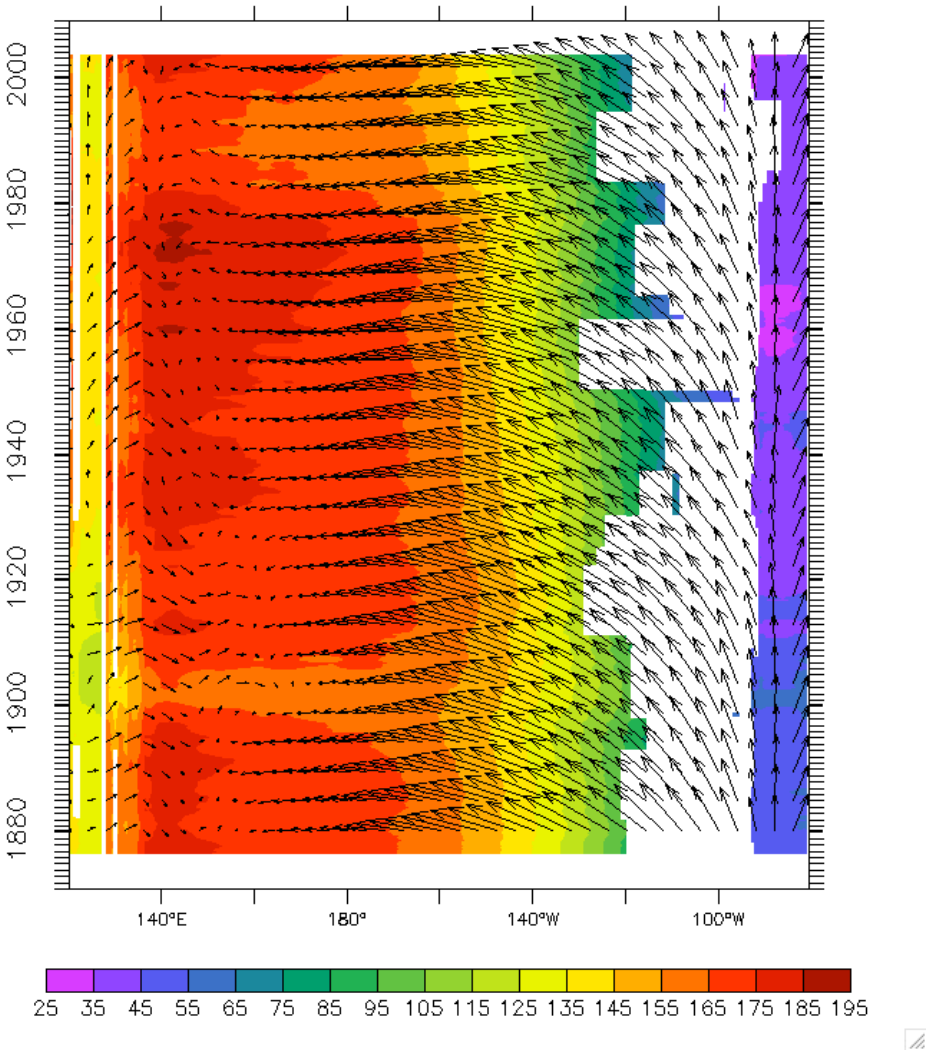

Figure 3. Yearly averaged 11-year climatology of depth of 20°C Isotherm at equatorial Pacific overlaid by yearly averaged 11-year climatology of wind vectors. Length of vectors is 0.05 m/s

The east-west SST gradient was sharp till the 1910s but from the 1950s onward the gradient relaxed with occasional strengthening and weakening of the zonal wind stress in the central/eastern equatorial Pacific (Figure 2b). The region of strong easterlies shifted westward from 1990s onward. The depth of 20°C isotherm in the equatorial Pacific, which is an indicator of the subsurface heat content does not show prominent

changes but is strongly influenced by the winds above in the eastern Pacific where it is shallow (Figure 3). It was 45m deep till the 1910s, but started to shoal by 10m thereafter. In the early 21st century the thermocline between 110°W-80°W shoaled to be about 35m.

Construction of Climatology

As the tropical Pacific undergo changes in its mean state (including slow changes in the seasonal cycle) that could affect the strength of the anomalous surface temperature and winds during El Niño and La Niña, we consider anomalies after removing climatology constructed using an 11-year window. This moving 11-year climatology (constructed each year with the plotted year at the center of the 11-year window) was constructed over the whole record of the reanalysis thereby removing decadal changes in the climatological state not associated with El Niño. The impacts of extended periods of El Niño/La Niña activity on the mean tropical Pacific climate was profound and had significant impact on the state of the tropical ocean-atmosphere interactions. Our approach was similar to that used by *Fedorov and Philander* [2001], thus a climatology was created that was long enough to be unaffected by strong El Niño/La Niña activity and short enough to remove decade-to-decade variability and trends that make the interannual signal difficult to analyze. The first five years (1871-1875) and the last five years (2004-2008) had a fixed climatology removed over their respective periods. Figure 4 shows the SST at different locations across the equatorial Pacific overlaid by the 11-year climatology of SST. The amplitude of seasonal cycle is larger in locations in eastern Pacific compared to that in western Pacific but the changes in the 11-year climatology is

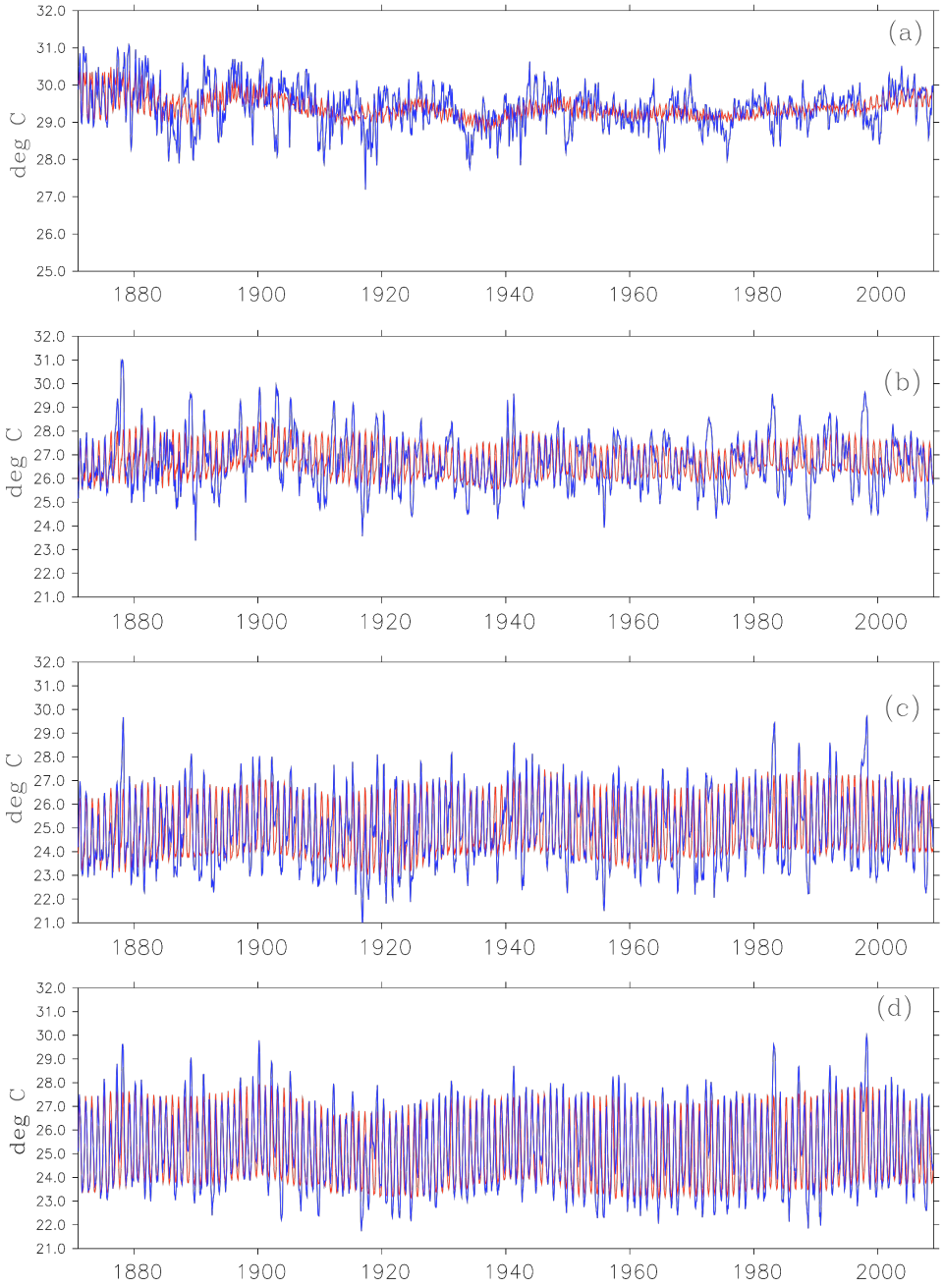

Figure 4. SST (blue) from SODA 2.2.4 at (a) 160°E, (b) 140°W, (c) 110°W, and (d) 90°W on the equator overlaid by an 11-year climatology (red) at the respective locations. A comparison of the variation in 11-year climatology at different longitudinal locations on the equatorial Pacific is shown.

prominent in the western Pacific. At 140°W there are changes in the amplitude of seasonal cycle, decreasing during 1900s, 1930s, 1970s but strengthening during 1880s, 1920s, 1940s, and decreasing during late 20th century. Changes in the amplitude of SST seasonal cycle at 110°W and 90°W are small, almost remaining constant in the latter half of the run. A comparison of the evolution of the SST anomaly after removing a constant climatology for 1871-2008 and an 11-year climatology is presented in Figure 5. Both show interannual warming and cooling in the eastern Pacific at similar times. The cold anomalies seem to be about 0.5°C stronger when a constant climatology is removed.

Niño 3.4 Index

Definition

The Niño 3.4 index is a standard metric to measure the strength of El Niño and La Niña in the tropical Pacific. The index is the SST anomaly averaged over a rectangular region in the central equatorial Pacific between 170°W-120°W and 5°S-5°N. An El Niño occurs when the average SST anomaly over the Niño 3.4 region exceeds 0.5°C for 3 consecutive months. Similarly, La Niña conditions prevail when the SST anomaly is less than -0.5°C for 3 consecutive months. The Niño 3 index, defined as the average SST anomaly over the eastern Pacific (150°W-90°W, 5°S-5°N) is also sometimes used as a measure of El Niño.

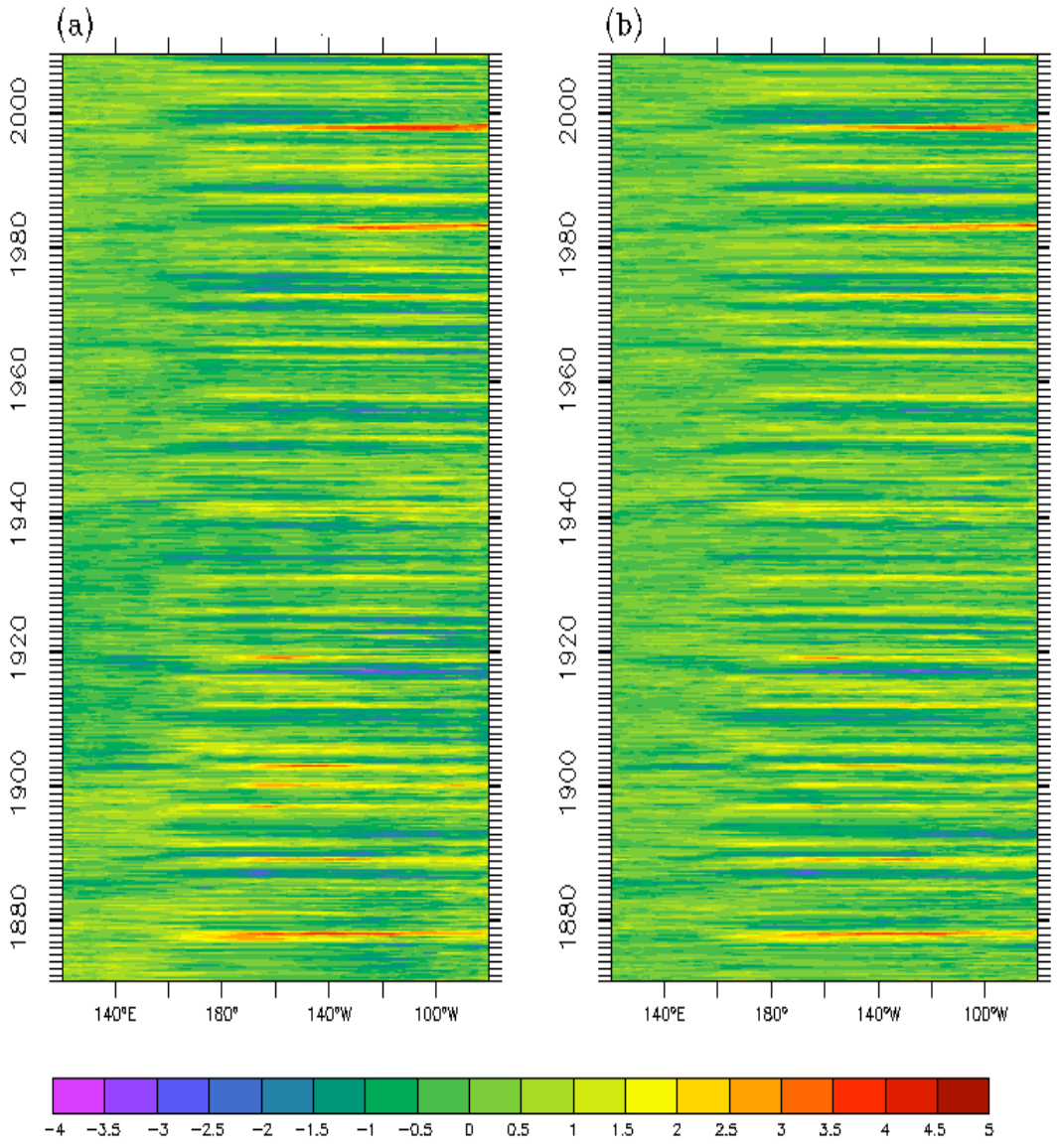

Figure 5. Time evolution of SST anomalies averaged over equatorial Pacific (5°S: 5°N) after removing a (a) constant climatology for 1871-2008 and (b) an 11-year climatology during 1871-2008. El Niño and La Niña events occur simultaneously in both.

Recent studies suggest existence of a different kind of El Niño in the tropical Pacific. *Trenberth and Stepniak* [2001] introduced the Trans-Niño Index (TNI) in addition to the Niño 3.4 index to identify different types of El Niño which they call flavors. TNI is the difference in the normalized SST anomalies averaged over the Niño 1+2 region (90°W - 80°W; 5°S - 5°N) and Niño 4 region (160°E - 150°W; 5°S - 5°N), which gives the gradient of SST anomalies across equatorial Pacific. The El Niño Modoki Index, which measures the difference in average temperature anomaly of the region 165°E-140°W, 10°S-10°N and half the sum of the region 110°W-70°W, 15°S-5°N and the region 125°E-145°E, 10°S-20°N is used to represent a different kind of El Niño, called the El Niño Modoki [*Ashok et al.,* 2007].

El Niño variation in SODA 2.2.4

The 138-year record of the ocean reanalysis SODA 2.2.4 was used to analyze the variations of El Niño and La Niña from 1871-2008. The 11-year running climatology of the Niño 3.4 region as computed from SODA 2.2.4 (Figure 6a) showed little variation in 1871-2008. This indicates that the climatological state of the surface temperature over the Niño 3.4 region did not change drastically from the late 19th Century through the end of the 20th Century. Figure 6b shows the SST anomaly after removing a fixed climatology (in black) and an 11-year moving climatology (in red).

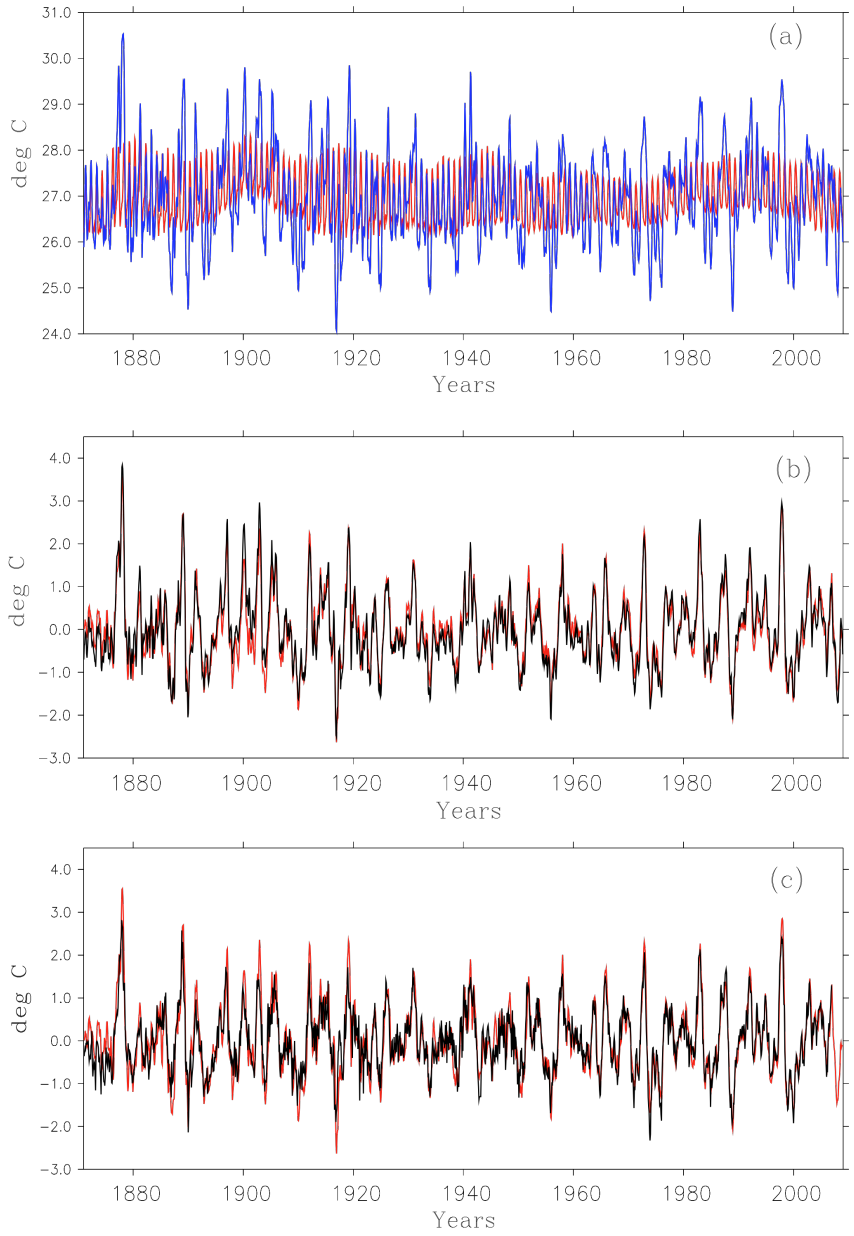

Figure 6. (a) Nino 3.4 region (170°W to 120°W and 5°S to 5°N) SST from SODA 2.2.4. Superimposed in red is an 11-year running climatology. (b) Niño 3.4 SST anomaly from SODA 2.2.4 plotted with the 11-year running climatology removed (red line) and with a constant climatology of the period 1871 – 2008 removed (black line). (c) Niño 3.4 SST anomaly from SODA 2.2.4 (red line) and from HadISST (black line). An 11-year running climatology has been removed from both.

El Niños in the late nineteenth Century and early twentieth Century were weaker after removing an 11-year moving climatology than after removing a fixed climatology. The El Niños during 1920-1970 were stronger after removing an 11-year climatology than after removing a fixed climatology.

The Niño 3.4 index from SODA 2.2.4 showed a prominent decadal variability in El Niño with strong events occurring at both the beginning and the end of the record. The middle of the twentieth century, 1930-1950, had weaker El Niño events, with no events from 1930-1940. The strength of El Niño does not show a trend during 1871-2008. Using Niño 3.4 SST anomaly as a measure of strength of El Niño shows that the El Niño of 1877/78 was the strongest in the record with an anomaly of 3.8°C followed by the El Niño of 1997/98 with an anomaly of 3°C. La Nina in Niño 3.4 index show little variation in its strength. The only strong La Niña in the record is the La Niña of 1917/18 with an anomaly of -2.6°C while the rest of the La Niña events are below an anomaly of - 2.0°C. The strengthening and weakening of El Niño is not seen in the strength of La Niña. On other hand, the El Niños are much stronger than the La Niñas. This indicates an asymmetry in the strengths of El Niño and La Niña.

Figure 7 shows comparison of Niño 3.4 index from SODA 2.2.4 and SODA 2.2.0, which is a simulation only. Since 1951 marks the year from when there was a gradual increase in marine observations, the correlation of Niño 3.4 index from SODA 2.2.4 and SODA 2.2.0 are shown separately for the two periods, 1871-1950 (period of

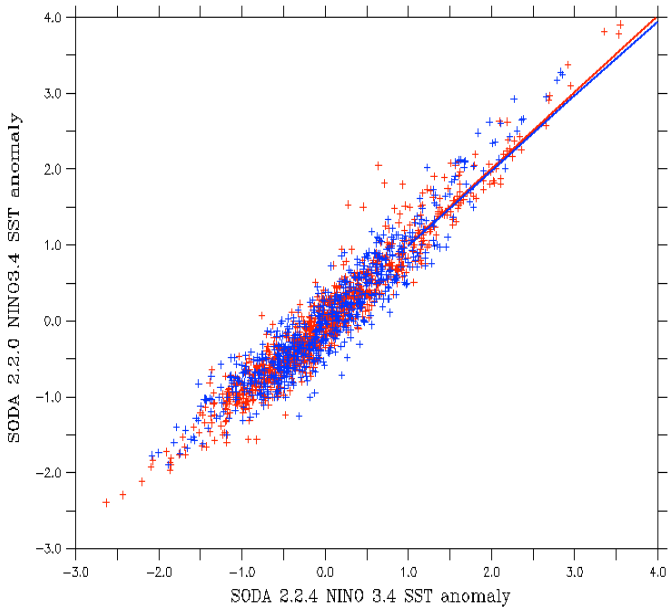

Figure 7. NINO 3.4 index from SODA 2.2.0 plotted as a function of NINO 3.4 index from SODA 2.2.4. Values from 1871 through 1949 are shown in red and values from 1950 through 2008 are shown in blue. The least squares regression for both periods of time are shown as a solid line.

sparse data) in red and 1951-2008 (period of dense data) in blue. The Niño 3.4 SST anomalies from the two runs (Figure 7) were highly correlated (0.95) with each other. The positive anomalies of Niño 3.4 index were better correlated (0.91) than the negative anomalies (0.8). The high correlation that was found during both the data sparse periods 1871-1950 (0.96) and the data dense period 1951-2008 (0.94) implies that model bias has negligible impact on the measure of the strength of El Niño and La Niña events. The El Niño events in SODA 2.2.0 were warmer than SODA 2.2.4 by 0.2°C during data dense period of 1950-2008 indicates that assimilation dampens the SST anomaly in the model.

El Niño variation in HadISST

The Niño 3.4 index from the reanalysis highly correlates (0.9) with HadISST. The times of El Niño and La Niña events matched remarkably well between the two datasets (Figure 6c). It was expected that the two products would agree well during periods of dense observations (1950-2008), but it was interesting to find them in modest agreement during periods of sparse observations in the early twentieth century (1871-1949). The number of observations that went in the Niño 3.4 SST reconstruction in the early twentieth century was limited. HadISST used spatial patterns of tropical Pacific SST (Empirical Orthogonal Functions, EOFs) from data dense periods (in the 1980s and 1990s) to extrapolate into data-sparse periods (for example the early twentieth century). Thus, SST reconstructions rely heavily on the assumed geographic pattern together with SST observations outside Niño 3.4 region during the early twentieth century and should be considered tentative. In fact, disagreement exists in the strength of El Niño and La Niña events between the two products during the first half of the 20th Century (Figure 6c). El Niño and La Niña events at the beginning of the record in SODA 2.2.4 are relatively strong. This is particularly evident during strong El Niño and La Niña events; SODA 2.2.4 showed the El Niño of 1877/78 was warmer than HadISST by 0.75°C and the strong La Niña event of 1917/1918 was colder by 1°C in SODA 2.2.4. Such big differences in the strengths of El Niño and La Niña between SODA 2.2.4 and HadISST do not exist in the late 20th Century, for example, the 1997/98 El Niño in SODA 2.2.4 was warmer by only 0.3°C. The reanalysis showed periods of strong El Niño activity at the beginning and end of the twentieth century with periods of weak activity in the mid

twentieth century (1920-1970). Similar decadal variation in strength of El Niño activity is present in the reconstructed SST anomaly from HadISST (Figure 6c). The difference between the two products is most prominent in the spatial structure of the December-January-February (DJF) averaged SST anomaly during the El Niño of 1877/78. Figure 8 shows the spatial patterns of the DJF SST anomaly during the El Niño of 1877/78 and 1997/98 from four different records: SODA 2.2.4 (Figure 8a and 8b), HadISST (Figure 8c and 8d), ERSST v3 (Figure 8e and 8f), and Kaplan v2 (Figure 8g and 8h). The El Niño of 1997/98 in HadISST (Figure 8d) resembles SODA 2.2.4 (Figure 8b). However the spatial structure of the El Niño of 1877/78 in HadISST (Figure 8c) differs from SODA 2.2.4 (Figure 8a). Interestingly, in HadISST the DJF SST anomaly of the El Niño 1877/78 closely resemble the DJF SST anomaly of the El Niño of 1997/98 (Figure 8c and 8d).

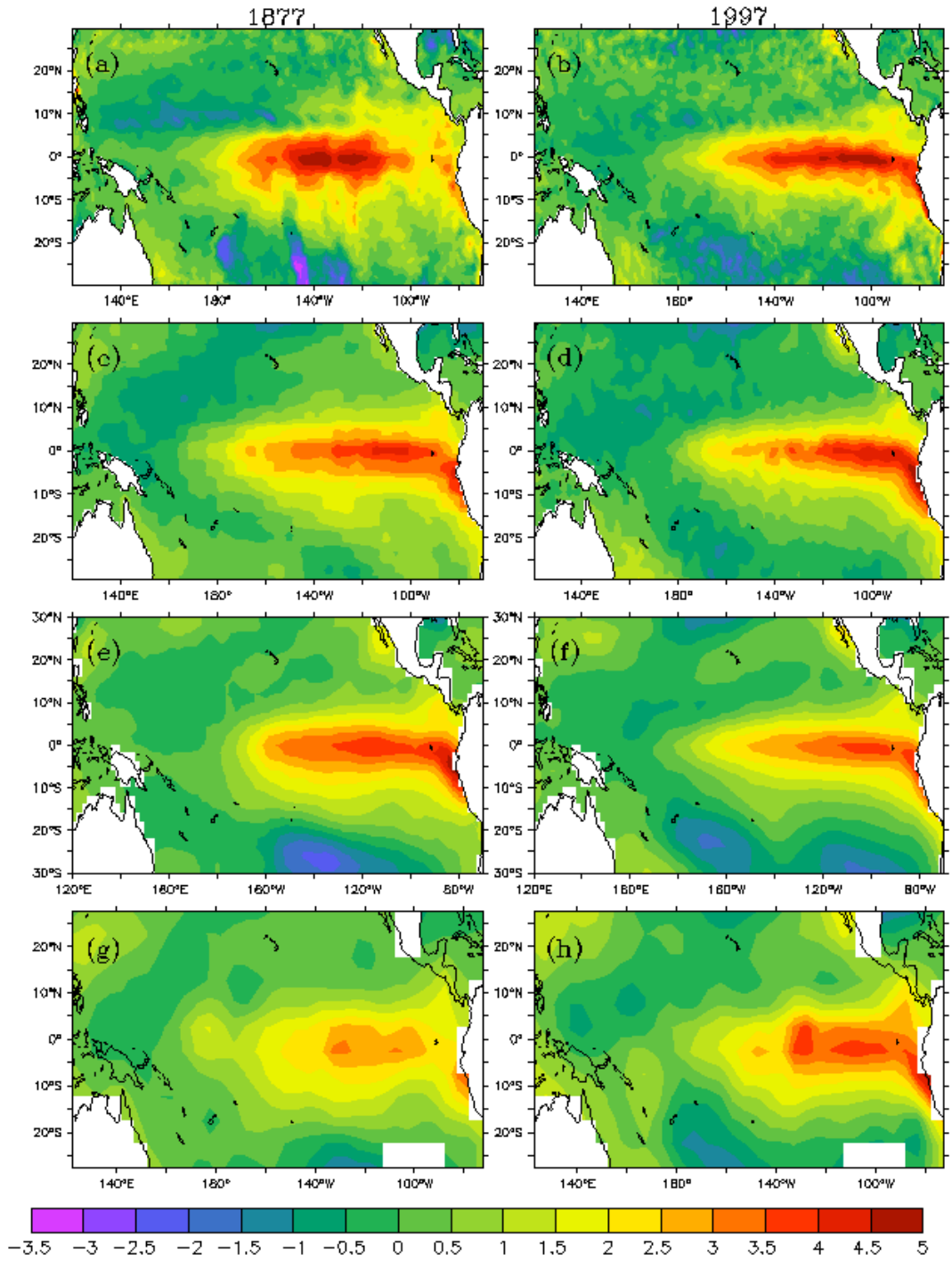

Figure 8. DJF averaged SST anomaly for El Niño of 1877/78 (left panel) and El Niño of 1997 (right) from SODA 2.2.4 (a and b), HadISST (c and d), ERSST v3 (e and f), and Kaplan v2 (g and h). A comparison of the two largest El Niños during 1871-2008 from four different records is shown.

El Niño variation in ERSST and Kaplan v2

Comparing the El Niño and La Niña events from SODA 2.2.4 to another reconstructed SST data set, the Extended Reconstructed SST (ERSST) version 3 (ERSSTv3) and version 3b (ERSSTv3b) created by National Ocean and Atmospheric Administration (NOAA), the Niño 3.4 indexes from the two records show a high correlation of 0.9. Comparing the Niño 3.4 indexes from SODA 2.2.4 and Kaplan's SST version 2 (Kaplanv2) also show a high correlation of 0.88. The El Niño of 1877/78 was one of the strongest in the whole period of study (1871-2008), but was surprisingly missing in the ERSST v3b, which is the latest version of ERSST and does not include satellite data. The spatial structure of the DJF SST anomaly of the El Niño of 1877/78 and the El Niño of 1997/98 in ERSSTv3 (Figure 8e and 8f) resemble each other closely. However the El Niño of 1997/98 is much stronger than the El Niño of 1877/78 in Kaplan v2 (Figure 8g and 8h). Figure 9a shows the Niño 3.4 index from ERSST v3 and SODA 2.2.4 plotted simultaneously. The timings of individual events matched well among the all the products. The events in ERSST v3 (Figure 9a) are weaker than SODA 2.2.4 in the beginning of the record till 1930, after which the strengths of ENSO events between the two agree better. The ENSO events in Kaplan v2 Niño 3.4 index (Figure 9b) are weaker than SODA 2.2.4 and ERSST. The El Niño of 1877/78 was weaker by about 1.75°C in Kaplan v2 whereas it was weaker by 0.85°C in ERSSTv3 than in SODA 2.2.4; the 1888/89 El Niño is weaker by 0.7°C in Kaplanv2 whereas it is only weaker by 0.1°C in ERSSTv3 when compared to SODA 2.2.4.

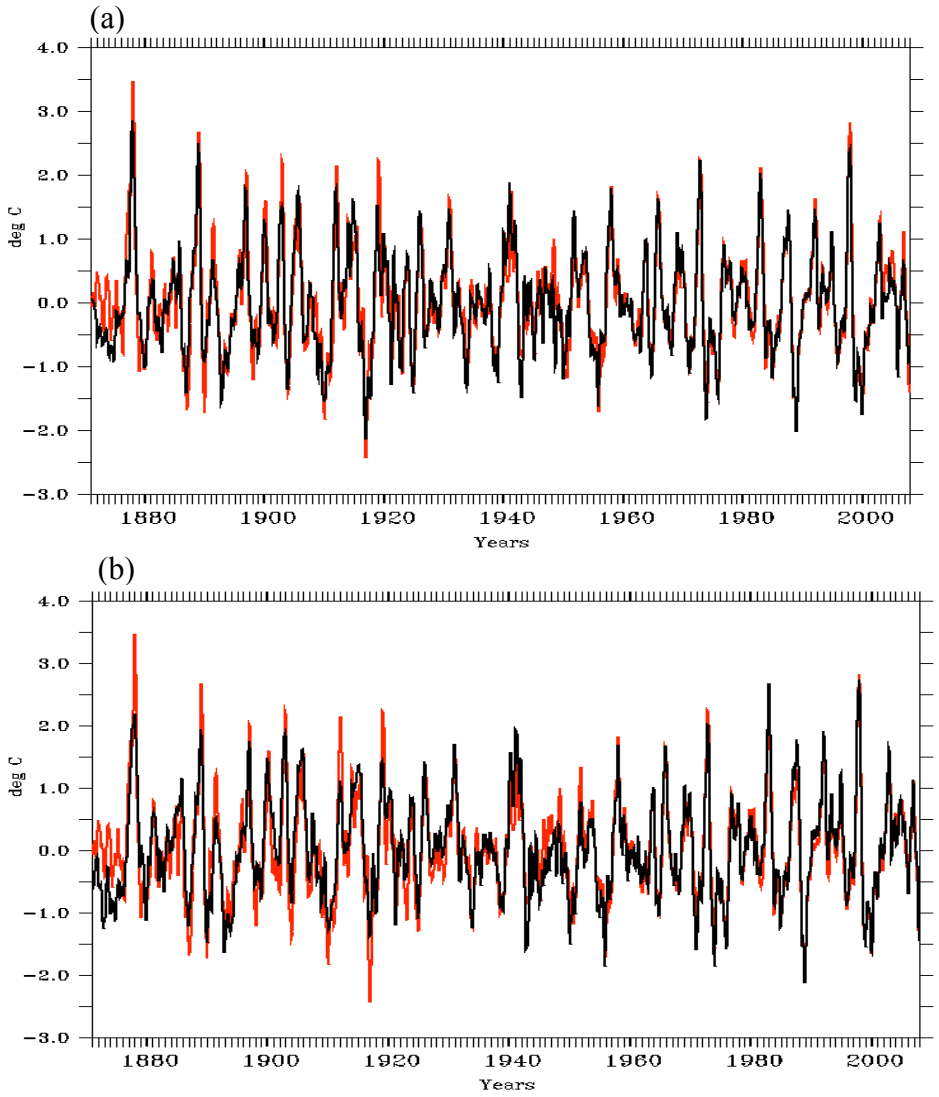

Figure 9. Niño 3.4 SST index from SODA 2.2.4 in red overlaid by Niño 3.4 SST index from (a) ERSST v3 and (b) Kaplan v2 in black. Comparison between the strength and times of El Niño and La Niña events in Niño 3.4 index from ERSST v3, Kaplan v2, and SODA 2.2.4 is shown.

Kaplan v2 shows an increasing trend in the strength of El Niño from the late nineteenth century to the end of twentieth century. Figure 10 shows the correlation plot of Niño 3.4 index from SODA 2.2.4 with HadISST (Figure 10a), ERSST v3b (Figure 10b), and Kaplan v2 (Figure 10c). ERSST v3b agree with SODA 2.2.4 better than HadISST in the data-dense period (1950-2008).

The fact that El Niño in HadISST/ERSST/Kaplan v2 are similar and that El Niño in HadISST/ERSST/Kaplan v2 is different than SODA 2.2.4 raises two issues of concern. First, the reconstructed SSTs rely on SST anomaly patterns obtained during data-dense periods to extrapolate into regions where observations are sparse in the early twentieth century. Second, it is possible that the Niño 3.4 index is an inaccurate measure of the strength of the El Niño when the maximum warming is not located in the Niño 3.4 region. For example, the maximum warm anomaly lies in Niño 3.4 region during the El Niño of 1877/78 (Figure 8a) but lies outside that region during the El Niño of 1997/98 (Figure 8b).

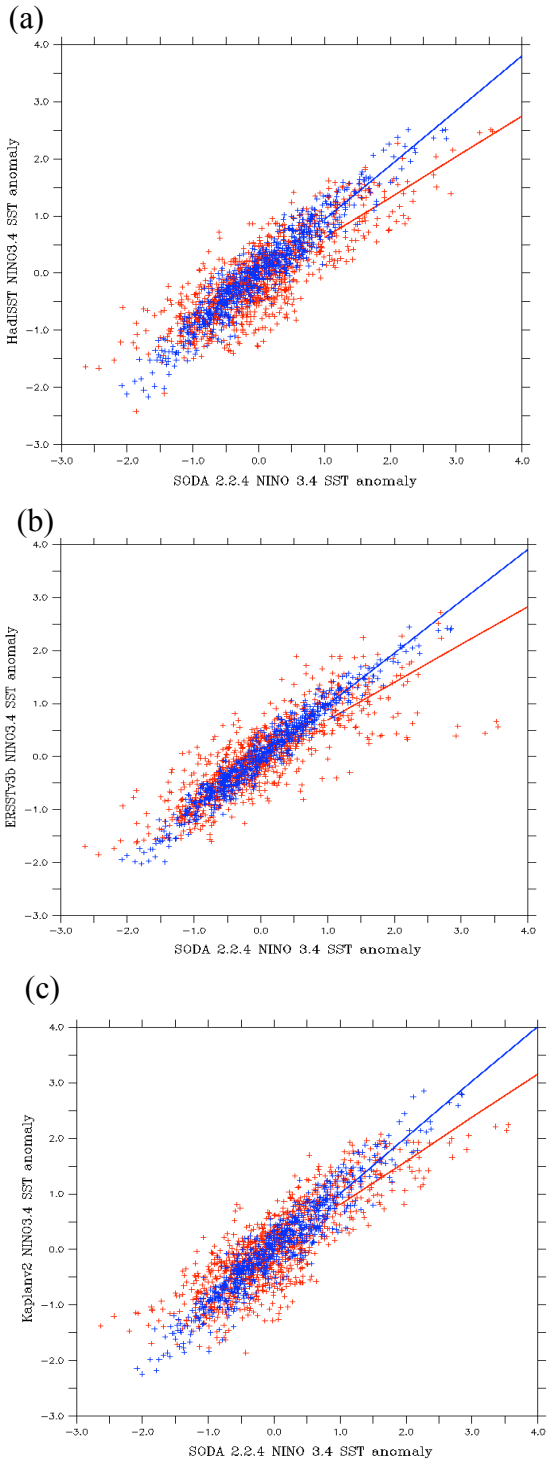

Figure 10. Niño 3.4 SST index from (a) HadISST, (b) ERSSTv3b and (c) Kaplan v2 plotted as function of Niño 3.4 SST index from SODA 2.2.4. Values from 1871 through 1949 are shown in red and values from 1950 through 2008 are shown in blue. The least squares regression for both periods of time are shown as a solid line.

The Niño 3.4 Index Is Inadequate

Assumption of El Niño variation at a fixed location

The primary reason for using the Niño 3.4 index as a measure of El Niño and La Niña was its location in the equatorial Pacific. The index covered mostly the location where El Niño warming and La Niña cooling conventionally occurs. However it is possible that significant ENSO warming can straddle or even be outside the Niño 3.4 region. During the El Niño of 1997/98 the warmest region resides to the east of Niño 3.4 region (Figure 8b) resulting in a weaker estimation of this powerful event. The El Niño of 1877/78 appeared stronger than the El Niño of 1997/98 using the Niño 3.4 Index (Figure 6c) whereas the El Niño of 1997/98 is stronger than the maximum anomaly during the El Niño of 1877/78 in the DJF SST anomaly pattern (Figure 8a and 8b). These differences occur because the strong anomaly in the winter of 1997/98 was confined to the coastal regions of South America and hence was not recorded by the Niño 3.4 Index. In some respects the Niño 3.4 index is not sufficient to record the strength of El Niño and La Niña when the positions of warming or cooling vary during El Niño and La Niña. In an attempt to measure the anomalous warming independent of its location in the equatorial Pacific during El Niño events, we propose a new index that records the location of the weighted center of the warming or cooling.

Center of Heat Index

Definition

The new index, which we term the Center of Heat Index (CHI), is the first moment of the SST anomaly. Anomalies greater than 0.5°C are considered when the area of the warm anomaly is greater than the surface area covered by the Niño 3.4 region. The search region is the equatorial Pacific (120°E: 70°W and 5°S: 5°N). The index gives the temperature-weighted center of mass (in terms of longitude) of the warm surface waters greater than 0.5°C of anomaly. The CHI has three components: the CHI longitude, given by

$$CHI\ Longitude = \frac{\sum sst\_anom \times longitude}{\sum sst\_anom} \qquad (1)$$

where *sst_anom* is the SST anomaly > 0.5°C over a surface larger than the Niño 3.4 region; the second component is the CHI amplitude, given by

$$CHI\ amplitude = \frac{\sum sst\_anom \times area}{\sum area} \qquad (2)$$

where *area* is the area over which the SST anomaly > 0.5°C. The third component is the CHI area, which is the sum of the *area* above 0.5°C of anomaly and must be at least the size of the Niño 3.4 area.

Three different metrics

The CHI components for El Niño from SODA 2.2.4 are shown in Figure 11. Figure 11a shows the CHI amplitude, which represents the strength of warm events in the equatorial Pacific. The CHI amplitude is the average SST anomaly above 0.5°C over

a region at least the size of the Niño 3.4 box. The CHI amplitudes in the start of the record are as strong as those in the last part of the record. The maximum value of CHI amplitude is 2.9°C. The mean value of CHI amplitude in 1.13°C and varies within ±0.4° about the mean. The location of El Niño represented by CHI longitude is shown in Figure 11b. The CHI longitude is the center of the warming and Figure 11b shows that it varies from the dateline eastward till 100°W in the eastern Pacific. The circle in Figure 11b is proportional to the CHI amplitude. The mean location of CHI longitude is at 139°W. Figure 11c shows the magnitude of area covered by the warm anomaly at the surface. The size of circles is once again proportional to the strength of the CHI amplitude. Strong El Niños tend to cover a larger area. The weak warm anomalies seem to be covering both small and large surfaces. Notably the 1877/78 El Niño covers a larger area than the 1997/98 El Niño, although they are comparable in their strength.

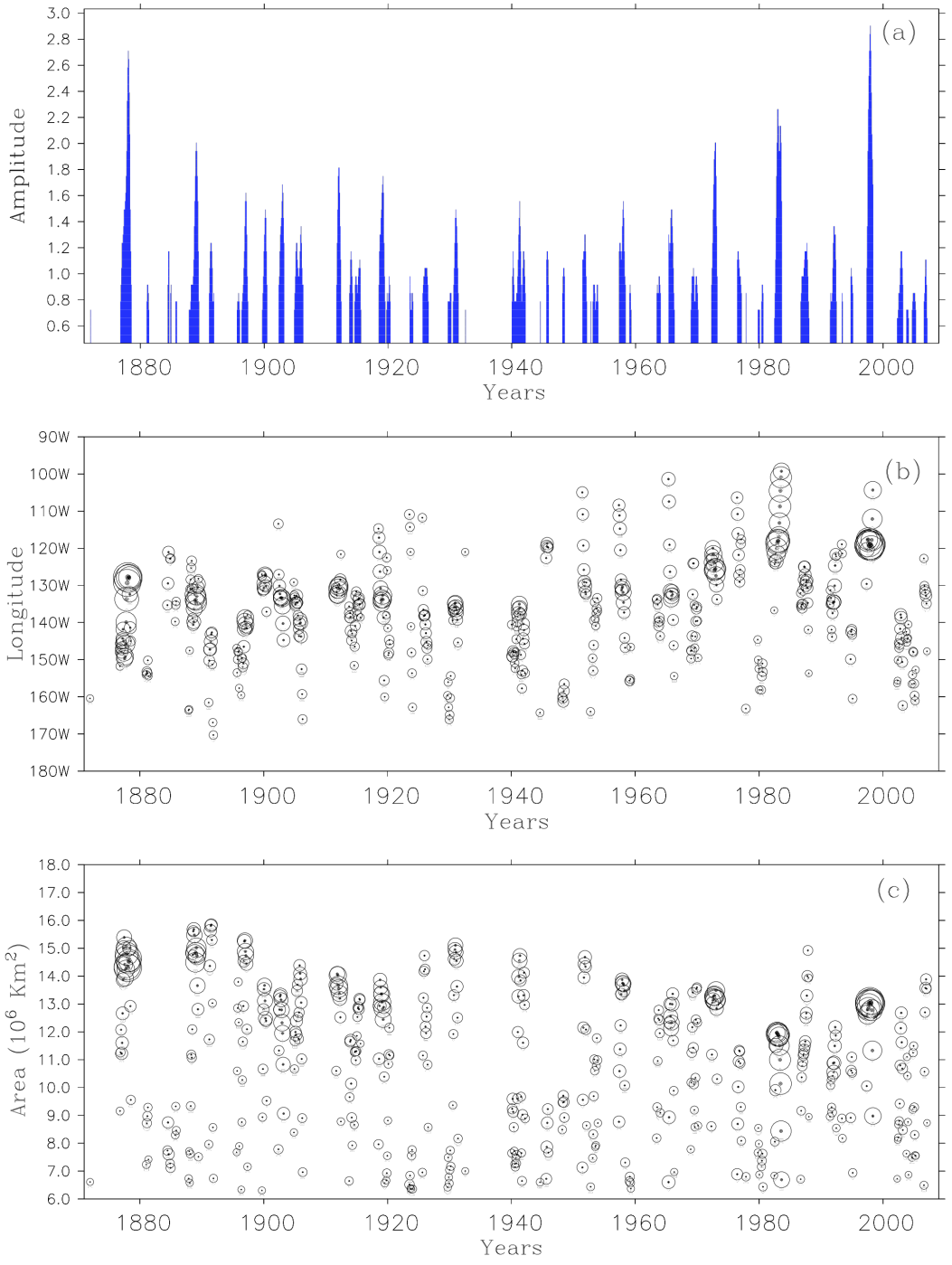

Figure 11. (a) CHI amplitude in °C, (b) CHI longitude, and (c) CHI area in 10^6 km^2 for warm events during 1871-2008. In both (b) and (c) the size of the circle is proportional to the amplitude.

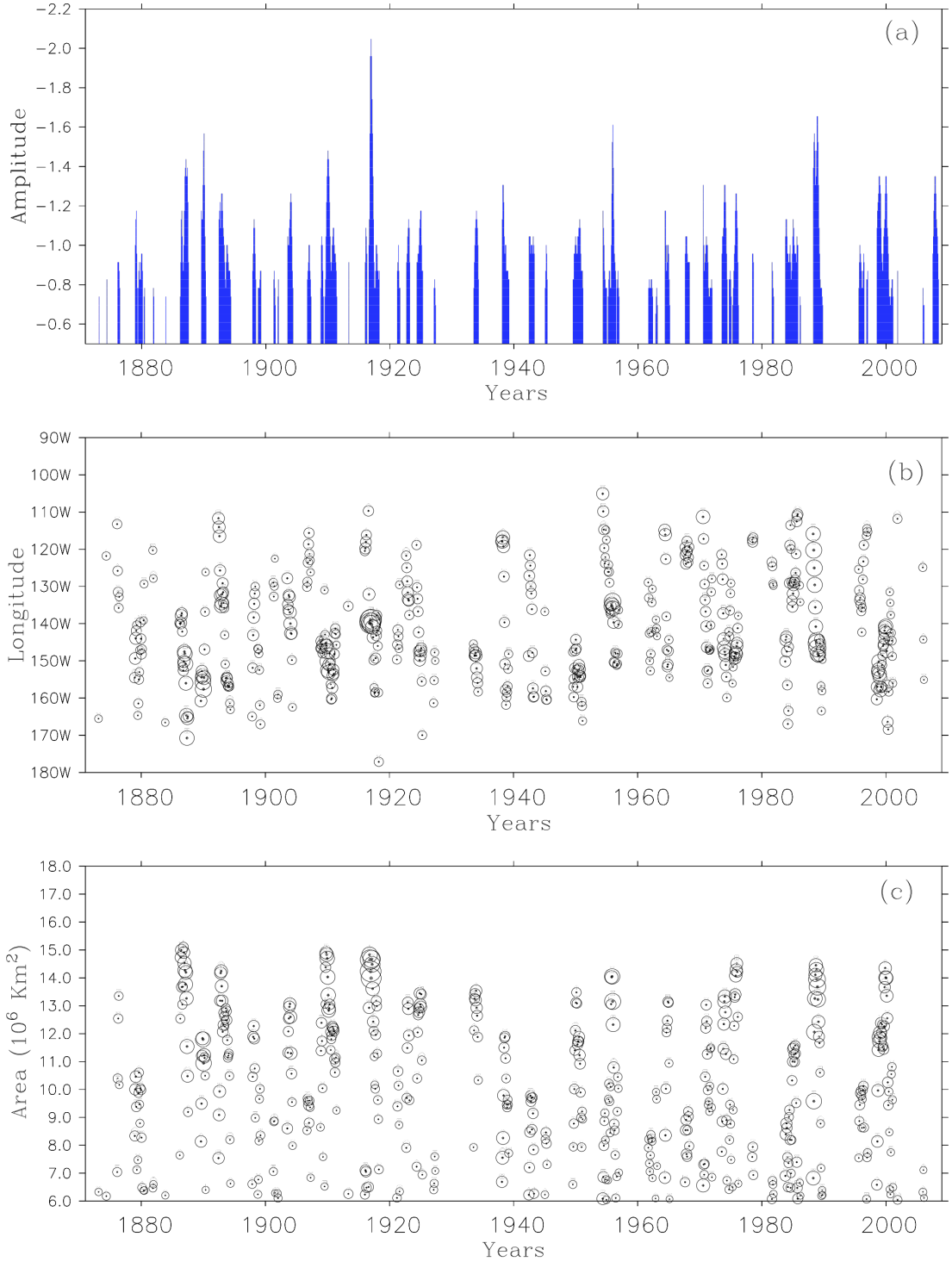

Figure 12. As in Figure 11, but for cold events.

CHI can also be used for La Niña by using SST anomalies less than -0.5°C over a region of at least the size of Niño 3.4 box. Figure 12a shows the CHI amplitude, which has a minimum value at -2°C. Otherwise La Niña strength is fairly consistent about its mean value of -0.99°C over the whole record without showing particular periods of strengthened or weakened amplitude. Figure 12b shows the distribution of CHI longitude for La Niña events over time, with circle size proportional to the CHI amplitude. The CHI longitude for La Niña is distributed between the dateline and 100°W in the eastern Pacific, similar to the CHI longitude for El Niño. The mean location of CHI longitude is at 140.1°W. Figure 12c shows the CHI area representing the size of La Niña events. Again the circle size is proportional to the CHI amplitude. The growth rate of La Niña seems to be smaller than that of El Niño.

Figure 13 shows the distribution of CHI amplitude for warm events (upper panel) and for cold events (lower panel). The warm events are stronger (maximum value 2.9°C) than cold events (minimum value -2.1°C) in CHI amplitude, which is particularly evident in the skewness of CHI amplitude for warm events (1.8) and cold events (-1.4) events.

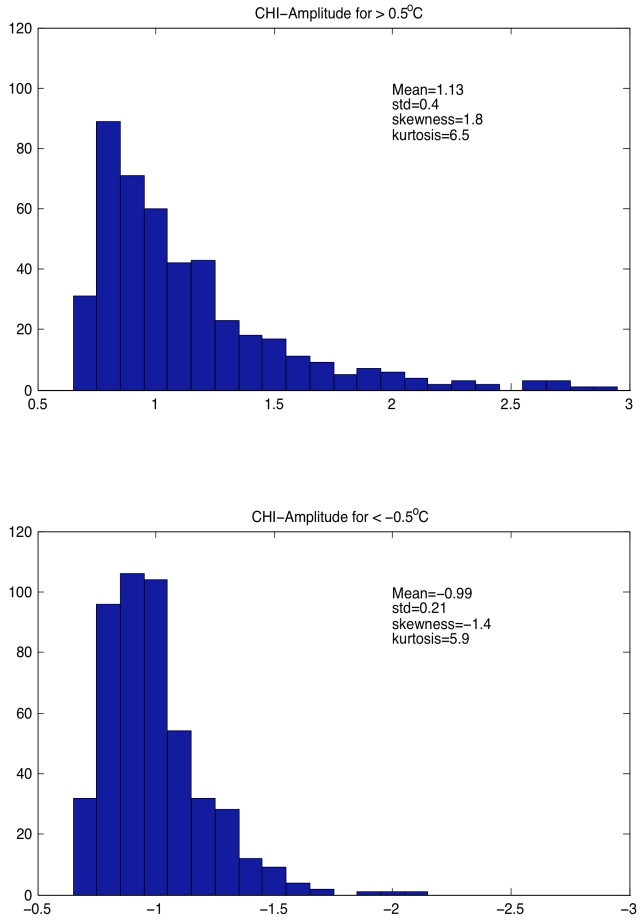

Figure 13. Histogram of CHI amplitude for warm (upper panel) and cold (lower panel) events during 1871-2008. The mean, standard deviation, skewness and kurtosis of each distribution are shown in the plot for each case. The distribution of the strengths of El Niño and La Niña is shown. The heavy-tailed distribution of El Niño strength indicates stronger El Niño events compared to La Niña events.

The comparative larger spread in the strength of El Niño events to that in La Niña events is evident in the standard deviations of the distributions of CHI amplitude for warm events (0.4) and cold events (0.21). Earlier studies [*Jin et al.,* 2003; *An and Jin*, 2004; *McPhaden and Zhang*, 2009] describe the asymmetry in the strength and

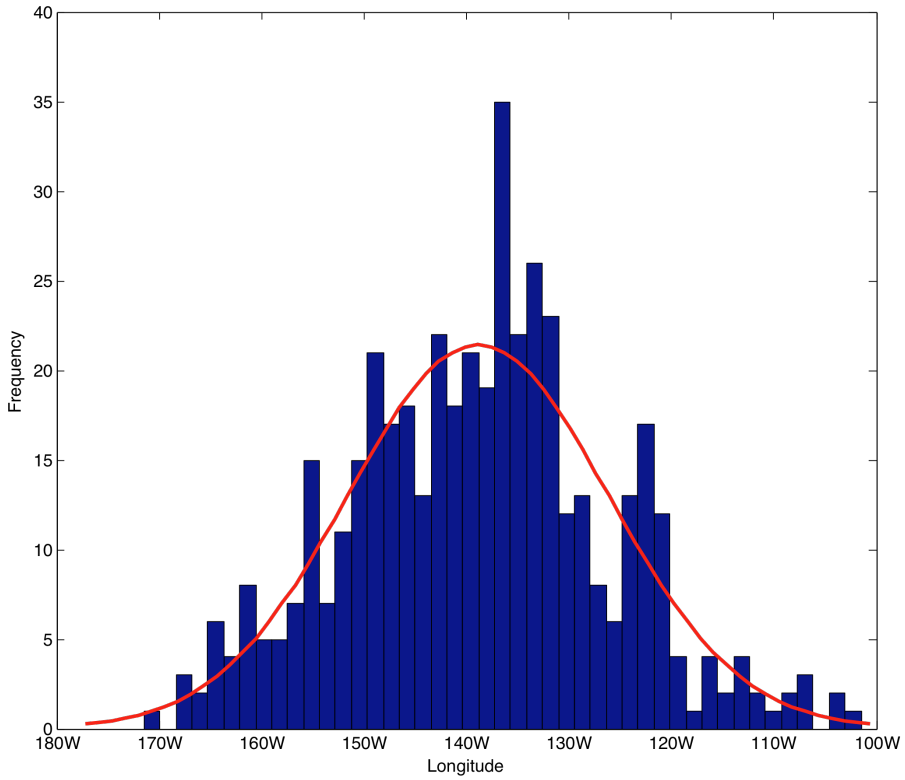

Figure 14. Histogram of CHI longitude for El Niño events. A Gaussian curve with the same mean and standard deviation as the CHI longitude is shown in red. A single peak in the distribution demonstrates a unique mean location of El Niño. See text for more discussion.

direction of propagation between El Niño and La Niña events. Figure 14 shows the histogram of CHI longitude of warm events.

The CHI longitude is distributed between 170°W in central Pacific to 100°W in the eastern Pacific. The distribution has a mean of 139°W and a standard deviation of 12.8°. The distribution seems to have a single peak and resembles a normal distribution when overlaid by a Gaussian of the same mean and standard deviation as the data. Figure 15 shows the histogram of CHI longitude for cold events. The CHI longitude

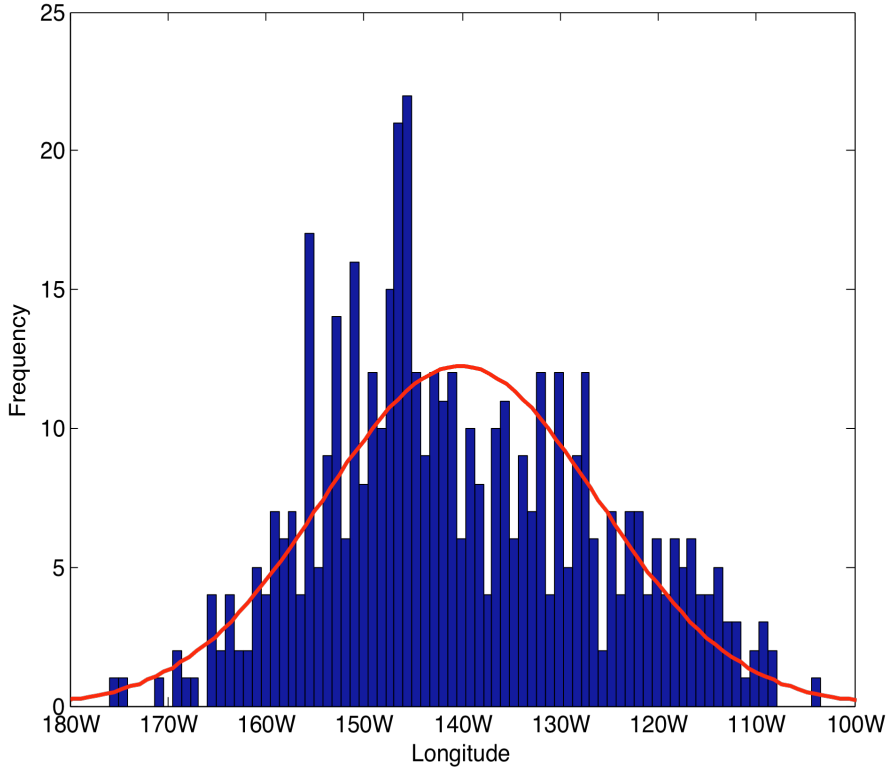

Figure 15. Histogram of CHI longitude for cold events during 1871-2008. A Gaussian curve with the same mean and standard deviation as the CHI longitude is shown in red. The distribution shows a sharp peak around 147°W.

varies between the dateline and 100°W. The mean of the distribution is at 140.1°W near to the mean location of CHI longitude for warm events. The standard deviation of the distribution is 14°, broader than CHI longitude for warm events (12.8°).

Compare CHI to Niño 3.4

We begin our analysis of CHI by comparing CHI to the Niño 3.4 index. Figure 16 shows the CHI amplitudes for El Niño and La Niña events compared to the Niño 3.4 index. For El Niño events the CHI amplitude correlates well (r=0.9) with Niño 3.4 index. When El Niño is weak the CHI measure tends to be stronger than suggested by the Niño

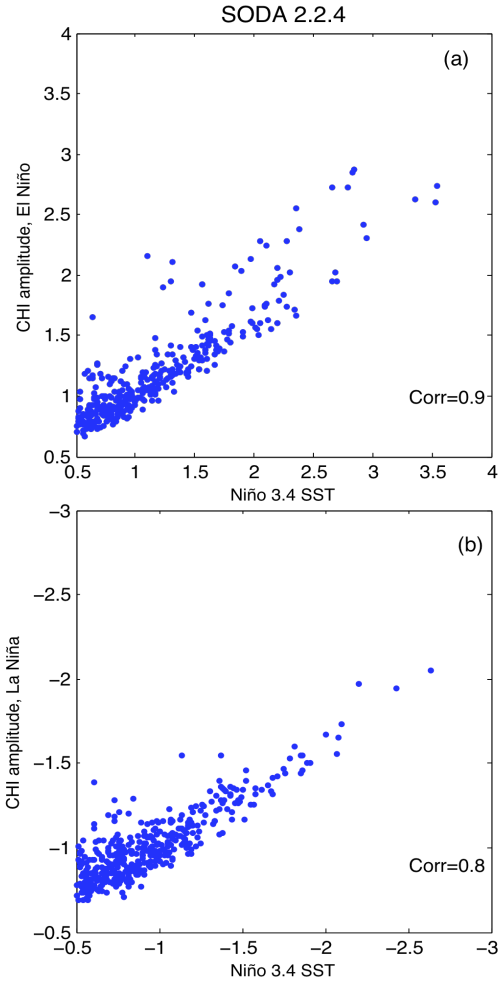

Figure 16. (a) CHI amplitude from SODA 2.2.4 (y-axis) plotted as a function of Niño 3.4 SST anomaly from SODA 2.2.4 (x-axis) for El Niño events. (b) CHI amplitude from SODA 2.2.4 (y-axis) plotted as a function of Niño 3.4 SST anomaly from SODA 2.2.4 for La Niña events. The respective correlation coefficients are mentioned in the figures.

3.4 index. This is because weak El Niño events tend to be small and so the warm anomaly is not entirely captured by Niño 3.4 index. Strong El Niño events tend to be stronger using the Niño 3.4 index compared with CHI because Niño 3.4 is smaller in area than actual El Niños, giving the possibility that its average is larger than for CHI.

Figure 16b shows the correlation between CHI amplitude and the Niño 3.4 index for La Niña events. The CHI amplitude and Niño 3.4 index for La Niña events are also highly correlated (0.8). Although the CHI metric is used as an alternate to Niño 3.4 index, the high correlation with the index show sufficient agreement of El Niño and La Niña strength between the two indices.

Relation between the metrics

The comparison of CHI metrics highlights issues such as whether there is location specific dependence of strength of ENSO. Figure 17 shows CHI amplitude as a function of CHI longitude (upper panel) and CHI amplitude as a function of CHI area (lower panel) for warm events. Figure 18 shows a similar plot but for cold events. In general strong warm events tend to occur in the eastern Pacific and are larger in size. Strong cold events, although bigger in size, seem to occur anywhere between the dateline to 100°W in the eastern Pacific. The warmest CHI longitude is at ~120°W with an anomaly of ~2.9°C, and the coolest CHI longitude is at ~ 140°W with an anomaly of -2.1°C. The correlation between CHI amplitude and CHI area is stronger than that between CHI amplitude and CHI longitude, implying strong El Niño or La Niña covers a larger area. The correlation between CHI amplitude and CHI area is 0.6 in case of warm events and is -0.6 in case of cold events. Although the correlation between the CHI amplitude and CHI longitude is poor (0.4) for warm events but is uncorrelated for cold events.

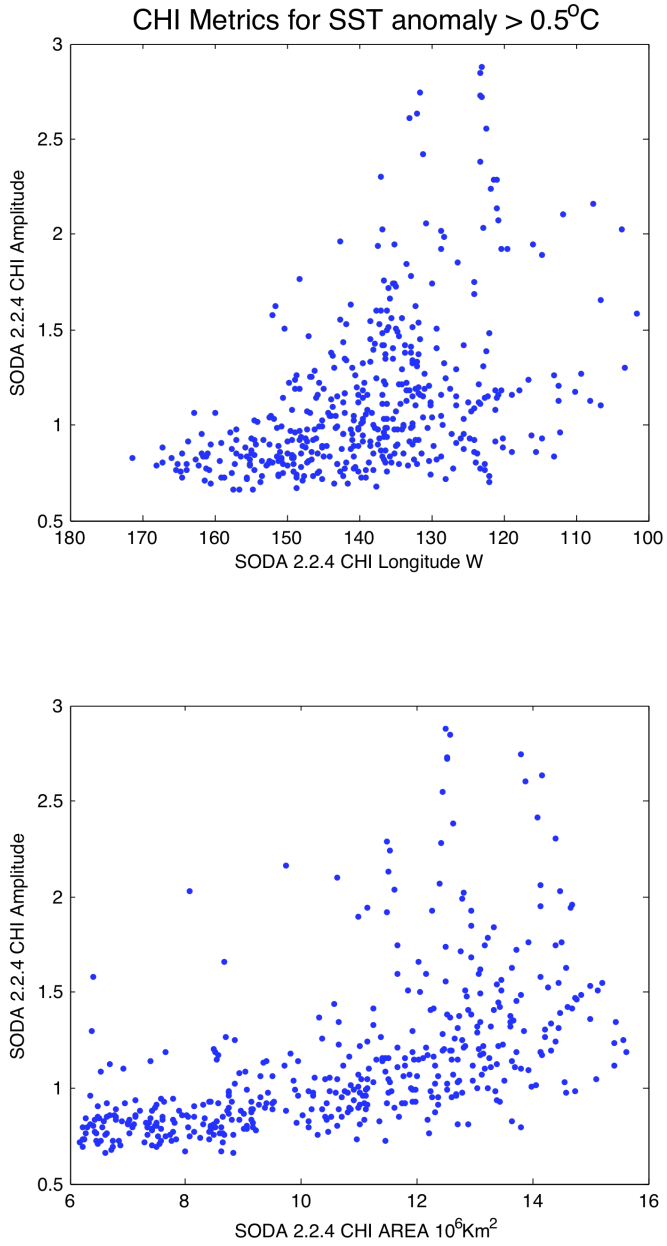

Figure 17. (Upper panel) CHI amplitude for warm events plotted as a function of CHI longitude for warm events. (Lower panel) CHI amplitude plotted as a function of CHI area for warm events.

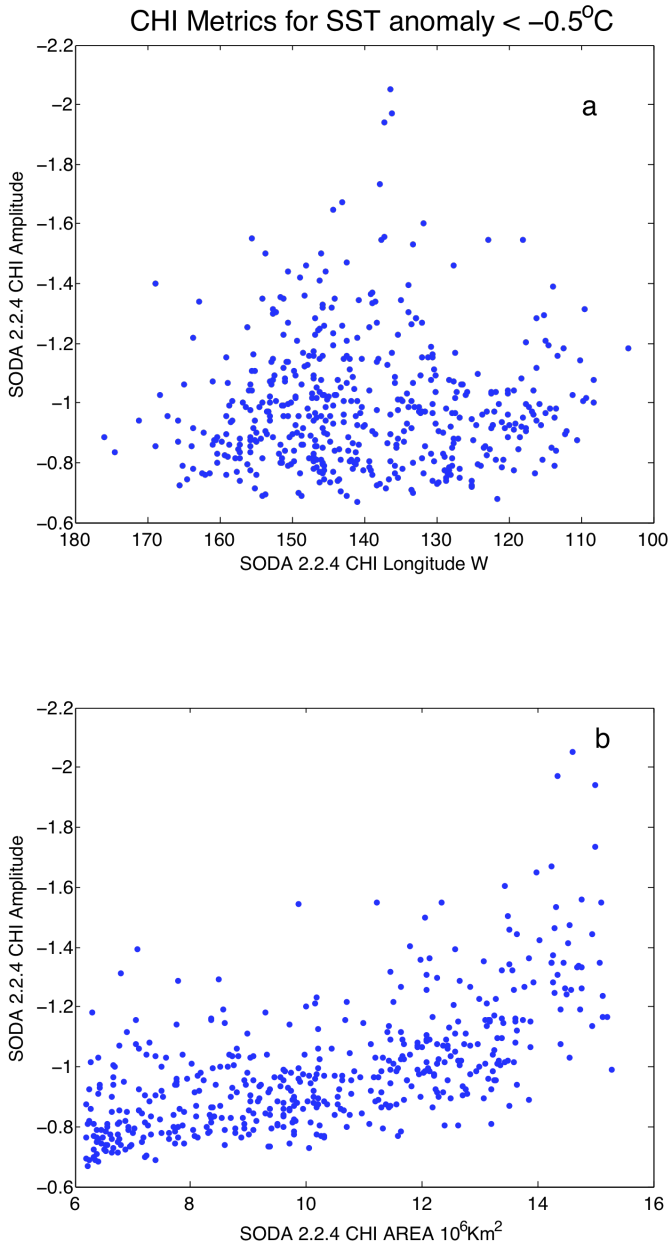

Figure 18. As in Figure 17 but for cold events.

Table 1. List of El Niño and La Niña years based on CHI amplitude (described in the text). To qualify as an El Niño or La Niña there must be 5 consecutive months for which the CHI amplitude exceeds 0.5° C or is below -0.5° C respectively.

	DJF	JFM	FMA	MAM	AMJ	MJJ	JJA	JAS	ASO	SON	OND	NDJ
1871												
1872												
1873												
1874												
1875												
1876		-0.9	-0.9	-0.9	-0.9	-0.8				0.8	0.9	1.1
1877	1.2	1.3	1.3	1.4	1.5	1.5	1.6	1.6	1.8	2.0	2.3	2.6
1878	2.7	2.6	2.4	2.1	1.5	1.2	0.9					-1.0
1879	-1.1	-1.2	-1.0	-0.8		-0.8	-0.9	-0.9	-0.8	-0.8	-0.9	-1.0
1880	-0.9	-0.9										
1881	0.8	0.9	0.9	0.8	0.7							
1882												
1883												
1884												
1885												
1886			-0.8	-0.9	-1.1	-1.2	-1.1	-0.9	-0.9	-1.0	-1.2	-1.3
1887	-1.4	-1.4	-1.4	-1.3	-1.4	-1.2	-0.9				0.8	0.7
1888	0.7	0.8	0.9	0.9	0.9	0.9	1.0	1.1	1.3	1.6	1.8	2.0
1889	2.0	1.9	1.8	1.5	1.2	0.8		-1.2	-1.1	-1.1	-1.3	-1.5
1890	-1.6	-1.3	-1.0	-0.9	-0.7							
1891		0.8	1.0	1.2	1.2	1.3	1.2	1.1	0.8	0.8	0.8	
1892						-1.1	-1.2	-1.2	-1.1	-1.2	-1.3	-1.3
1893	-1.2	-1.1	-1.0	-1.0	-0.9	-0.8	-0.8	-0.9	-1.0	-1.0	-1.0	-0.9
1894	-0.9	-0.9	-0.9	-0.8	-0.8							
1895								0.7	0.8	0.8	0.8	0.8
1896	0.7				0.7	0.8	0.8	0.9	1.0	1.2	1.4	1.5
1897	1.6	1.6	1.3	1.0	0.8						-0.9	-1.0
1898	-1.1	-1.1	-1.1	-1.0	-0.8					-0.8	-0.8	-0.8
1899	-0.8	-0.9	-0.9						0.7	0.8	1.0	1.2
1900	1.3	1.5	1.5	1.4	1.2	0.9						
1901												
1902					0.9	1.0	1.2	1.3	1.4	1.4	1.6	1.7
1903	1.6	1.4	1.3				-1.1	-1.0	-1.0	-1.1	-1.2	-1.2
1904	-1.3	-1.2	-1.1	-0.9	-0.8						0.7	0.9
1905	1.0	1.2	1.2	1.2	1.1	1.0	1.0	1.0	1.0	1.2	1.3	1.4
1906	1.2	1.0	0.9	0.9					-0.8	-0.9	-0.9	-1.0
1907	-1.0	-0.9	-0.8	-0.7								
1908											-0.8	-1.0
1909	-1.1	-1.0	-0.9	-0.8			-0.7	-0.8	-1.0	-1.2	-1.4	-1.4
1910	-1.5	-1.4	-1.4	-1.2	-1.1	-0.9	-0.9	-0.9	-1.0	-1.1	-1.1	-1.1
1911	-1.0	-1.0	-1.0	-0.9	-0.9	-0.7			0.9	1.2	1.5	1.7
1912	1.8	1.8	1.6	1.4	1.1	0.8						
1913										0.8	0.9	1.1
1914	1.2	1.1	1.0	0.8				0.8	0.9	1.0	1.0	0.9
1915	0.9	0.9	1.0	1.0	1.1	1.1	1.0	0.7				
1916								-1.0	-1.2	-1.6	-1.9	-2.1
1917	-2.0	-1.7	-1.6	-1.4	-1.2	-0.9	-0.8	-0.8	-0.9	-1.0	-1.0	-1.0
1918	-0.9	-0.9	-0.9	-0.9			1.0	1.2	1.3	1.3	1.4	1.5
1919	1.6	1.7	1.7	1.6	1.3	1.0	0.8			0.7	0.9	0.8
1920	0.8	0.9	1.0	0.9	0.8							
1921			-0.9	-0.9	-1.0	-0.9	-0.8	-0.8				
1922									-0.9	-1.0	-1.0	-1.1
1923	-1.2	-1.1	-0.9				1.0	0.9	0.7	0.7	0.8	0.9
1924	0.8				-0.9	-0.9	-1.0	-1.0	-1.0	-1.1	-1.1	-1.2
1925	-1.2	-1.0	-0.9	-0.9				0.8	0.9	1.0	1.0	1.0
1926	1.0	1.1	1.1	1.1	1.0	0.9	0.8					
1927												
1928												
1929									0.8	0.8	0.8	0.8
1930	0.8	0.8	0.8				0.8	0.9	1.1	1.2	1.4	1.5
1931	1.4	1.3	1.2	1.0	0.9							
1932												
1933							-0.8	-0.9	-1.0	-1.1	-1.2	-1.2
1934	-1.1	-1.1	-1.0	-0.8								
1935												
1936												
1937												
1938		-1.1	-1.3	-1.3	-1.2	-1.0	-1.0	-1.0	-1.0	-0.9	-0.9	-0.9
1939	-0.9	-0.8	-0.8									

	DJF	JFM	FMA	MAM	AMJ	MJJ	JJA	JAS	ASO	SON	OND	NDJ
1940	0.8	1.0	1.1	1.1	0.9	0.8	0.8	0.8	0.8	0.9	0.9	1.0
1941	1.1	1.3	1.5	1.5	1.4	1.1	0.9	0.8	0.9	1.0	1.1	1.2
1942	1.1	1.0	0.9			-1.0	-1.0	-1.0	-1.0	-1.0	-1.0	-1.0
1943	-1.0	-1.0	-1.0	-0.9								
1944												
1945	-0.8	-0.9	-1.0	-1.0	-0.8			1.1	1.2	1.2	1.1	0.9
1946												
1947												
1948			0.8	1.0	1.1	1.1	1.0					
1949							-0.8	-0.8	-0.9	-1.0	-1.0	-1.0
1950	-1.0	-0.9	-1.0	-1.0	-1.1	-1.1	-1.1	-1.1	-1.1	-0.9	-0.9	-0.9
1951	-0.9	-0.8				1.1	1.1	1.2	1.2	1.3	1.3	1.2
1952	1.0	0.8										
1953		0.8	0.9	0.9	0.9	0.8	0.8	0.8	0.8	0.9	0.9	0.8
1954					-1.2	-1.1	-1.0	-0.9	-0.8	-0.8	-0.8	-0.8
1955			-0.7	-0.8	-0.9	-0.9	-0.8	-0.8	-1.0	-1.3	-1.5	-1.6
1956	-1.4	-1.2	-1.0	-0.9	-0.9	-0.8		-0.8	-0.8	-0.9	-0.8	-0.8
1957					1.2	1.3	1.2	1.2	1.1	1.2	1.3	1.5
1958	1.6	1.4	1.2	1.0	0.9							
1959												
1960												
1961									-0.8	-0.8	-0.8	-0.8
1962	-0.8	-0.8	-0.8	-0.8	-0.7							
1963						0.9	0.9	0.9	0.9	1.0	1.0	0.9
1964	0.8				-1.2	-1.2	-1.0	-0.9	-0.9	-1.0	-1.0	-1.0
1965	-0.8	-0.7			1.3	1.3	1.2	1.3	1.4	1.5	1.5	1.4
1966	1.2	1.1	0.9	0.7								
1967								-1.0	-1.0	-1.0	-1.0	-1.0
1968	-0.9	-0.9	-0.9	-0.9								0.7
1969	0.9	1.0	1.0	1.0	1.0	1.0	0.8	0.8	0.9	1.0	1.0	0.9
1970	0.8	0.8					-1.3	-1.0	-0.9	-0.9	-1.0	-1.0
1971	-1.0	-1.0	-1.0	-0.9	-0.8	-0.7	-0.7	-0.8	-0.8	-0.8	-0.8	-0.8
1972				0.9	1.1	1.2	1.5	1.7	1.9	1.9	2.0	2.0
1973	1.7	1.4	1.0				-1.0	-1.0	-1.1	-1.1	-1.2	-1.3
1974	-1.3	-1.2	-1.1	-1.0	-0.8				-0.8	-0.8	-0.9	-0.8
1975	-0.8			-0.7	-0.8	-0.9	-1.0	-1.0	-1.2	-1.3	-1.2	-1.2
1976	-1.1	-0.9	-0.7			1.1	1.2	1.2	1.1	1.1	1.0	1.0
1977	0.9	0.9										
1978												
1979												
1980												
1981												
1982						0.7	0.9	1.1	1.4	1.8	2.0	2.2
1983	2.3	2.1	1.9	2.0	2.1	2.2	2.0	1.6		-1.1	-1.2	-1.1
1984	-1.0	-0.9	-0.9	-0.9	-0.9	-1.0	-1.0	-0.9	-0.8	-0.9	-1.0	-1.0
1985	-1.1	-1.1	-1.0	-1.0	-1.0	-1.0	-0.9	-1.0	-1.0	-1.0		
1986									0.8	0.9	1.0	1.0
1987	1.0	1.0	1.0	1.1	1.2	1.2	1.2	1.2	1.2	1.1	1.0	0.8
1988	0.7			-1.4	-1.6	-1.6	-1.5	-1.3	-1.3	-1.5	-1.7	-1.7
1989	-1.5	-1.3	-1.1	-0.9	-0.8	-0.8	-0.8	-0.8	-0.7	-0.7		
1990												
1991						0.8	0.8	0.8	0.8	0.9	1.1	1.2
1992	1.4	1.3	1.3	1.3	1.1	0.8						
1993												
1994										1.0	1.1	1.0
1995	0.9	0.9						-0.8	-0.9	-1.0	-1.0	-0.9
1996	-0.9	-0.8	-0.8	-0.9	-1.0	-0.9						
1997					1.0	1.4	1.9	2.3	2.6	2.7	2.9	2.9
1998	2.7	2.4	2.1	1.9	1.7		-1.1	-1.2	-1.2	-1.3	-1.4	-1.4
1999	-1.3	-1.3	-1.1	-1.0	-0.9	-0.9	-1.0	-1.0	-1.1	-1.2	-1.3	-1.4
2000	-1.4	-1.3	-1.1	-1.1	-1.0	-0.8	-0.7	-0.7	-0.7	-0.7	-0.8	-0.8
2001	-0.8	-0.8										
2002				0.7	0.7	0.7	0.8	0.9	0.9	1.0	1.2	1.2
2003	1.2	1.1	0.9							0.7	0.7	0.8
2004	0.7	0.7							0.8	0.8	0.8	0.8
2005	0.9	0.8	0.7									
2006								0.8	0.9	1.0	1.1	1.1
2007	0.9	0.7					-1.0	-1.0	-1.2	-1.3	-1.4	-1.3
2008	-1.3	-1.2	-1.1	-1.0	-0.9	-0.8						

Defining El Niño and La Niña

Table 1 lists CHI amplitudes for El Niño and La Niña events from 1871 through 2008. For this table we require that the CHI amplitude be above 0.5°C for 5 consecutive months to qualify as an El Niño event (in red). Similarly, to qualify as a La Niña event (in blue) the CHI amplitude had to be below -0.5°C for 5 consecutive months. There is a general tendency for El Niño and La Niña events to peak during boreal winter (December, January, February, March) of year 0 [*Rasmusson and Carpenter*, 1982; *Mitchell and Wallace*, 1996). Figure 19 shows the month of maximum CHI amplitude from Table 1 plotted for each El Niño year. Year 0 is defined as the year of occurrence of an El Niño or La Niña event and Year 1 is the year following Year 0 whereas Year -1 is the one preceding. The plot shows that the month of largest anomaly can vary from as early as May of Year 0 (1915) to as late as October of Year 1 (1986).

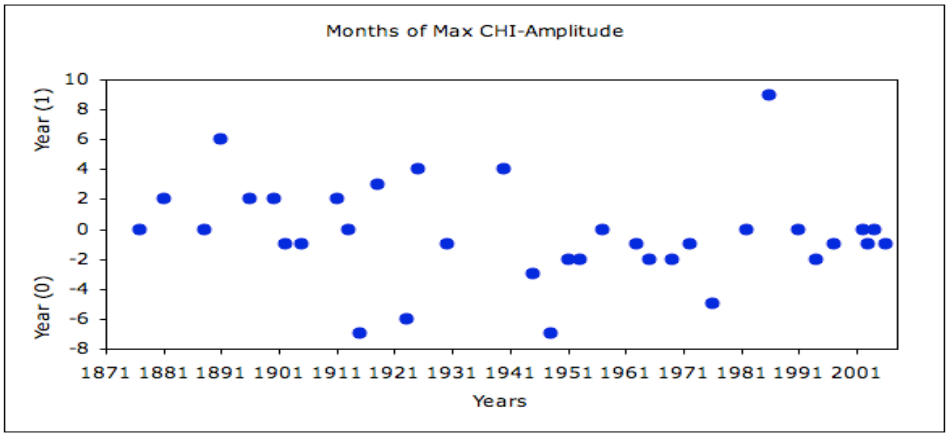

Figure 19. The warmest month in CHI amplitude for El Niño during 1871-2008. December of Year (0) is represented as 0 on the y-axis and is counted forward for Year (1) and backward for Year (0).

Table 2. Summary of El Niño and La Niña years in Table1. The mean of duration of either event is shown along with the mean and standard deviation of the strength of the events.

	El Niño Years	Duration (months)	Strength	La Niña Years	Duration (months)	Strength
1	1876/1877/1878	22	2.7	1876	5	-0.9
2	1881	5	0.9	1878/1879/1880	14	-1.2
3	1888/1889	20	2.0	1886/1887	17	-1.4
4	1891	10	1.3	1889/1890	10	-1.6
5	1895/1896/1897	19	1.6	1892/1893/1894	24	-1.3
6	1899/1900	10	1.5	1897/1898/1899	13	-1.1
7	1902/1903	11	1.7	1903/1904	11	-1.3
8	1904/1905/1906	18	1.4	1906/1907	8	-1.0
9	1911/1912	10	1.8	1908/1909/1910/1911	30	-1.5
10	1913/1914/1915	20	1.2	1916/1917/1918	21	-2.1
11	1918/1919/1920	21	1.7	1921	6	-1.0
12	1923/1924	7	1.0	1922/1923	7	-1.2
13	1925/1926	12	1.1	1924/1925	12	-1.2
14	1929/1930/1931	18	1.5	1933/1934	10	-1.2
15	1940/1941/1942	27	1.5	1938/1939	14	-1.3
16	1945	5	1.2	1942/1943	11	-1.0
17	1948	5	1.1	1945	5	-1.0
18	1951/1952	9	1.3	1949/1950/1951	20	-1.1
19	1953	11	0.9	1954/1955/1956	29	-1.6
20	1957/1958	13	1.6	1961/1962	9	-0.8
21	1963/1964	8	1.0	1964/1965	10	-1.2
22	1965/1966	12	1.5	1967/1968	9	-1.0
23	1968/1969/1970	15	1.0	1970/1971	18	-1.3
24	1972/1973	12	2.0	1973/1974/1975	28	-1.3
25	1976/1977	9	1.2	1983/1984/1985	25	-1.2
26	1982/1983	15	2.3	1988/1989	19	-1.7
27	1986/1987/1988	17	1.2	1995/1996	11	-1.0
28	1991/1992	13	1.4	1998/1999/2000	32	-1.4
29	1994/1995	5	1.1	2007/2008	12	-1.4
30	1997/1998	13	2.9			
31	2002/2003	12	1.2			
32	2003/2004	5	0.8			
33	2004/2005	7	0.9			
34	2006/2007	7	1.1			
					15.2	-1.3
	Mean	12.4	1.4			0.27
	St Dev		0.49			

Table 2 summarizes Table 1 and highlights individual El Niño and La Niña events. Using the above criteria for El Niño and La Niña events results in 34 El Niño events and 29 La Niña events during the period of our study (1871-2008). Dividing the time period by the number of events results in a mean interval of 4.2 years between El Niño events and 4.8 years between La Niña events. The list of El Niño years and La

Niña years also contains the duration of each event and the peak anomaly of each event. The mean duration of El Niño events is a little over a year (12.4 months) whereas for La Niña events the duration is 15.2 months, implying a longer persistence of cold events. The mean strength of El Niño events is 1.4°C and for La Niña events is -1.3°C. However El Niño events have a wider distribution of strength with a standard deviation of 0.49°C as compared to that of La Niña events with a standard deviation of 0.27°C. Using CHI, the El Niño of 1997/98 was the strongest event with a peak anomaly of 2.9°C followed by the El Niño of 1877/78 with a peak anomaly of 2.7°C. This is in contrast to the Niño 3.4 SST anomaly (Figure 6c), where the El Niño of 1877/78 was stronger than the El Niño of 1997/98 by 0.8°C. Other strong El Niños based on CHI includes the El Niño of 1982/83 (2.3°C), the El Niño of 1972/73 (2.0°C), and the El Nino of 1888/89 (2.0°C). The El Niños of 1911/12, 1902/93 and 1918/19 have an anomaly of 1.7°C or less. The strongest La Niña event was the 1917/1918 event with an anomaly of -2.1°C followed by the 1988/89 La Niña (-1.7°C), the 1889/1890 La Niña (-1.6°C), and the 1954/55 La Niña (-1.6°C).

Altering the threshold criteria for CHI

To test the robustness of the mean location of CHI longitude for warm and cold events we construct new experimental CHI metrics by altering the threshold criteria. The first experimental CHI constructed is using SST anomalies greater than 0.5°C covering a minimum area of half the size of the Niño 3.4 box. The second experimental CHI is constructed using SST anomalies having a minimum of 0.25°C and covering at least half the size of Niño 3.4 box. The third experimental CHI is constructed using SST

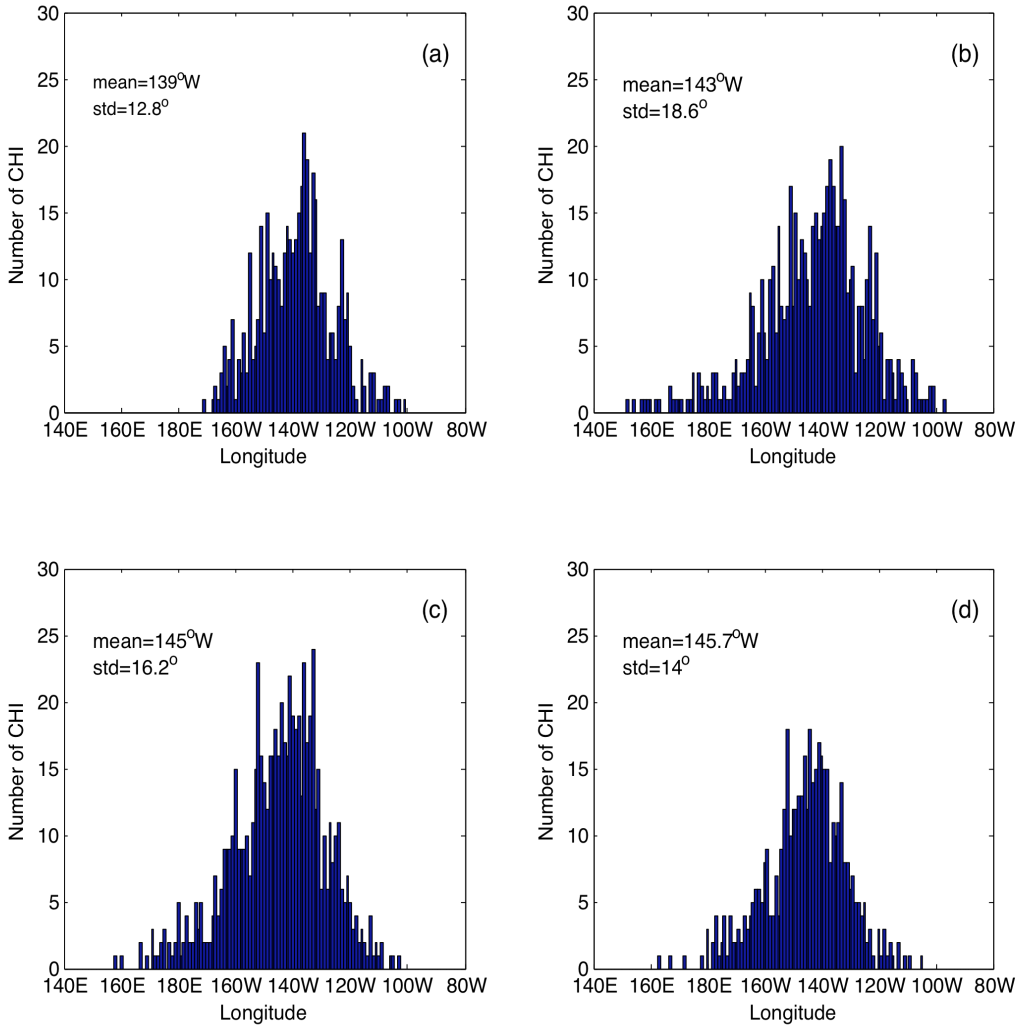

Figure 20. Histograms of CHI longitude for warm events using different thresholds: (a) for SST anomaly greater than 0.5°C and area at least the size of NINO 3.4 box, (b) for SST anomaly greater than 0.5°C and area at least half the size of NINO 3.4 box, (c) for SST anomaly greater than 0.25°C and area at least the size of NINO 3.4, (d) for SST anomaly greater than 0.25°C and area at least half the size of NINO 3.4. The mean and standard deviation of CHI longitude for case are listed in each plot. The mean location of El Niño does not change much due to altered definitions of CHI.

anomalies greater than 0.25°C covering an area at least the size of Niño 3.4 box. Figure 20 shows the histogram and means of CHI longitude for all three experimental CHI along with the original criterion for CHI metric (Figure 20a). Figure 20b shows the histogram of CHI longitude when the minimum affected area was reduced to half the size of the Niño 3.4 box. The mean location of CHI longitude is 4° west of the original location of mean CHI longitude (Figure 20a). The distribution also covers a broader region with a standard deviation of 18.6°. Figure 20c shows the distribution of CHI longitude for SST anomalies reduced to a cutoff at 0.25°C. The mean location of CHI longitude moves 6° west of the original mean position (139°W) along with a broader standard deviation of 16.2°. Figure 20d shows the distribution of CHI longitude when the cutoff for SST anomalies was reduced to 0.25°C and the area affected were reduced to half the size of the Niño 3.4 box. The mean location of CHI longitude shifts 7° westward from the original location of mean CHI longitude with a slightly broader standard deviation at 14°.

Altering the threshold criteria increasingly widens the histogram of CHI longitude as more data points from west of dateline satisfy the reduced criteria. Hence to ensure that none of the anomalous warming in this region in the western/central equatorial Pacific is happening due to a cold event in the eastern Pacific, filters are applied in the construction of the experimental metric in reduced threshold criteria. This step retained only the data that qualify for a warm event in the eastern-central Pacific. The mean location of CHI longitude did not shift by more than 7° among the different altered threshold criteria making a small change in the mean location of CHI.

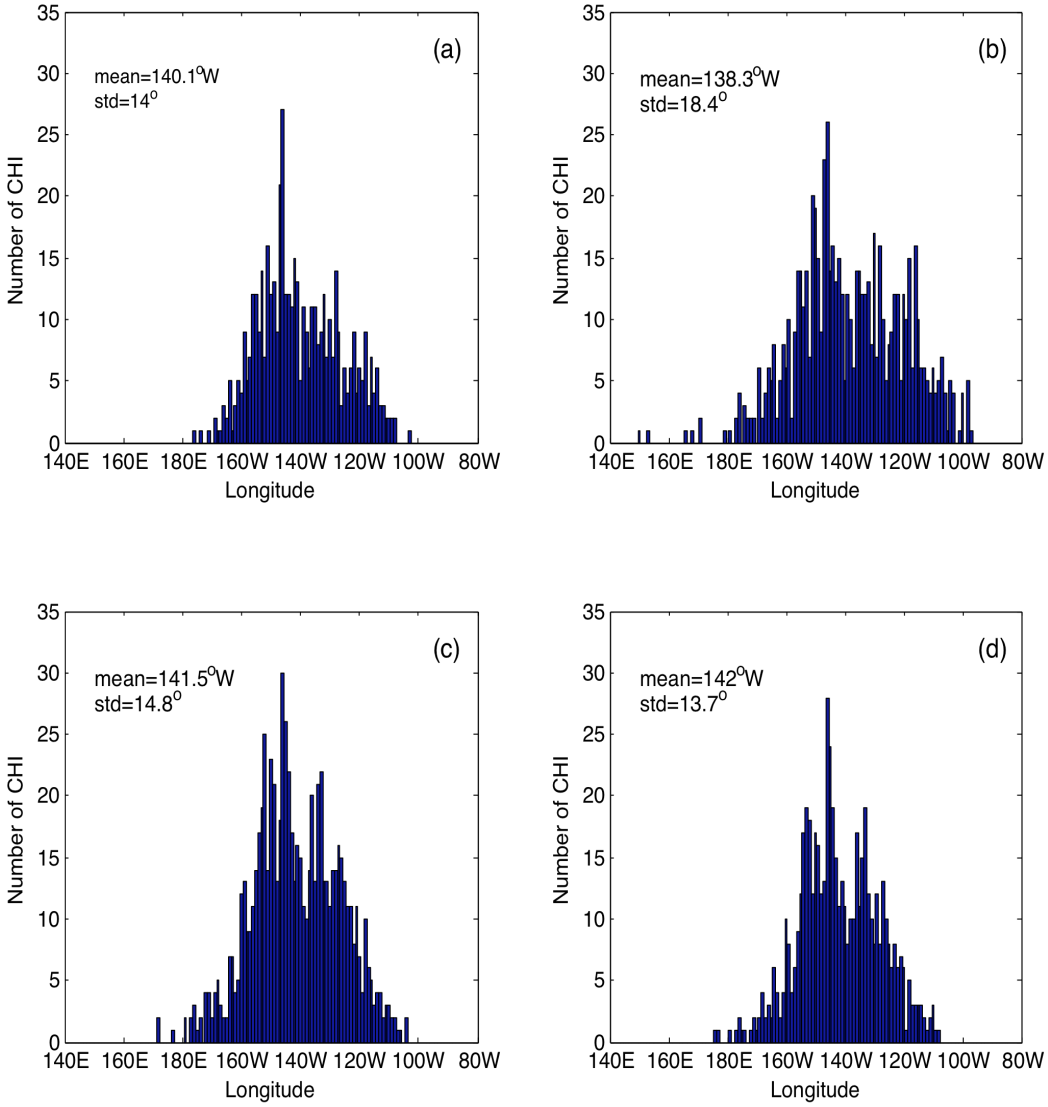

Figure 21. Histograms of CHI longitude for cold events using different thresholds: (a) for SST anomaly less than -0.5°C and area at least the size of NINO 3.4 box, (b) for SST anomaly less than -0.5°C and area at least half the size of NINO 3.4 box, (c) for SST anomaly less than -0.25°C and area at least the size of NINO 3.4, (d) for SST anomaly less than -0.25°C and area at least half the size of NINO 3.4. The mean and standard deviation of CHI longitude for case are mentioned inside each figure. The mean location of La Niña does not change much due to altered definitions of CHI metric.

The threshold criteria for cold events are also altered to check the robustness in location of CHI longitude. Figure 21 shows the histograms of CHI longitude using different thresholds and comparing them to the mean location of CHI longitude constructed originally (Figure 21a). Figure 21b shows the distribution of CHI longitude for cold events that cover at least an area half the area of the Niño 3.4 region. The mean location of CHI longitude shifts 2° east of the original mean location of CHI longitude for cold events (140.1°W). The distribution spreads over larger region than the original CHI longitude distribution (Figure 21a) with a standard deviation of 18.4°. Figure 21c shows the histogram of CHI longitude for reduced SST anomaly criteria at -0.25°C. The mean location of CHI shifts by 1° to the west of the original mean location of CHI longitude to 141.5°W. The standard deviation is almost the same at 14.8°. Figure 21d shows the distribution of CHI longitude for reduced threshold of both SST anomaly to -0.25°C and the area reduced to half the area of Niño 3.4 box. The mean position of CHI longitude shifts 2° to the west to 142°W. The standard deviation is not altered much at 13.7°. As with warm events, filters are applied to ensure that all the qualifying data points are related only to cold events in the eastern Pacific.

Latitudinal location of CHI

The latitudinal location of CHI (CHI latitude) is constructed to analyze the variation of CHI meridionally around equator. Figure 22 shows the histogram of CHI latitude between 2°S and 2°N. The distribution of CHI latitude is narrow compared to that of CHI longitude for warm events with a standard deviation of 0.4°, which is much

smaller than the standard deviation of CHI longitude of warm events (12.8°). The mean location of CHI latitude is near the equator at 0.14°S.

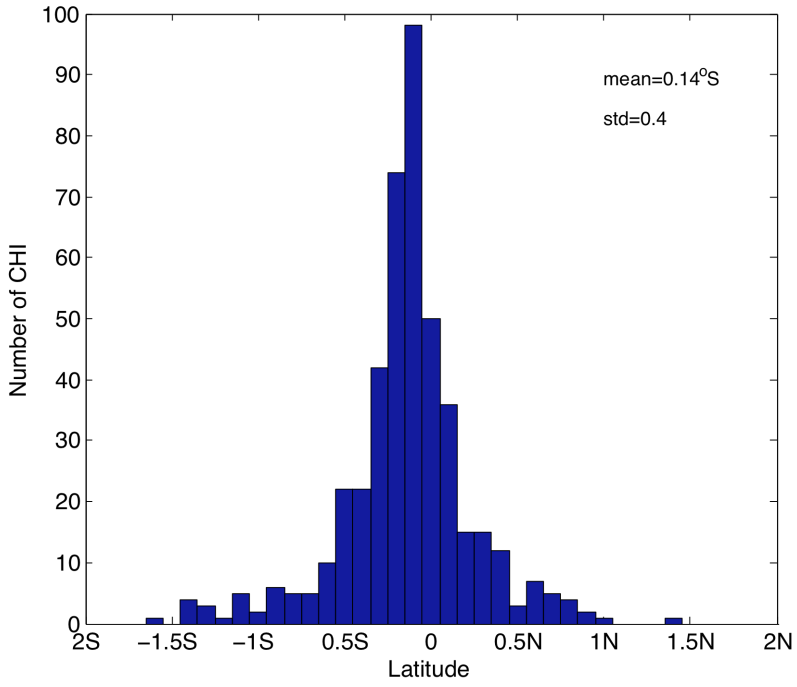

Figure 22. Histogram of CHI latitude for El Niño events. The mean and standard deviation of the distribution are shown in the plot.

Strength and location of westerly wind events

In order to analyze the relation between westerly wind stress and the strength of El Niño, a metric incorporating the first moment of zonal wind stress is constructed. The zonal wind anomaly is smoothed over 3 months and values larger than $0.02 N/m^2$ are filtered using a fetch that is at least half the length of the Niño 3.4 box. Using half the

Niño 3.4 region is required because the size of wind anomalies is smaller than for SST anomalies. This returned the average of the zonal wind anomaly representing the strength of the westerly wind stress anomaly and the location of the wind anomaly. Figure 23 shows the strength of warm anomaly plotted as a function of amplitude for the westerly wind anomaly (Figure 23a) and the location of warm anomaly as a function of the location of westerly wind anomaly (Figure 23b). The correlation between the locations (0.6) is better than that between their strengths (0.4). This indicates that the location of the westerly wind events could influence the location of El Niño but the strength of El Niño is less influenced by the strength of wind anomaly. It could be the subsurface that influences the strength of anomalous warming during El Niño.

CHI for subsurface

An analysis of the center of warming in the subsurface is performed to measure the subsurface anomalies and their location during El Niño. Since subsurface anomalies are larger than surface anomalies a two-dimensional CHI of the subsurface was constructed for anomalies greater than 1°C and which covers at least 0.01% of the Niño 3.4 area. The search region for the CHI is between 120°E to 70°W and between 0-400m of depth. The three metrics for measuring the subsurface warm anomaly during El Niño are the amplitude of the subsurface warming (CHI amplitude), the longitudinal location of the warming (CHI longitude), and the depth of the center of warming (CHI depth). Figure 24 shows the three metrics. Similar to the surface CHI, the bars in Figure 24a are the average warm anomaly (> 1°C) representing the strength of El Niño. The dots in Figure 24b are the longitudinal location of the subsurface CHI and the circles are

proportional to the CHI amplitude. Similarly the dots in Figure 24c represent the depth of CHI, and the circles are proportional to the CHI amplitude. The subsurface CHI amplitude has a mean of 1.8°C with a standard deviation of 0.5°C and a skewness of 1.14, which is close to that from CHI amplitude for surface (1.4).

Figure 25a shows the histogram of CHI longitude for the subsurface.The CHI longitude has a mean at 127.4°W, which is east of the mean location of surface CHI longitude (139°W) and has a smaller standard deviation of 11.6° than the surface CHI longitude (12.8°). Figure 25b shows the histogram for CHI depth, which has a larger spread than CHI longitude for subsurface as represented by its standard deviation (16.3 m).

The mean of depth of the subsurface CHI is 72 m although the maximum CHI depth is 120m. Figure 26a shows the subsurface CHI longitude as a function of surface CHI longitude. Although the subsurface CHI amplitude is well correlated to surface CHI amplitude (0.83), a correlation of only 0.6 exists between the two longitudes. Figure 26b shows the inter-metric correlation of CHI depth and CHI longitude for subsurface. The mean depth of 20°C isotherm is overlaid in red. This shows that the subsurface CHI are almost all located east of 170°E and have a depth that follows the 20°C isotherm longitude.

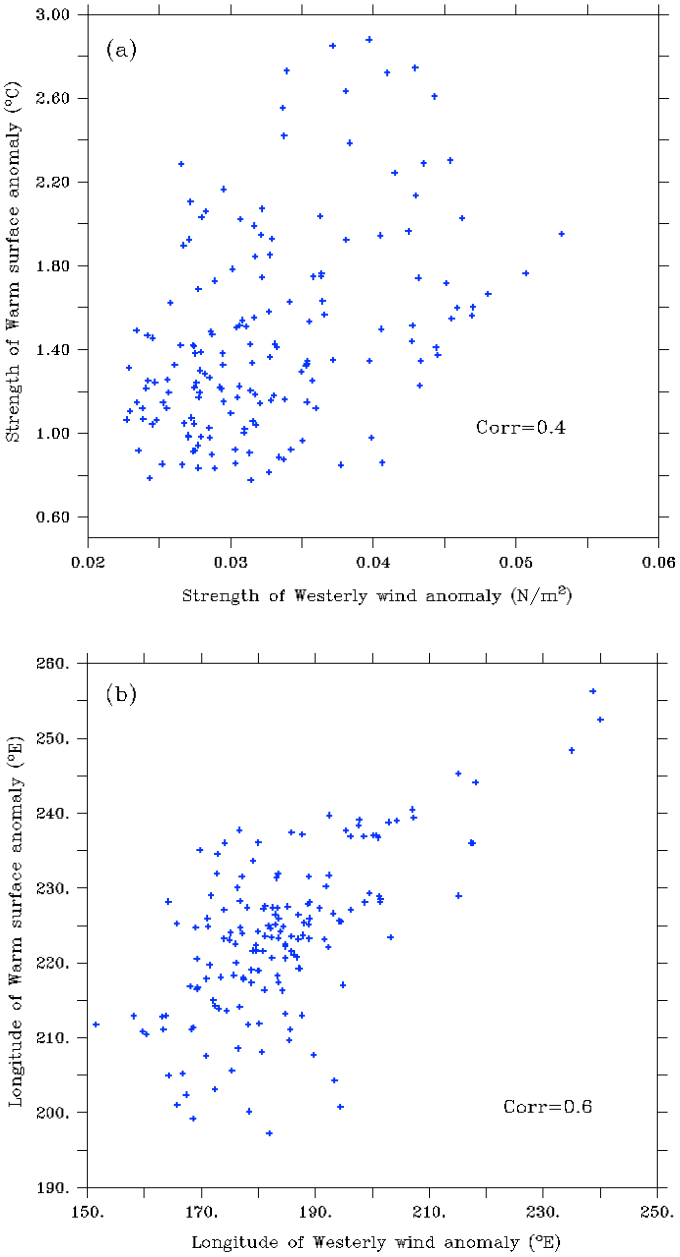

Figure 23. (a) Strength of warm SST anomaly plotted as a function of strength of zonal wind anomaly. The correlation between the two is shown in the figure. (b) Location of the warm SST anomaly plotted as a function of longitude of zonal wind anomaly.

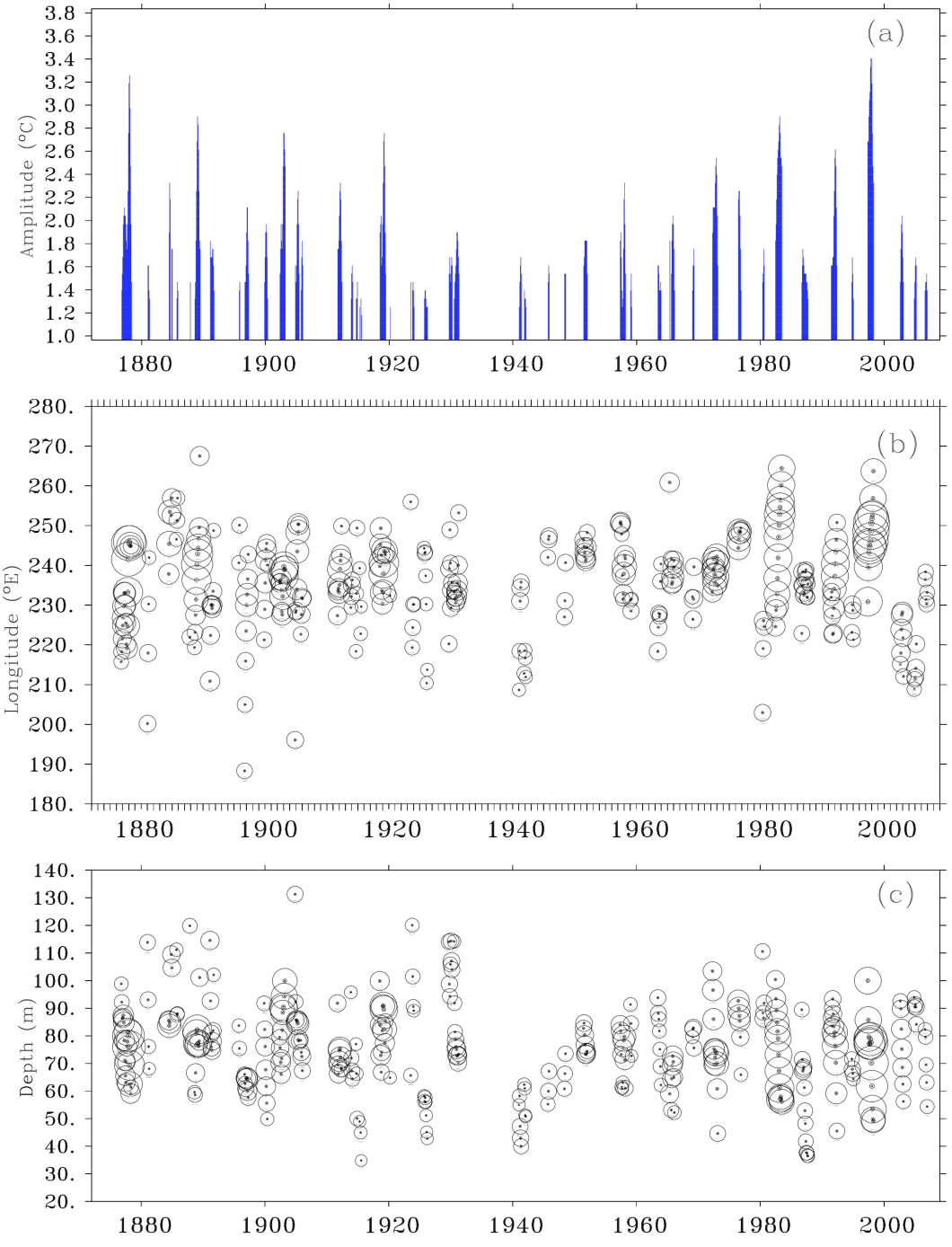

Figure 24. (a) The subsurface CHI amplitude (0-500m) for El Niño events in °C. (b) The subsurface CHI longitude from SODA 2.2.4 in degrees E longitude. (c) The subsurface CHI depth from SODA 2.2.4. In both (b) and (c) the size of the circle is proportional to the amplitude. Regression line is fitted in red for (b) and (c).

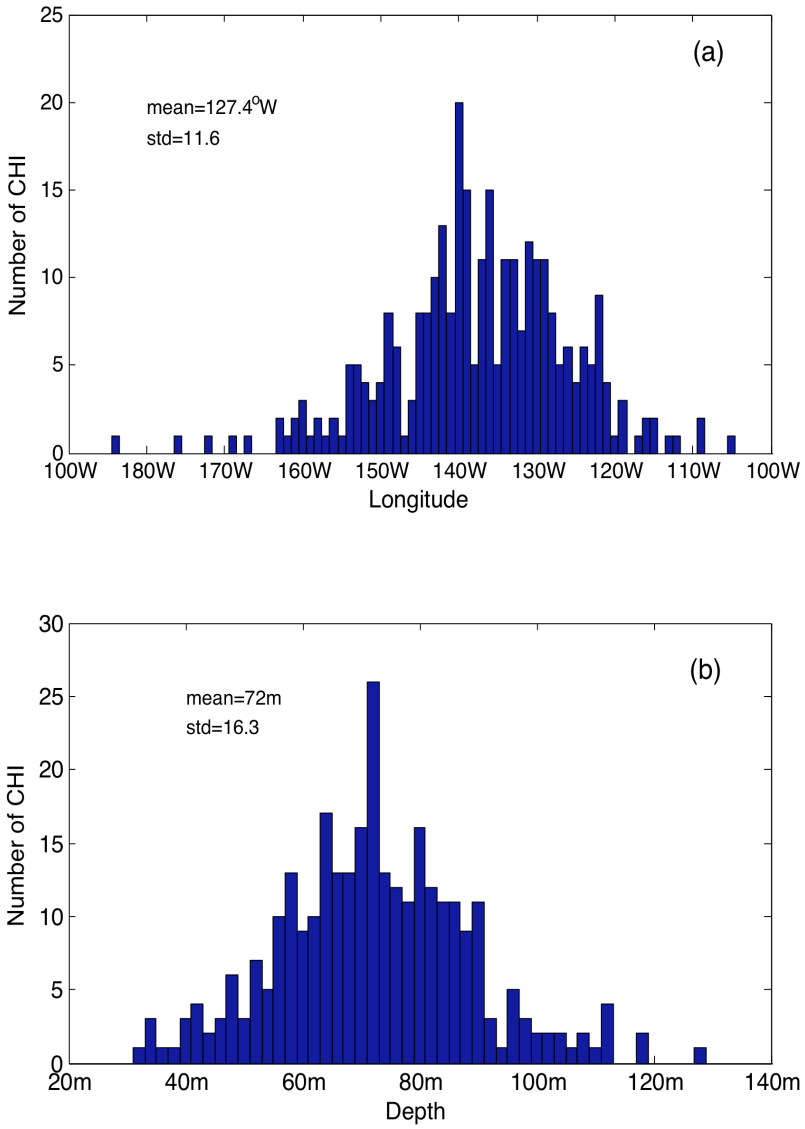

Figure 25. Histogram of subsurface CHI longitude and subsurface CHI depth for temperature anomaly greater than 1°C, for depth range of 0-400m. Mean and standard deviation of each distribution is shown in the figure.

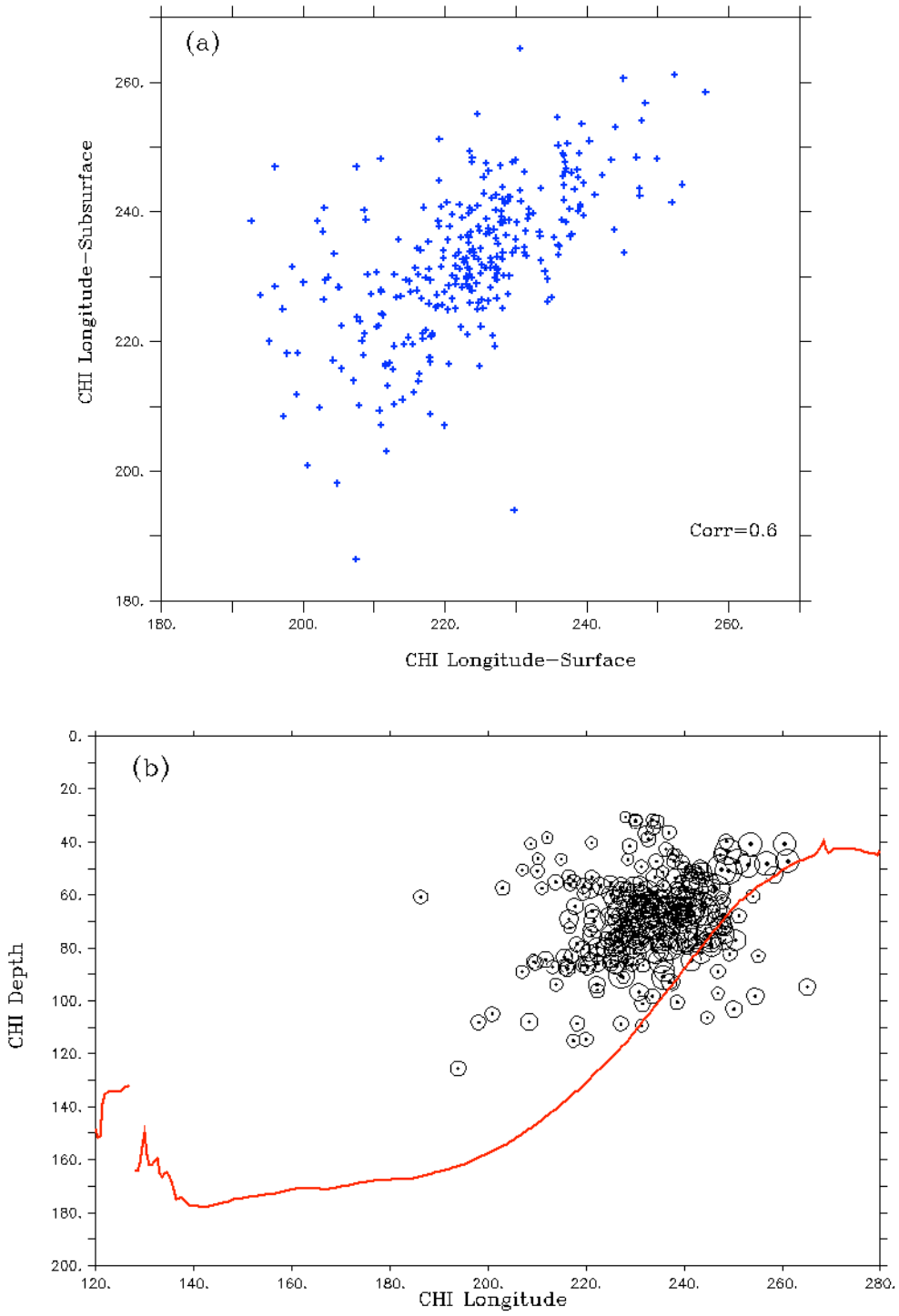

Figure 26. (a) Subsurface CHI longitude for temperature anomaly greater than 1°C plotted as a function of CHI longitude for SST anomaly greater than 0.5°C. The correlation between the two values is shown inside the plot. (b) CHI depth for subsurface temperature anomaly greater than 1°C plotted as a function of CHI longitude for the same subsurface anomaly and overlaid by the mean position of the 20°C isotherm.

CHI from reconstructed SSTs

CHI is further exploited to measure the strengths and locations of El Niño and La Niña from other long records, such as the reconstructed SST records from ERSST, HadISST, and Kaplan SST. Figure 27 shows the CHI amplitude for warm events from ERSST (Figure 27a), HadISST (Figure 27b), and Kaplan SST (Figure 27c). The variation in CHI-amplitude from ERSST and HadISST resemble closely the CHI amplitude from SODA 2.2.4 (Figure 11a). Both ERSST and HadISST show strong El Niño periods in the late nineteenth and the late twentieth century with weaker events in between, similar to that from SODA 2.2.4. However the CHI amplitude from Kaplan v2 shows a trend towards strengthening of El Niño from the late nineteenth century to the late twentieth century and is very dissimilar to the CHI amplitude from SODA 2.2.4 (Figure 11a). Figure 28 shows the CHI longitude for El Niño events from ERSST (Figure 28a), HadISST (Figure 28b), and Kaplan v2 (Figure 28c). The location of CHI longitudes is in degrees east and the size of circles is proportional to the CHI amplitude. The CHI longitude record for ERSST at the beginning of the record seems unrealistic as the onset and decay stages of the warm events occurs in a small longitudinal region in the eastern Pacific before 1920. Instead CHI longitude from HadISST shows reasonable distribution over the record and varies about the mean location of 130°W. The CHI longitude form Kaplan v2 moves more towards western Pacific than either in ERSST or in HadISST or in SODA 2.2.4. A comparison of CHI amplitude and CHI longitude for El Niño events between the reconstructed SSTs and SODA 2.2.4 shows how different the products are in terms of measuring El Niño. Figure 29 shows CHI longitudes for

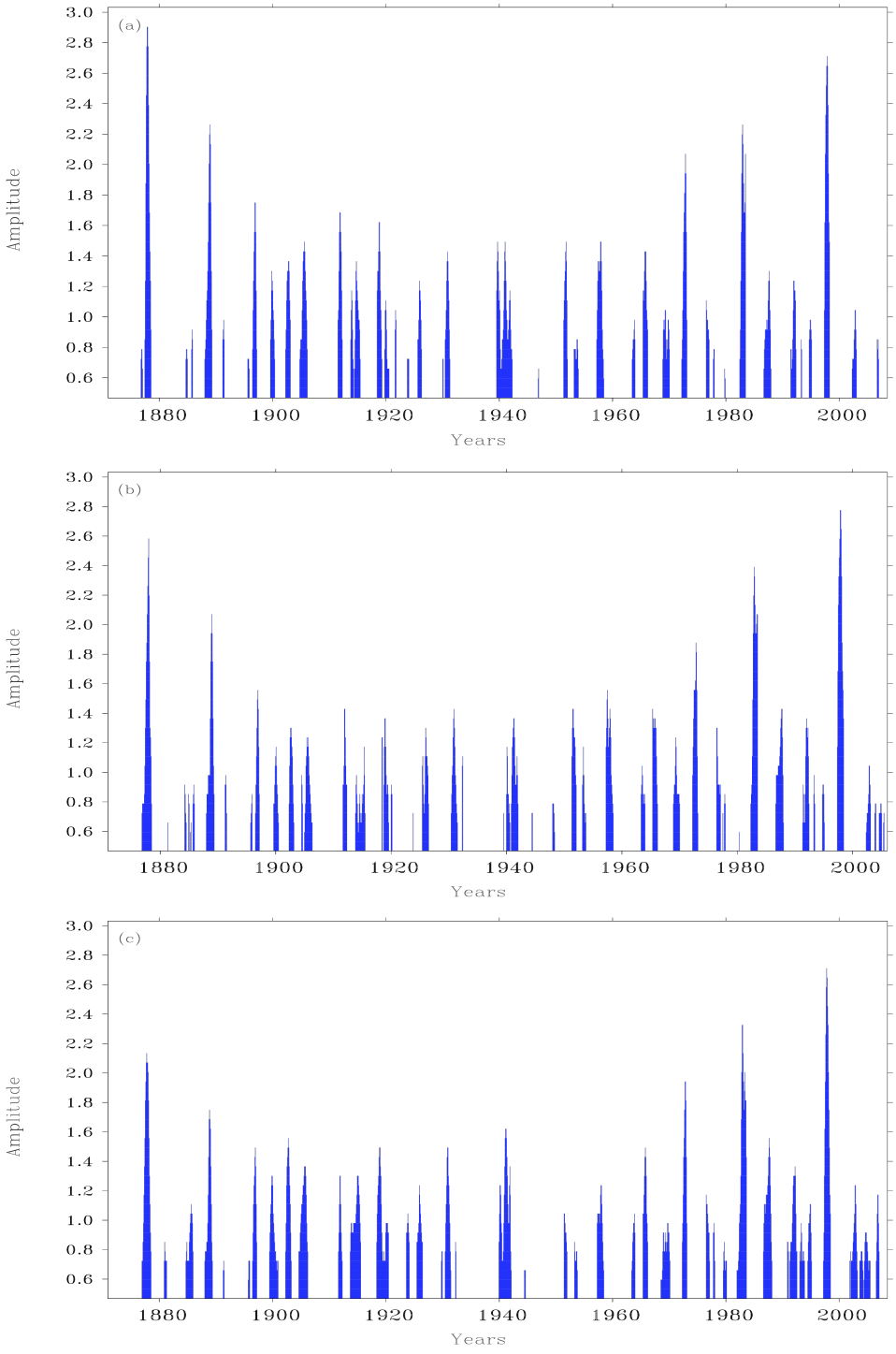

Figure 27. CHI amplitude for SST anomalies greater than 0.5°C constructed from (a) ERSST v3, (b) HadISST, and (c) Kaplan v2.

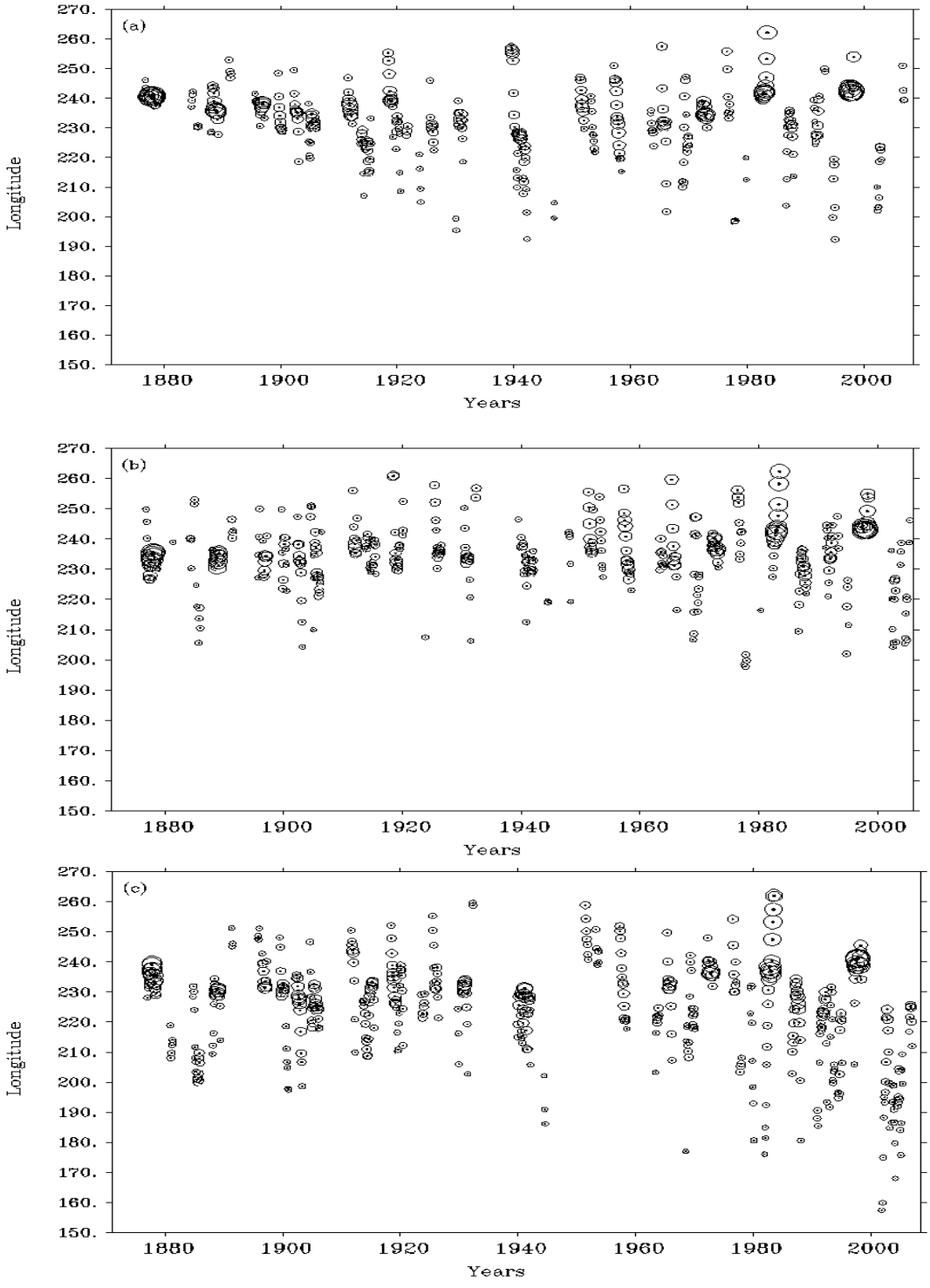

Figure 28. As in Figure 27 but for CHI longitude.

El Niño events from ERSST plotted against the same from SODA 2.2.4 (upper panel). The lower panel of Figure 29 shows the CHI amplitude for El Niño from ERSST plotted against the same from SODA 2.2.4. To distinguish the products for periods of varying density of observations, the data sparse periods (1871-1949) are plotted in red and the data dense periods (1950-2008) are plotted in blue. The CHI amplitudes of the two products agree very well (0.96) and the CHI longitude is correlated at 0.87 during periods of dense observations. Although the correlation between the CHI amplitudes (0.76) is relatively high that of CHI longitudes (0.45) is poor during periods of sparse observations. Figure 30 shows similar plots as Figure 29 but for CHI amplitudes and CHI longitudes from HadISST. The CHI amplitudes are correlated at 0.94 and CHI longitudes are correlated at 0.77 during periods of dense observation. During periods of sparse observations the correlation between CHI amplitudes is 0.78 and CHI longitudes are uncorrelated. Figure 31 shows the same again but for CHI longitudes and CHI amplitudes from Kaplan v2. The correlations of the CHI metric in Kaplan v2 do not agree as well as other reconstructed products. Overall, SODA 2.2.4 shows better agreement with ERSST than either HadISST or Kaplan v2. The difference in CHI-longitude between reconstructions and SODA 2.2.4 is prominent west of 140°W in the central-western Pacific. This is probably due to the method used to construct reconstructed SST data in data sparse periods (already discussed in Introduction). The debate of long-term variability in the position of El Niño warming therefore becomes complicated using the reconstructed data products. Although the strengths of the El Niño are comparable between the reanalysis and the reconstructions the locations of warming

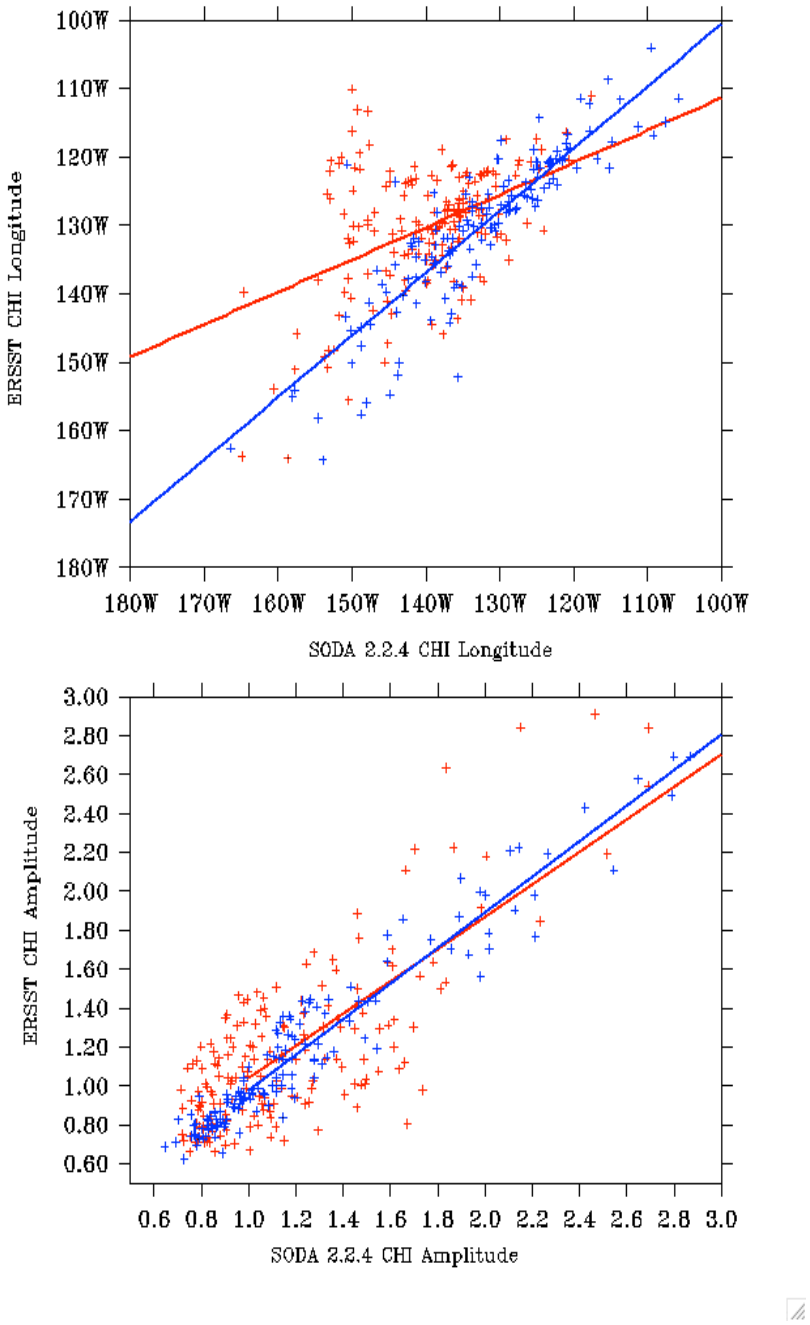

Figure 29. (Top) CHI longitude from ERSST v3 (y-axis) plotted as a function of CHI longitude from SODA 2.2.4 (x-axis) for warm events. (Below) CHI longitude from ERSST v3 (y-axis) plotted as a function of CHI longitude from SODA 2.2.4. Values from 1871 through 1949 are shown in red and values from 1950 through 2008 are shown in blue. The least squares regression for both periods of time are shown as a solid line.

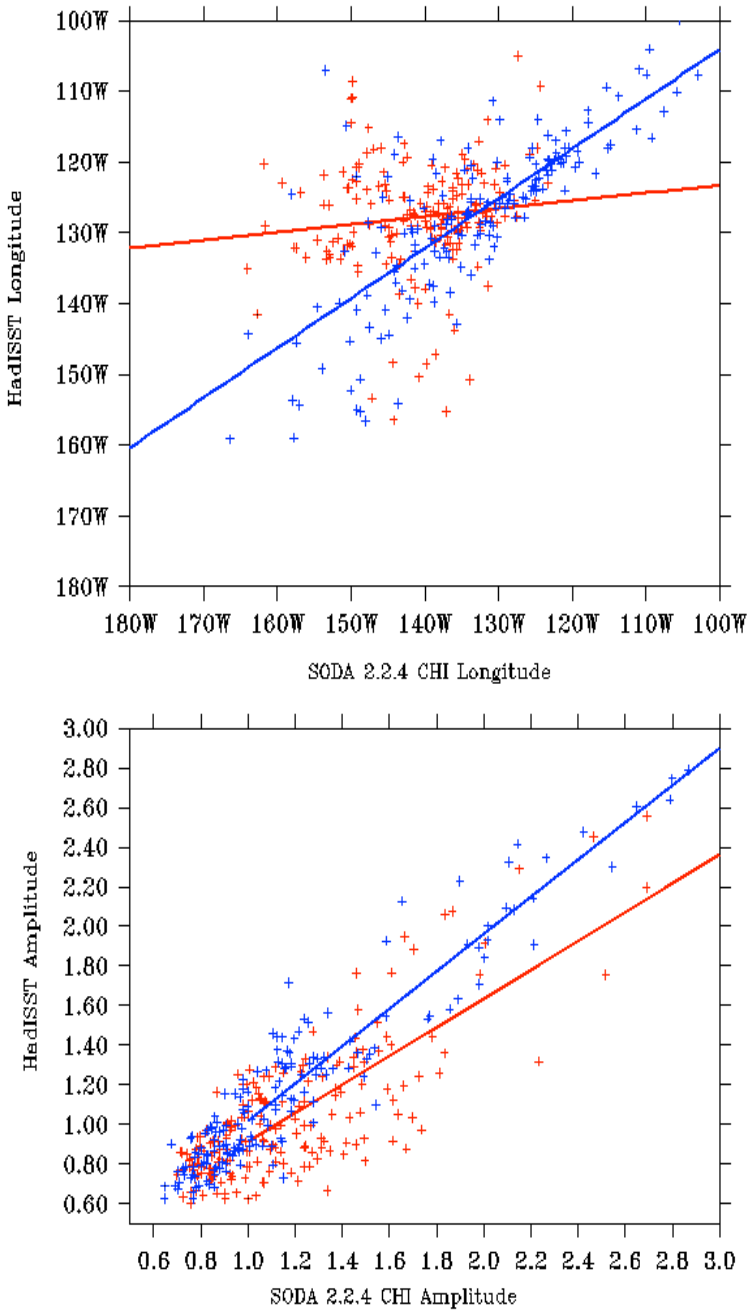

Figure 30. (Top) CHI longitude from HadISST (y-axis) plotted as a function of CHI longitude from SODA 2.2.4 (x-axis) for warm events. (Below) CHI longitude from HadISST (y-axis) plotted as a function of CHI longitude from SODA 2.2.4. Values from 1871 through 1949 are shown in red and values from 1950 through 2008 are shown in blue. The least squares regression for both periods of time are shown as a solid line.

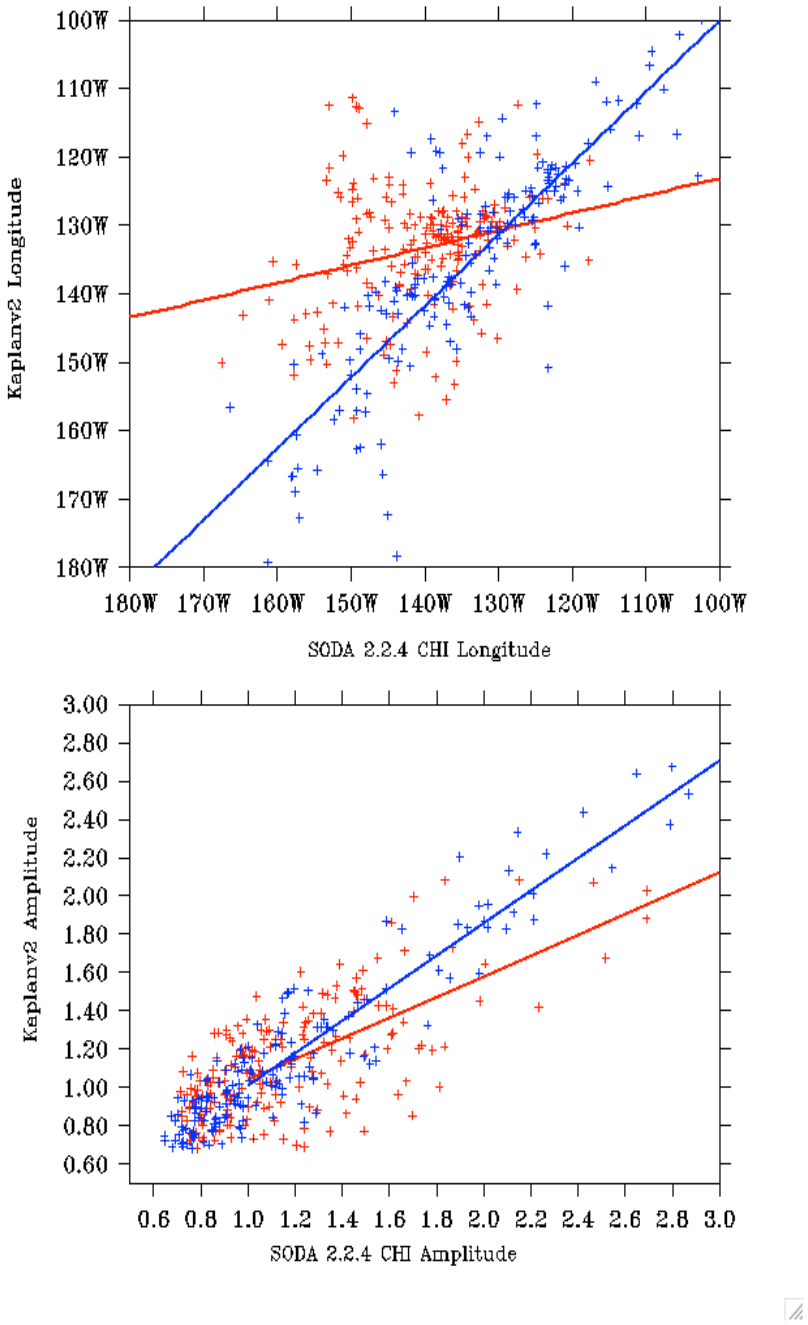

Figure 31. (Top) CHI longitude from Kaplan v2 (y-axis) plotted as a function of CHI longitude from SODA 2.2.4 (x-axis) for warm events. (Below) CHI longitude from Kaplan v2 (y-axis) plotted as a function of CHI longitude from SODA 2.2.4. Values from 1871 through 1949 are shown in red and values from 1950 through 2008 are shown in blue. The least squares regression for both periods of time are shown as a solid line.

disagree significantly. Figure 32 shows histograms of CHI longitude from the two reconstructions, ERSST and HadISST, along with that from SODA 2.2.4 and SODA 2.2.0. The mean location of CHI longitude of El Niño events in ERSST (130°W) and HadISST (127.2°W) is east of that in SODA 2.2.4 (139°W). The mean location of CHI longitude in SODA 2.2.4 (139°W) and SODA 2.2.0 (143.3°W) differ at most by 4°. Notably the standard deviation of CHI longitude in ERSST (10.8) and HadISST (10.9) compared to SODA 2.2.4 (12.5) and SODA 2.2.0 (14.5) indicates a localized occurrence of El Niño in ERSST and HadISST compared to the reanalysis. The distributions of CHI longitude are negatively skewed in ERSST (-0.65) and in HadISST (-0.56), which is in contrast to that in SODA 2.2.4 (0.1). This implies that the center of the warm anomaly during El Niño is eastward in the reconstructions compared to that in reanalysis. Figure 33 show histograms of CHI longitude of El Niño events from SODA 2.2.4, ERSST, and HadISST for periods of sparse observations (1871-1949) and periods of dense observations (1950-2008) separately. The distribution of CHI longitude from SODA 2.2.4 during the two periods 1871-1949 (Figure 33a) and 1950-2008 (Figure 33d) do not look similar and the mean location of CHI longitudes differ by 6°. The mean location of CHI longitude during the two periods of 1871-1949 (Figure 33b) and 1950-2008 (Figure 33e) differ only by one degree in both ERSST and HadISST. That the location of ENSO is so similar in the two periods may be due to the pre-determined EOF pattern of SST of the data dense periods (1950-2005) used to reconstruct SST data in the data spare periods (1871-1949). The SST reconstructions in data sparse periods could thus be dominated by the strong El Niño events of 1982-83 and 1997-97, which could result

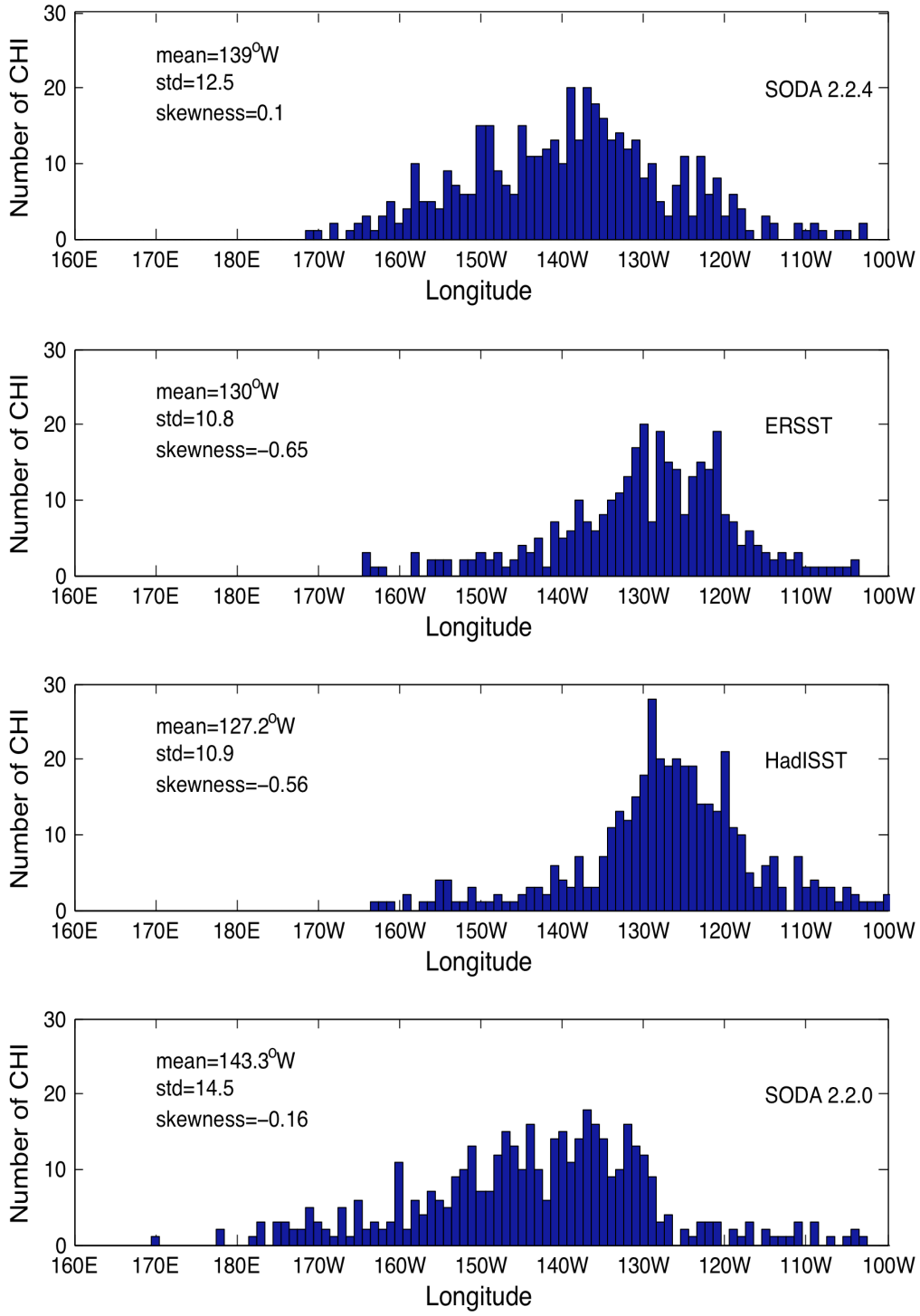

Figure 32. Histograms of location of El Niño events from SODA 2.2.4, ERSST, HadISST, and SODA 2.2.0. respectively. The mean, standard deviation and skewness of each distribution are shown in the figure.

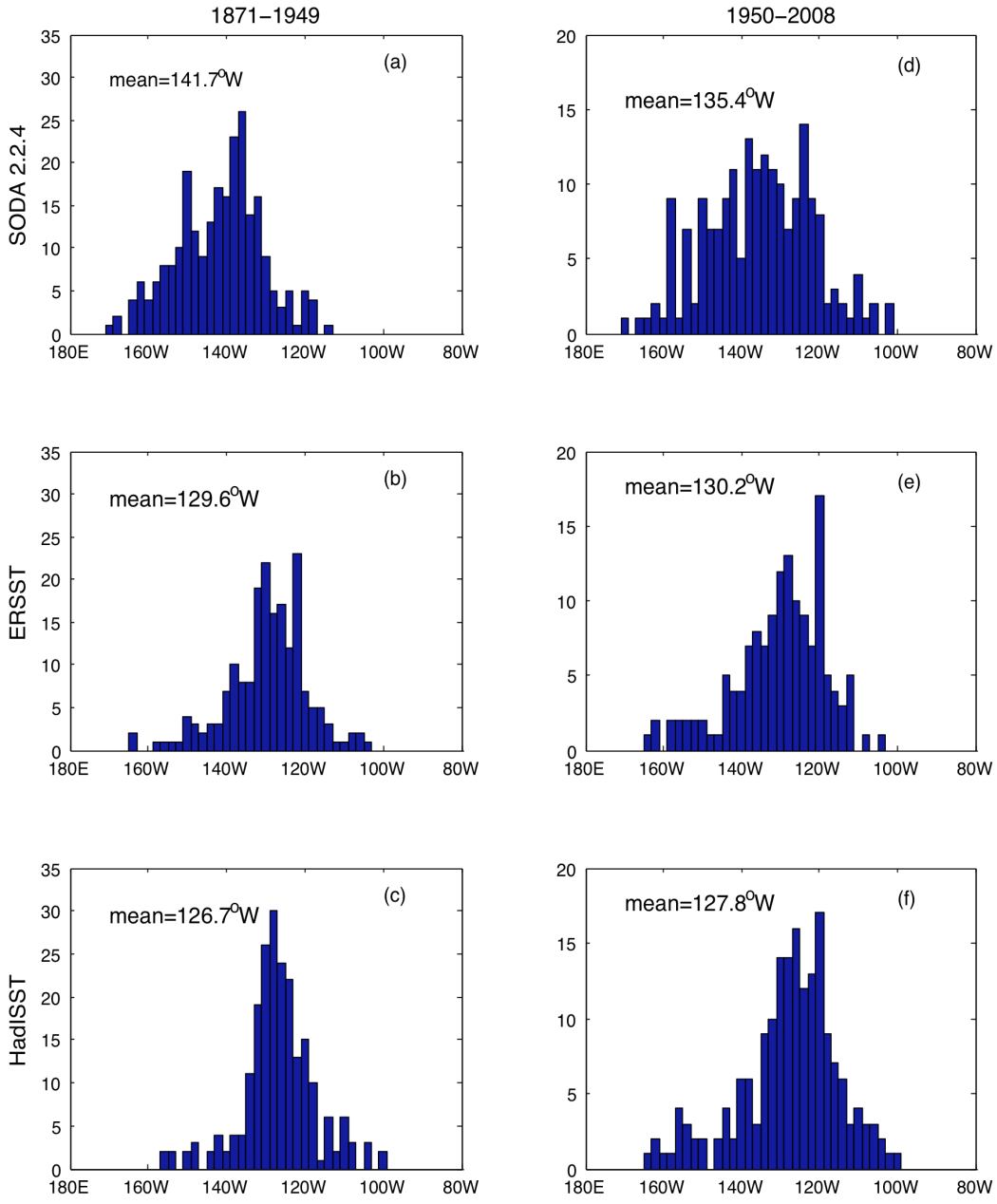

Figure 33. Histograms of CHI longitude for El Niño events shown separately for 1871-1949 (a, b, c) and for 1950-2005 (d, e, f) periods as constructed from SODA 2.2.4 (a and d), ERSST (b and e), and HadISST (c and f) respectively. The distribution of location of El Niño events is shown in each plot with the mean location.

in the sharp peak in the CHI longitude histograms with low standard deviations.

Changes in ENSO

Changes in amplitude

The CHI amplitude for El Niño from SODA 2.2.4 shows strong variability (Figure 11a), with strong warm events at both the beginning (between 1875-1920) and end (1970-2008) of the record and weak events in between (1920-1969). The period 1930-1940 was distinct due to absence of El Niño and weak La Niña events. North America experienced severe dust storms and drought during these years, and the years came to be known as the Dust Bowl years. *Schubert et al.* [2004] suggest that a cool tropical Pacific and a warm Atlantic ocean accompanied and aided the dry conditions of North America during the Dust Bowl years. El Niño in the Pacific is associated with excess wintertime rainfall in North America. Thus reduced El Niño during these years could influence the dry conditions in North America at the time. On the other hand La Niña brings below average rainfall in the region, but weakened activity of La Niña during the time does not explain the severe drought conditions that North America experienced at the time. Most of the El Niños up to 1930 were strong with very few weak El Niño events occurring in between. After a brief period of null El Niño activity during 1930-1940 moderate-to-strong El Niño events start from 1940 onwards. Strong El Niños start strengthening from 1960 onwards, although weak El Niño events seem to occur throughout.

Variation in the strength of La Niña has been more regular than the strength of El Niño during 1871-2008. Apart from the La Niña of 1917/18 no other cold event recorded a temperature anomaly below -1.6°C (Figure 12a). In addition there do not appear periods of heightened or weakened La Niña activity and there is little trend in strength of La Niña.

Changes in location

The location of El Niño given by CHI-longitude (Figure 11b) does not show much variation during the 138 years of study. Instead the locations of El Niño are randomly distributed between the Dateline and 100°W about the mean location of CHI longitude at 139°W. A gradual strengthening of each event occurs irrespective of whether the warming propagates eastward or westward during the growing stage. To explore recent suggestions that there are spatially different kinds of El Niños we explored the CHI-longitude from the reanalysis to search for different types of El Niños. The histogram of CHI longitude from SODA 2.2.4 for the period from 1871 to 2008 (Figure 14) resembled that of a Gaussian distribution. The distribution of the data was Gaussian at the 5% significance level with a p-value of 0.14 and test statistic of 0.04. A Lilliefors test was performed to test the normality of the data. The Lilliefors test is similar to Kolmogorov-Smirnov test but does not require a predetermined cumulative distribution function to test the null hypothesis that the two distributions are from the same family of Gaussian curves. The Gaussian that gives the smallest RMS (root-mean-square) difference from the CHI-longitude distribution is shown as a red line (Figure 14). The null hypothesis that El Niño events have a single mean location was tested. The

test demonstrates that the location of CHI longitude can be represented as a Gaussian distribution about the mean. The Gaussian that was fitted to the data has the same mean of the data and the standard deviation was the square root of the unbiased estimate of the variance of the data; this was considering the data was a sample from a normal distribution. The fitted Gaussian verified the location of CHI-longitude was around a particular longitude on the equatorial Pacific. Thus, using the Lilliefors test, the null hypothesis that the distribution of CHI longitude is a Gaussian cannot be rejected.

The location of La Niña occurs between the Dateline to 100°W in the eastern Pacific (Figure 12b). Unlike El Niño events La Niña events do not show either strengthening or weakening during its developing stages although the location of cold anomalies propagate across the equatorial stretch between 100°W and the Dateline. The distribution of the location of La Niña has a standard deviation of 14° and a mean of 140.1°W. Similar to the analysis for single mean location of El Niño, the location of La Niña was explored with similar tests. The distribution of CHI longitude for La Niña fails the Lilliefors test indicating that the distribution of CHI longitude for cold events is not Gaussian. Unlike the CHI longitude for El Niño events, the CHI longitude for La Niña events does not have a single mean location with all the other locations distributed about this mean location. Thus the existence of multiple locations of La Niña event cannot be rejected. The distribution of CHI longitude for La Niña (Figure 15) shows high positive skewness (0.3) compared to that from El Niño events (0.1), which implies that most La Nina events occur towards the central Pacific.

Changes in frequency

Figure 34 shows the frequency of El Niño during the period 1871-2008 in terms of the elapsed time between consecutive El Niño events. The longest elapsed time occurs between the El Niño of 1929/31 and the El Niño of 1940/42. There were frequently occurring El Niños during the late nineteenth and the beginning of the twentieth century, during the 1950s, and during the end of the twentieth century. Overall there was no trend in the frequency of El Niño. The histogram of the frequency of El Niño has a mean of 3.9 years (46.6 months) and a standard deviation of 1.9 years (22.8 months). A high

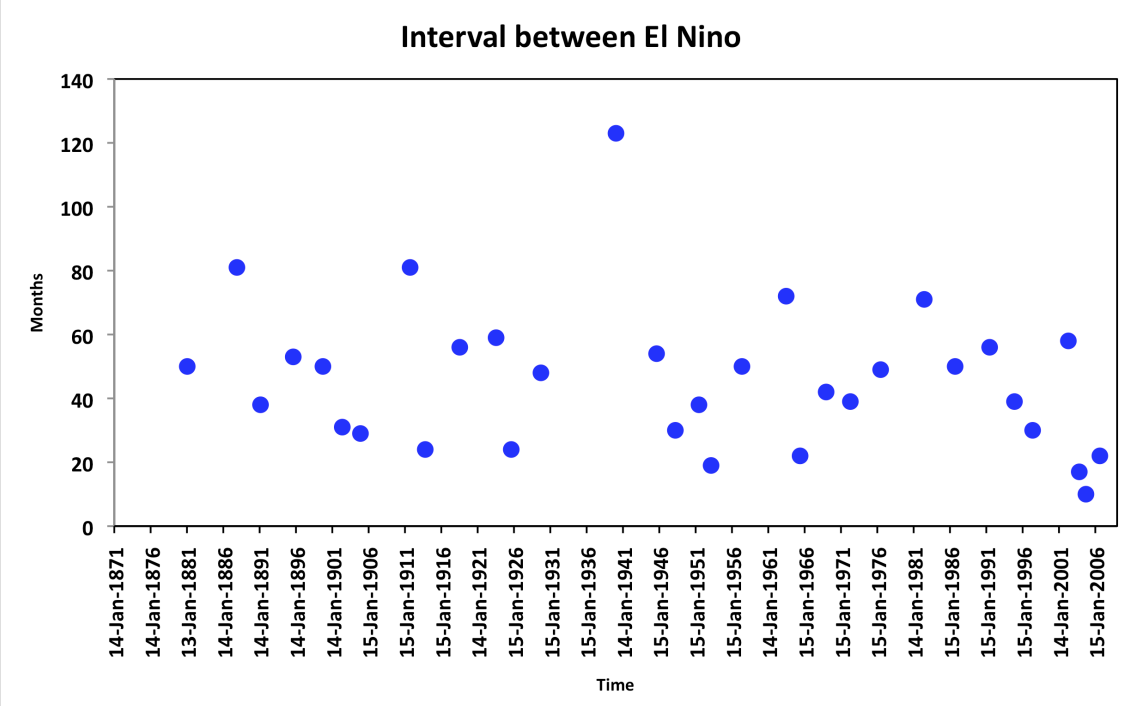

Figure 34. Interval between El Niño events in months during 1871-2008. Dots located at the year of El Niño shows the months since the previous event.

skewness of 1.12 in the distribution indicates occurrence of elongated wait times. By Lilliefors test the distribution of wait times of El Niño events resemble a Gaussian with a p-value of 0.12 and a test statistic of 0.14. We explore using statistical tests the minimum events required to reliably determine a change in the mean wait time (frequency) of El Niño events at 95% confidence level. The tests show that many El Niño events are required to detect such change and the current record is not long enough. The test is described briefly as follows. We consider a normally distributed population of wait times of El Niño events. Two samples of n_1 and n_2 events are considered from the population. The sample n_1 represents the 34 El Niño events from the reanalysis. m_1, m_2 and σ_1, σ_2 represents the means and standard deviations of the frequencies. Thus m_1 is 46.6 months and σ_1 is 22.8 months. We want to find the n_2 events that would have a mean wait time of m_2 and a standard deviation of σ_2. We assume the difference between m_1 and m_2 is represented by δ_i at 5% significance level. We then calculate n_2 using Student's t-test for $\delta_1 = 4$ months, $\delta_2 = 8$ months, and $\delta_3 = 12$ months. This returned 42 events for n_2 that would be needed to reliably detect a change in the mean frequency by 8 months and 251 events to detect a change in the mean frequency by 4 months at a 5% significance level when the standard deviation of n_2 events is same as n_1 events. Table 3 shows the number of events (n_2) needed for different changes in the mean frequency (δ_i) of events and for varied standard deviations (σ_2) at a 5% significance level. The table shows that as the standard deviation of the distribution of the second sample decrease, the number of events required to detect the same change in the mean frequency decreases too. In the method the distribution of wait time for the second sample, which

can be identified with future El Niño events, is kept the same as the past events (the 34 El Niños in the reanalysis). However such an assumption is not flawless, as any change in the distribution of wait time for future El Niño events is possible. Thus tests with added assumptions on different distribution of future El Niño events could be made, but would necessitate a more complex method. Nevertheless, this analysis showed that 34 El Niño events (if not less) in 138 years were not sufficient to identify a change in the mean frequency of El Niño events. *Enfield and Cid* [1995] performed similar statistical analysis of multi-century climate data to show that El Niño frequency had not changed since 1525.

Table 3. Number of El Niño events (n_2) needed to determine a change in the period of El Niño. n_2 is shown for different mean wait times (m_2) and different standard deviation (σ_2). δ_1, δ_2 and δ_3 represent the change in the mean frequency.

Standard deviation	Number of events = $\mathbf{n_2}$		
σ_2	m_2=50.6 ($\delta_1 = 4$)	m_2=54. 6 ($\delta_2 = 8$)	m_2=58. 6 ($\delta_3 = 12$)
34.8	602	114	14
22.8	251	42	3
10.8	92	22	3

Figure 36 shows the frequency of La Niña events from 1871-2008 in terms of the waiting time between consecutive La Niña events. The intervals between consecutive La

Niña events are distributed much wider than El Niño events. Both long and short intervals are present more irregularly than El Niño events. After 1976 there are fewer La Niña events compared to El Niño events that occur after long waiting times. The mean frequency of La Niña is 55.6 months (~5 years). The standard deviation of the frequency for La Niña is 29 months (~2.5 years). Both mean and standard deviation for La Niña events are larger than El Niño events.

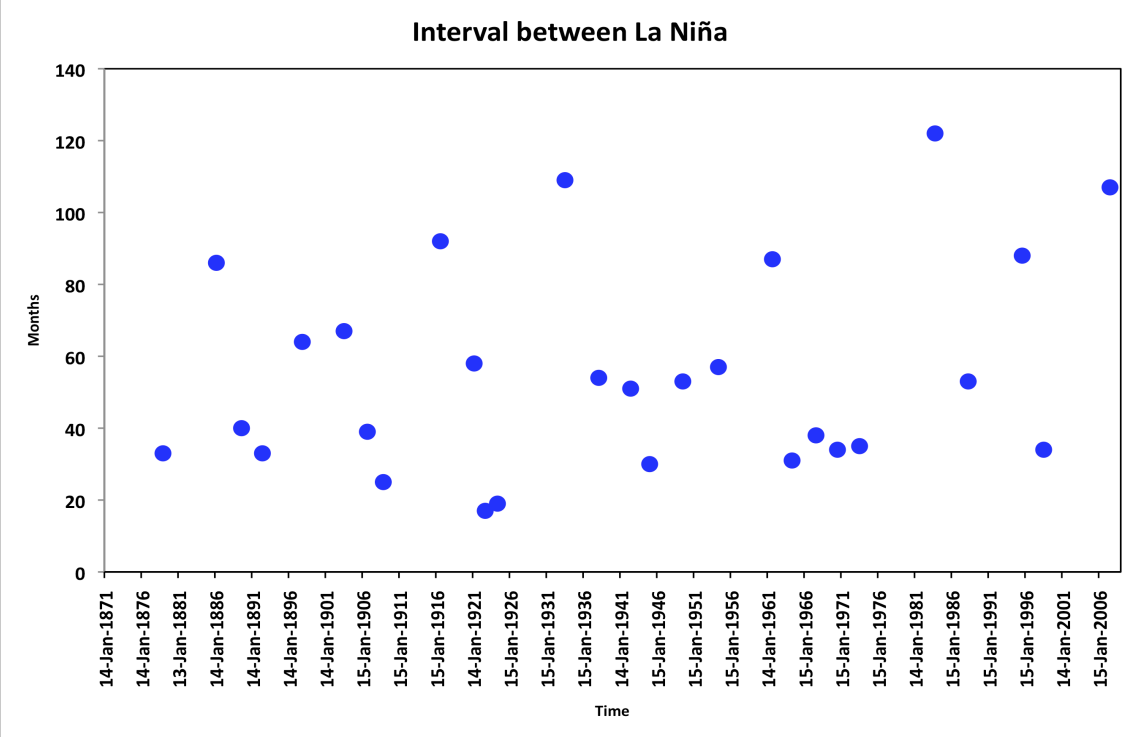

Figure 35. Interval between La Niña events in months during 1871-2008. Dots located at the year of La Niña shows the months since the previous event.

Changes in duration

Figure 36 shows the variation in the duration of El Niño events from 1871-2008. The mean duration for El Niño events is 12.4 months with a standard deviation of 5.7 months. The duration of El Niño is highly variable ranging from 5 months (1881, 1945, 1948, 1994/95, 2003/04) to 27 months (1940-42). The longest event being the El Niño of 1940-42, which occurred after a prolonged period without an El Niño, as discussed earlier. El Niño before 1940-42 warming were either of long duration of almost two years or are as short as 10 months. But after the El Niño of 1940-42 most of the El Niño

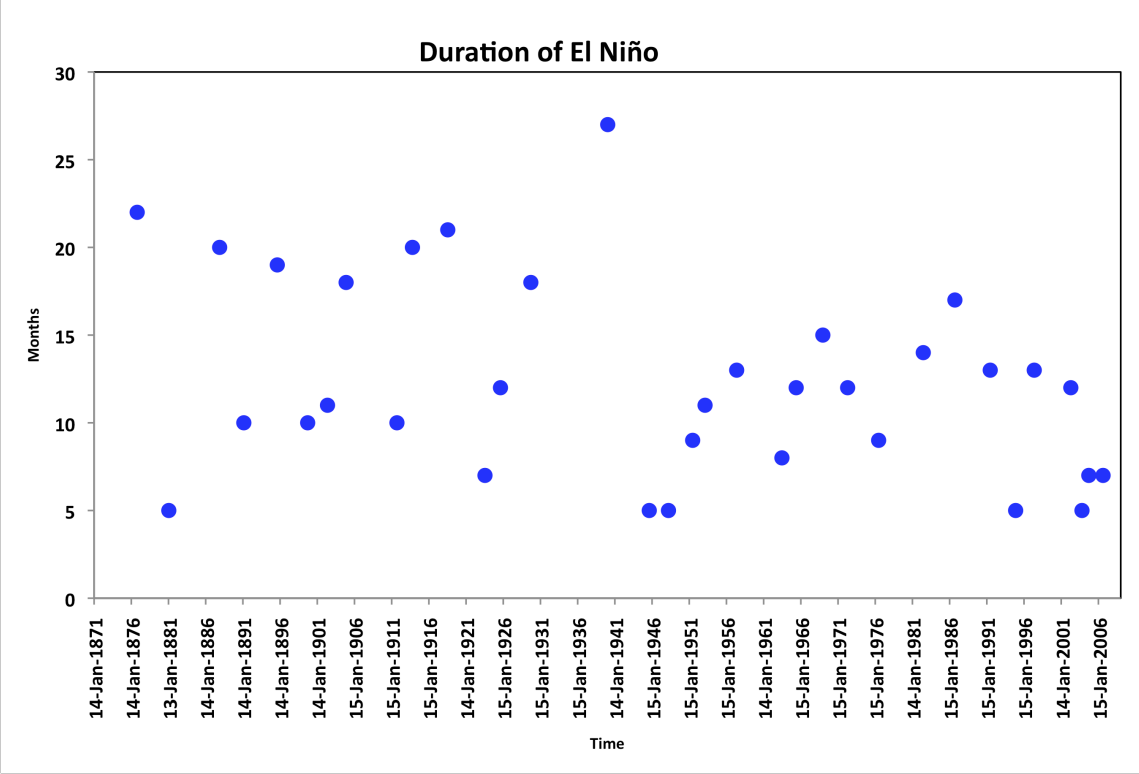

Figure 36. Duration of El Niño events in months during 1871-2008. Dots located at the year of El Niño event and denote the number of months the warm anomaly (>0.5°C) persist.

events were of a year in duration on average. El Niños in the early twenty-first century were much shorter, with a period of around 5-6 months. Figure 37 shows the duration of La Niña events over the 138-year record of study. The time series of duration shows that both short-lived and long-lived La Niña events occur consistently throughout the record. The mean duration for La Niña events is 15.2 months with a standard deviation of 8 months. The duration of La Niña is highly variable ranging from 5 months (1876, 1945) to 30 months (1998-2000). Earlier we noted the period between 1930-1940 experienced weak La Niña events; Figure 37 shows that the duration of the La Niña is short as well. Comparing Figure 36 and Figure 37 shows that in recent years short duration El Niño events occur whereas the duration of La Niña is generally long (compare with Figure 35). The mean duration of La Niña events is longer than the mean duration of El Niño events. *Okumura and Deser* [2010] suggests the influence of Indian Ocean on wind anomalies of western equatorial Pacific as a possible cause for asymmetry in the duration of El Niño and La Niña. They suggest that the warming of the Indian Ocean basin during El Niño increases tropospheric temperatures which forces atmospheric Kelvin waves to propagate to the western Pacific. This induces anomalous surface easterlies in the western equatorial Pacific, which counteracts and reduces the anomalous surface westerlies forced by the eastward shift of anomalous precipitation in the central equatorial Pacific. This brings rapid termination of anomalous warming during El Niño. In La Niña, the cooling of the Indian Ocean induces surface westerlies in the western Pacific that are subdued by the strong anomalous easterlies forced by negative precipitation anomalies in the equatorial Pacific. This prolongs the duration of cold

anomaly during La Niña and requires slow ocean adjustment processes to terminate the event. *Okumura et al.* [2011] demonstrates this hypothesis through AGCM experiments and also show the additional contribution of off equatorial winds influencing the SST anomalies in the equatorial Pacific.

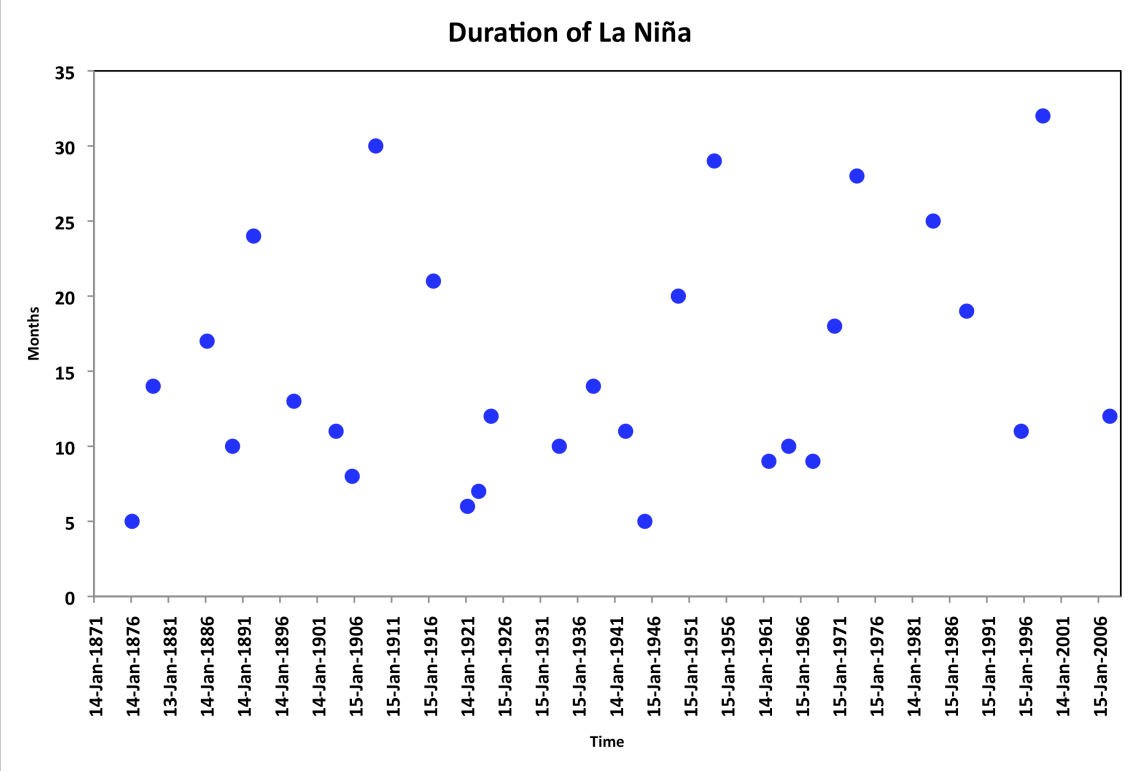

Figure 37. Duration of La Niña events in months during 1871-2008. Dots located at the year of La Niña event and denote the number of months the cold anomaly (<-0.5°C) persist.

Changes in propagation

Fedorov and Philander [2001] proposed a theory explaining eastward and westward propagating anomalies of El Niño. They argue that a deep thermocline with weak background winds favors eastward propagation and a shallow thermocline with strong background winds favor a westward propagation during El Niño. *McPhaden and Zhang* [2009] explores the direction of El Niño for the period from 1950-2002. They use *Reynolds et al*. [2002] blended satellite/in situ SST analysis for the period 1981-2008 and the *Smith et al.* [2008] in situ SST analysis for the period 1950-1981 to show a change in the phase propagation of SST anomalies during El Niño from westward to eastward after the mid-1970s. Their analysis showed no change in phase propagation of La Niña anomaly. Figure 38a shows the composite of 34 El Niños from SODA 2.2.4 for the period from 1871-2008. The first indication of positive anomalies occurs in early year 0 near the Dateline and propagates eastward. However, anomalies greater than 0.5°C seem to have a weak westward propagation. From the composite of the entire record there does not seem to be a significant propagation of anomalies during El Niño. Figure 38b shows the composite over the period 1980-2008, as shown by *McPhaden and Zhang* [2009].

The composite shows weak warm anomalies from year -1 near the Dateline, which then propagates eastward in the middle of year 0. The warmest anomalies show negligible phase propagation. Figure 38c shows the composite of SST anomalies for 1950-1976, which was also analyzed by *Mcphaden and Zhang* [2009]. During this period the composite shows a westward propagating anomaly in agreement with *McPhaden and Zhang* [2009]. Figure 38d shows the composite of El Niño for the period 1871-1941. There seems to be an eastward propagation of anomalies warmer than 0.5°C. However the anomalies across the equatorial Pacific basin seem to start and end simultaneously during the period. The composite of zonal wind anomalies during the El Niño events of 1871-2008 is shown in Figure 39a. There is a prominent eastward zonal phase propagation of westerly wind anomalies. Similar eastward phase propagation is seen in the composites of 1980-2008 (Figure 39b) and 1871-1941 (Figure 39d). However the composite of 1950-1976 (Figure 39c) show westerly wind anomalies moving eastward west of the Dateline and moving westward east of the Dateline.

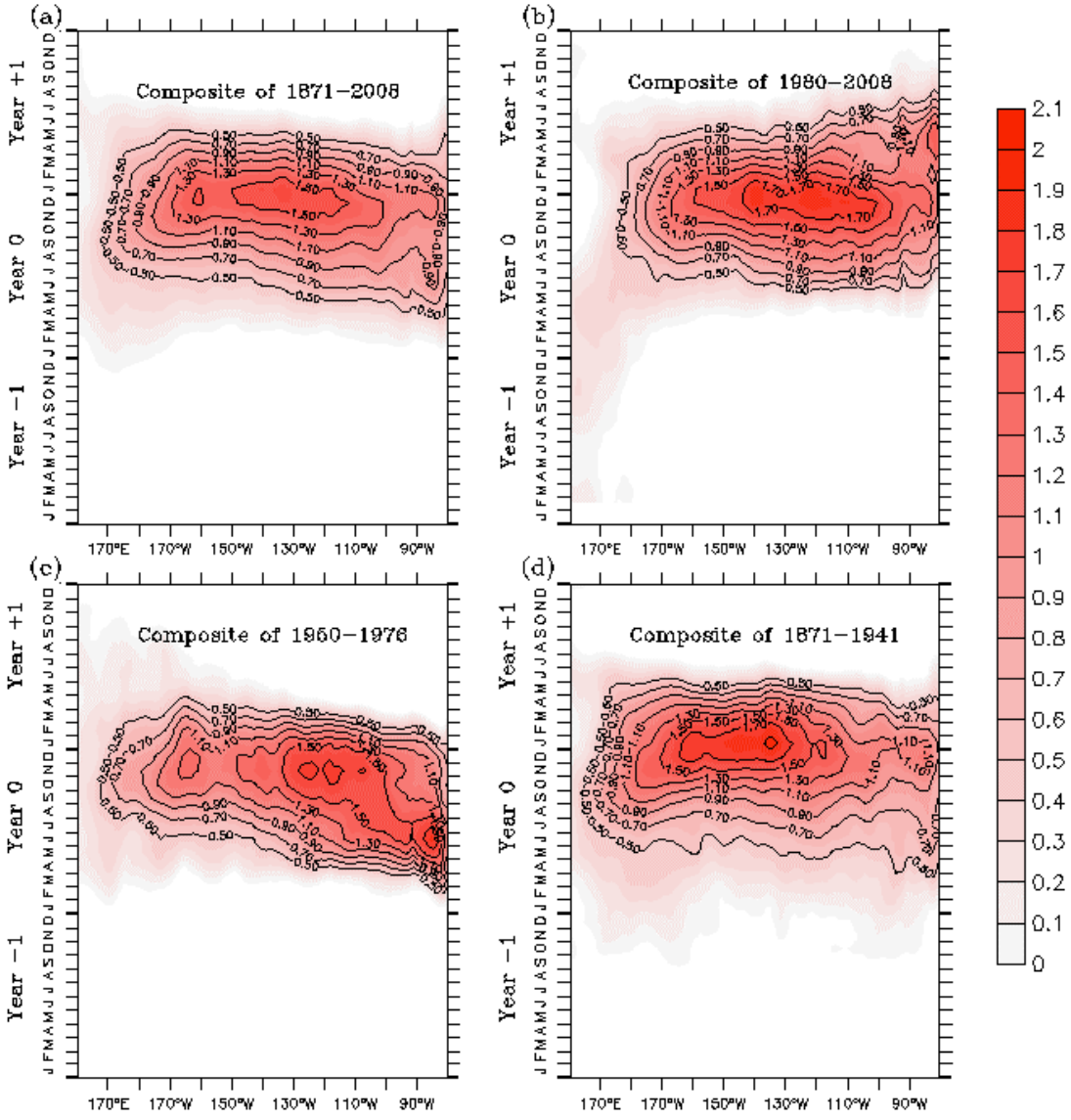

Figure 38. Composite time evolution of SST anomalies during El Niño averaged from 5°S: 5°N. Composites of El Niños during (a) 1871-2008, (b) 1980-2008, (c) 1950-1976, and (d) 1871-1941. Anomalies greater than 0°C are shaded and anomalies greater than 0.5°C are contoured at an interval of 0.2°C. The composites from year -1, year 0, and year 1 is shown.

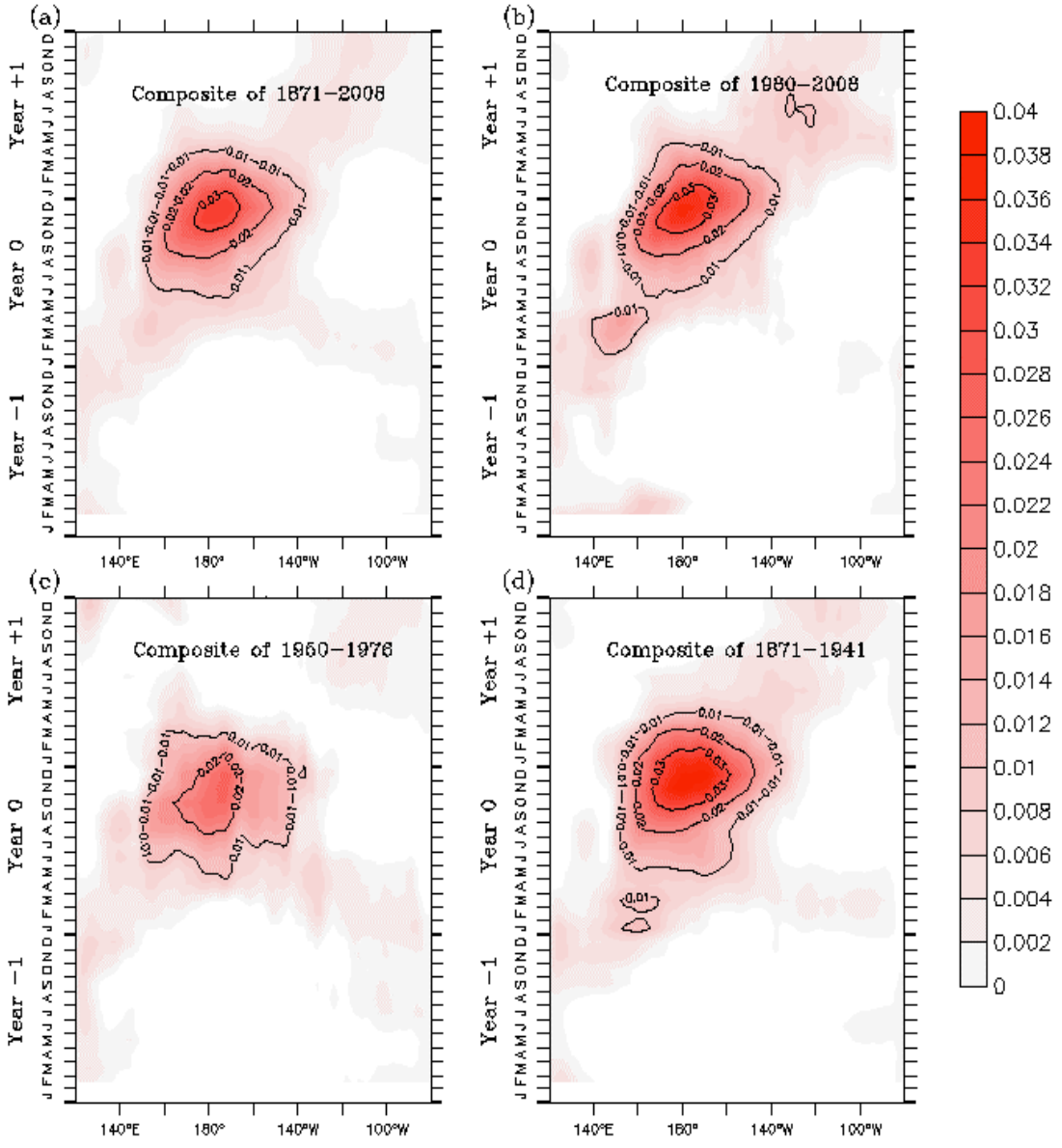

Figure 39. Composite time evolution of taux anomalies during El Niño at the equator. Composites for El Niño during (a) 1871-2008, (b) 1980-2008, (c) 1950-1976, and (d) 1871-1941. Westerly zonal wind anomalies are shaded and anomalies greater than 0.01 dynes/cm^2 are contoured at an interval of 0.1 dynes/cm^2. The composites from year -1, year 0, and year 1 is shown.

Figure 40a shows the composite SST anomaly for La Niña events over a span of four years during 1871-2008. The composite shows a slight westward propagation of anomalies colder than -0.5°C although the conditions returns to normal simultaneously across the basin. Figure 40b shows the composite of SST anomalies for La Niña event during the period 1980-2008. During this time there is a prominent reappearance the cold anomalies in the end of year +1. This elongates the duration of La Niña events during this period further as is also evident in Figure 37. Figure 40c shows the composite of anomalies of SST for La Niña during 1950-1976. This period shows a clear westward propagation of cold anomalies. Figure 40d shows the composite of SST anomalies for La Niña events during 1871-1949. The period also shows westward propagating anomalies. The westward zonal phase propagation of SST anomalies during La Niña is evident in all the composites. Figure 41 shows the composite of zonal wind anomalies during the similar periods as in Figure 40. Very little zonal propagation is evident in the composite of zonal wind anomalies of composite of all La Niña in 1871-2008 (Figure 41a). There is an eastward propagation of easterly wind anomaly during 1980-2008 and the anomaly persists till the middle of Year 2, which perhaps forces the cold anomalies to reappear in the year the La Niña.

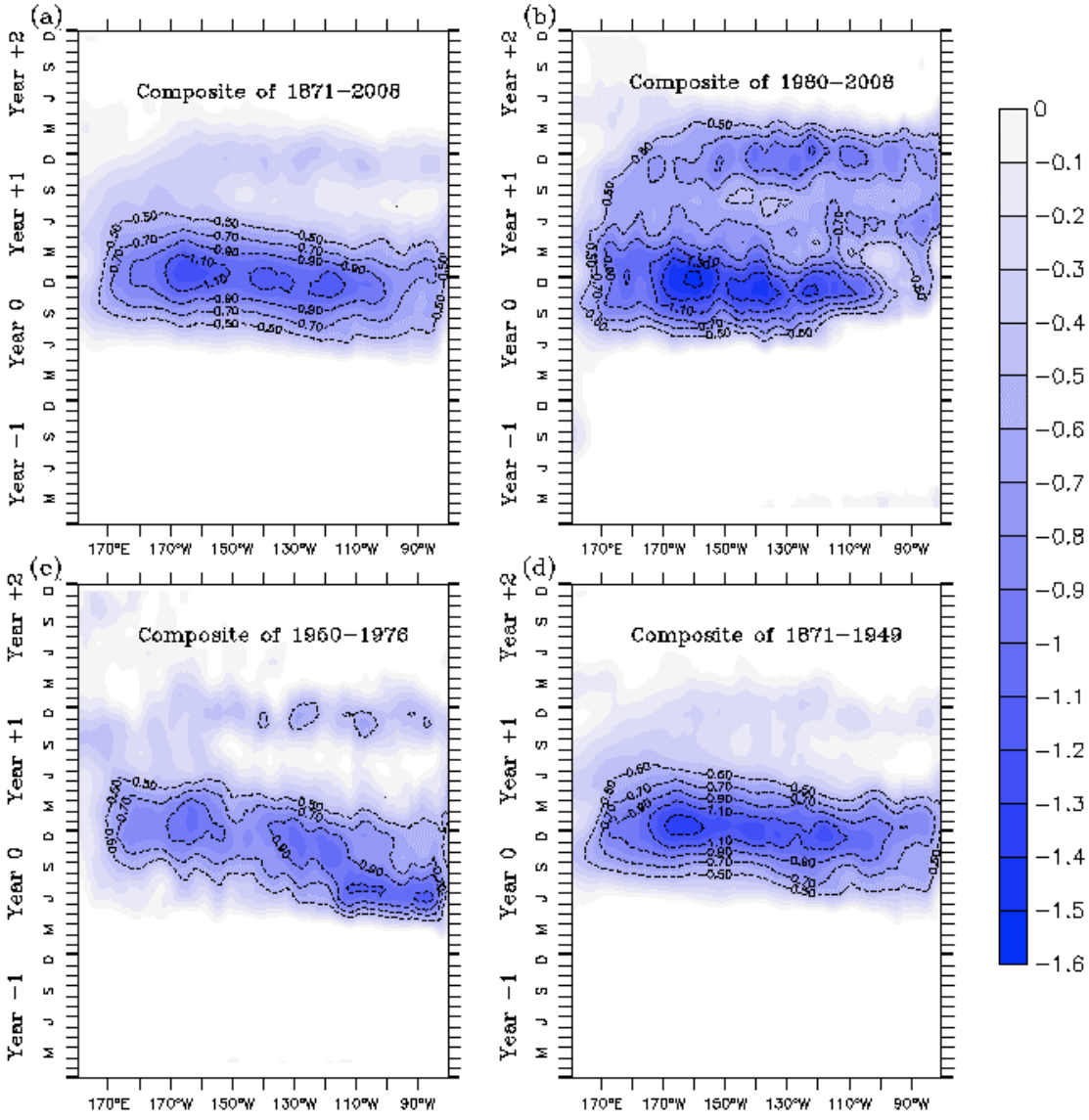

Figure 40. Composite time evolution of SST anomalies during La Niña averaged from 5°S: 5°N. Composites for La Nina during (a) 1871-2008, (b) 1980-2008, (c) 1950-1976, and (d) 1871-1941. Anomalies less than 0°C are shaded and anomalies less than -0.5°C are contoured at an interval of 0.2°C. Year 2 is included due to elongated duration of La Niña.

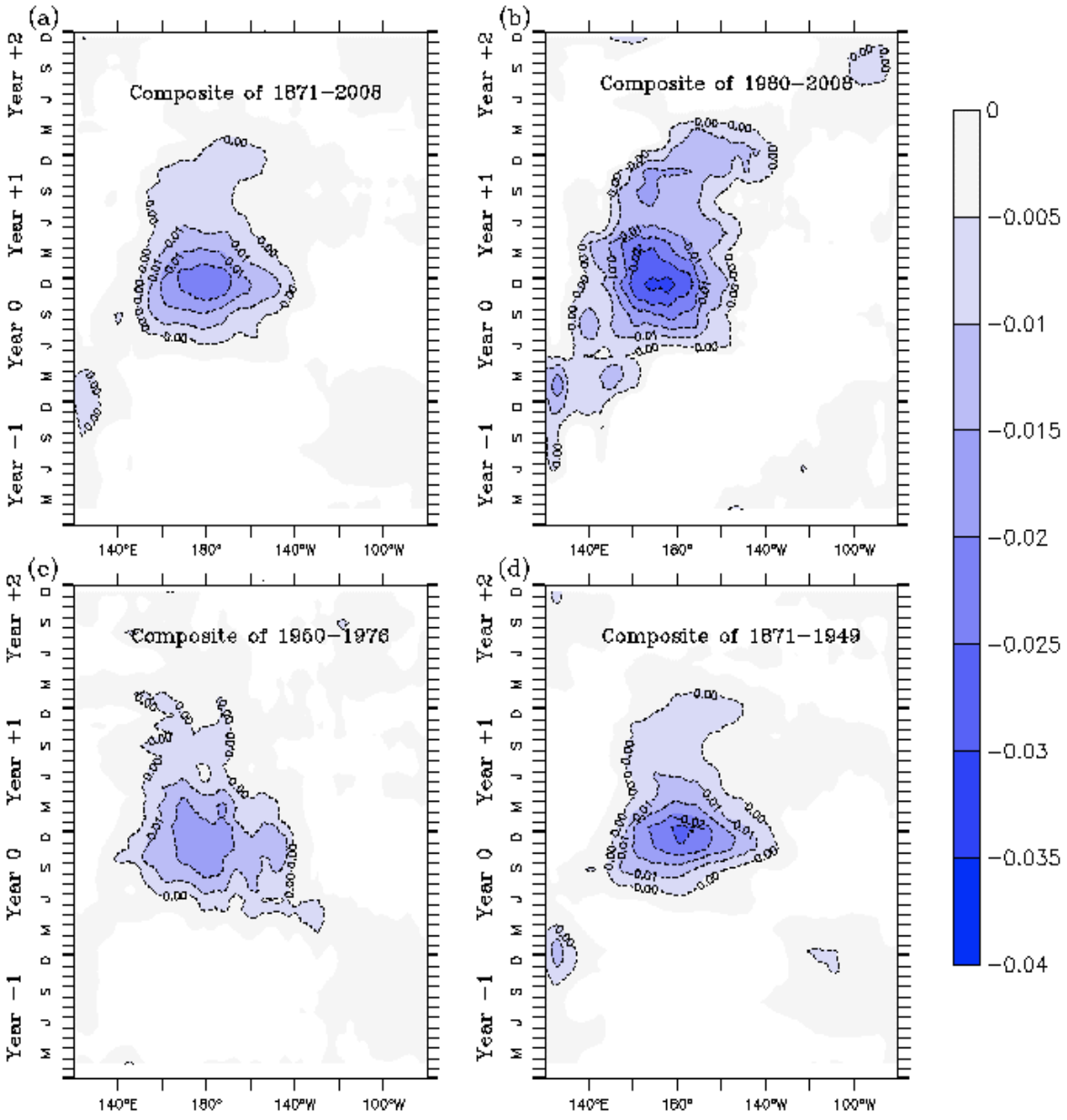

Figure 41. Composite time evolution of taux anomalies during La Niña at the equator. Composites for La Niña during (a) 1871-2008, (b) 1980-2008, (c) 1950-1976, and (d) 1871-1941. Easterly zonal wind anomalies are shaded and anomalies less than -0.01 dynes/cm^2 are contoured at an interval of 0.1 dynes/cm^2. Year 2 is included due to elongated duration of La Niña.

Change in subsurface temperature

The long-term variation of the strength of subsurface warming during El Niño resembles that of surface warming (compare Figure 24a and Figure 11a). El Niño in the beginning of the record shows strong subsurface warming and strong warming occurs again at the end of the twentieth century. The longitudinal location of subsurface El Niño warming does not show prominent variation over the record. The strength of warming grows with location in few El Niño events. The location of subsurface El Niño warming as a function of depth shows that there are shallower warm events in the late twentieth century. The longitudinal location and depth of El Niño warming in the subsurface equatorial Pacific follows the mean depth of the 20°C isotherm (Figure 26b). Thus the depth of El Niño warming in eastern Pacific is shallow along with the depth of 20°C isotherm and contributes strongly to surface warm anomaly. *Vecchi and Soden* [2007] shows through climate model experiments performed for IPCC AR4 that the zonal tropical atmospheric circulation (Walker circulation) has reduced in recent years. This affects the tropical ocean circulation through reduced surface easterlies, decreased mean depth of equatorial thermocline and reduced zonal equatorial thermocline slope. It could be that with a reduced mean depth of the equatorial thermocline, an eastward propagating Kelvin wave prior to the peak phase of El Niño generates a strong warm anomaly in the subsurface, whose center of warming would be closer to the surface. This probably could be the reason that El Niño events over the last few decades have shallow center of warm anomaly.

Variation of heat budget terms with strength and location of El Niño

Earlier studies suggest region specific contribution of individual heat budget terms in El Niño anomaly. Studies suggest zonal advection contributes to El Niño anomaly that is located in central Pacific and vertical advection term dominating the anomalies in the eastern Pacific. This section discusses how the heat budget terms vary with El Niño strength and location as defined by CHI metric. Figure 42 shows the temperature tendency and the advection terms of heat budget terms plotted as a function of the strength of El Niño, as represented by CHI amplitude. Interestingly, none of the heating terms shows a strong correlation with the strength of El Niño. It is likely that all terms contribute to warming, so that no individual term has a high correlation. Figure 43 shows the same set of plots as Figure 42 but the heat budget terms are now plotted as function of the location of El Niño represented by CHI longitude. As for CHI amplitude, the CHI longitude is relatively uncorrelated with the heating terms.

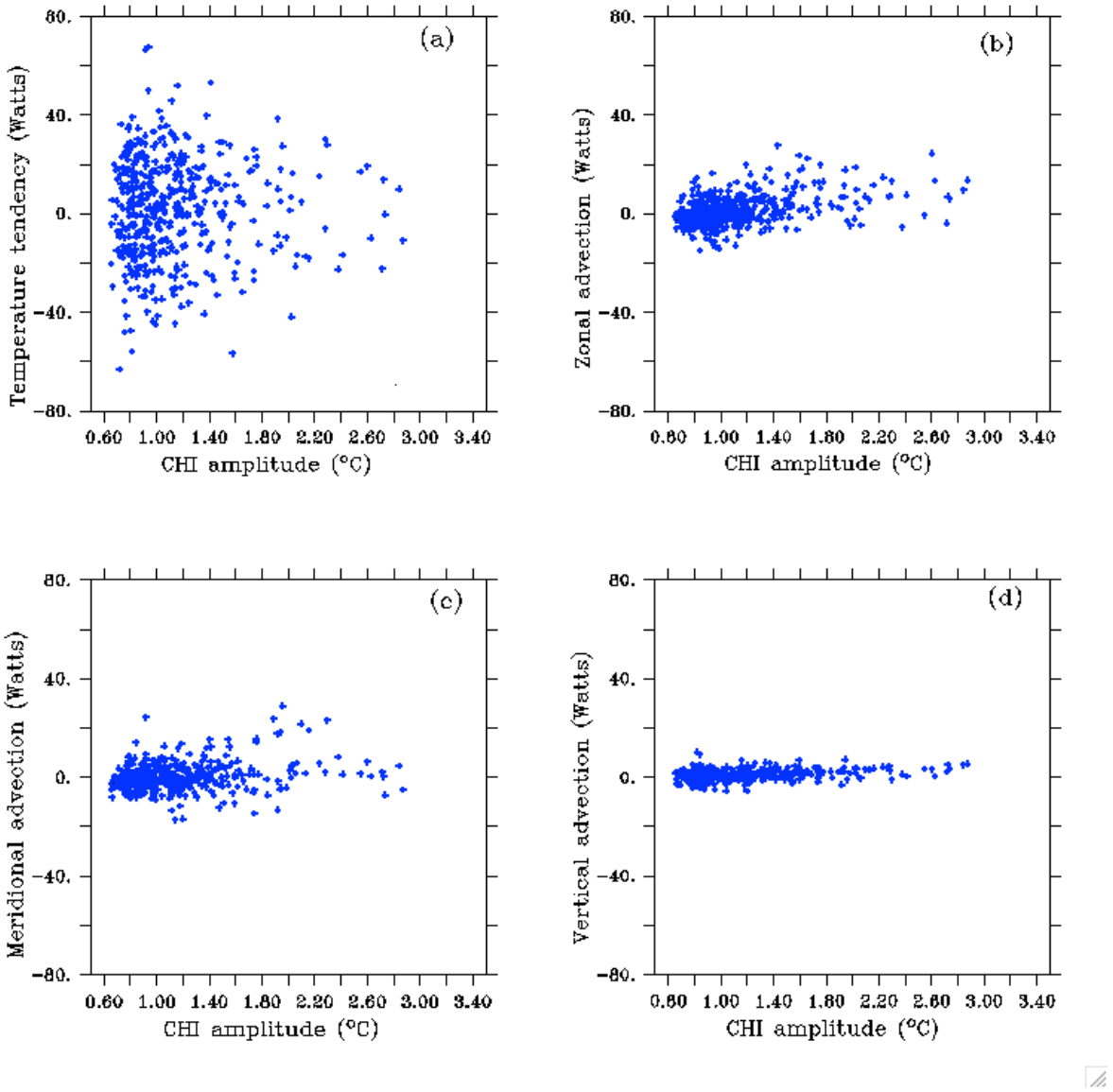

Figure 42. Mixed layer heat budget anomaly terms in watts of (a) temperature tendency, (b) zonal advection, (c) meridional advection, and (d) vertical advection plotted as a function of CHI amplitude for El Niño.

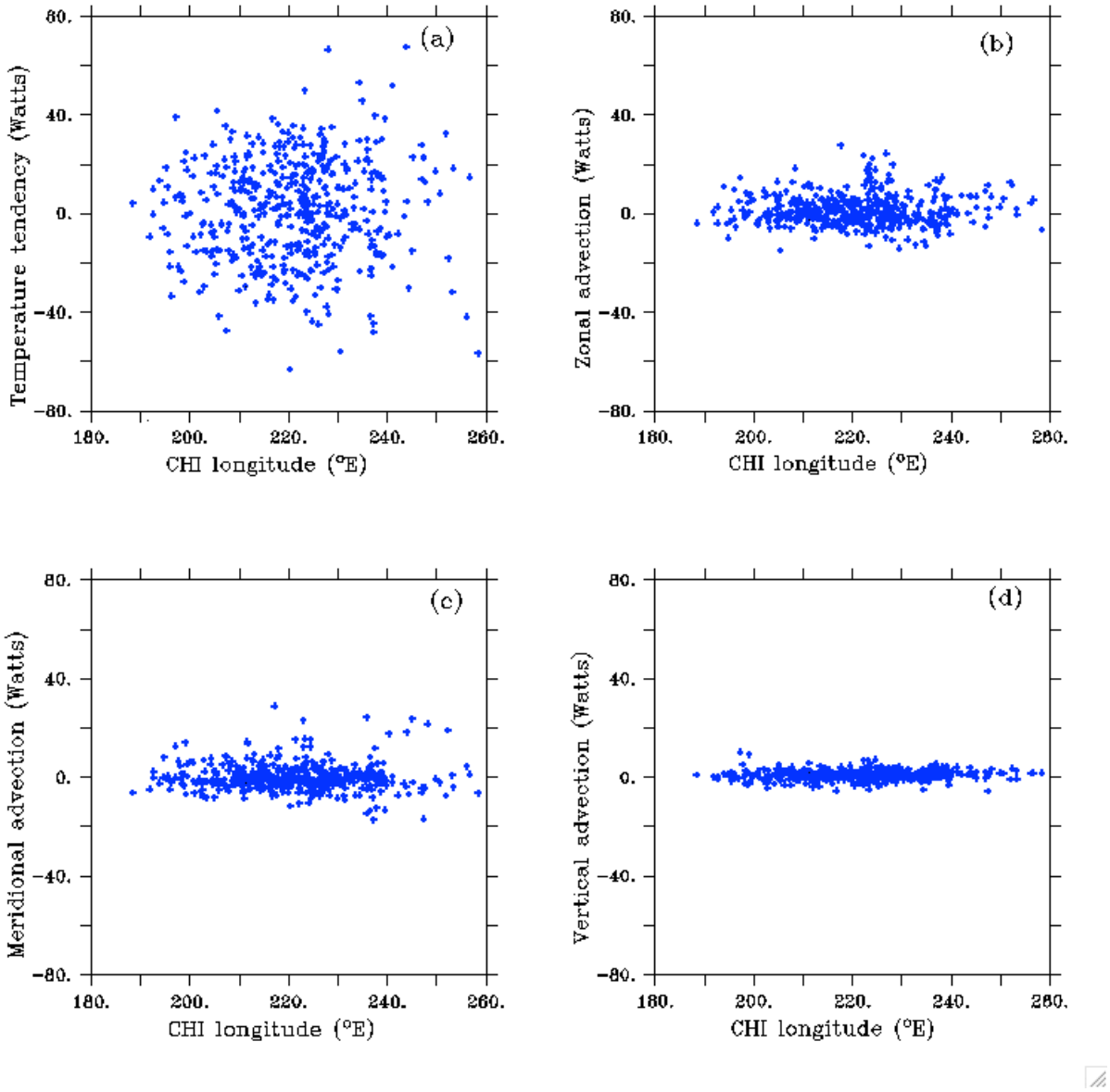

Figure 43. Mixed layer heat budget anomaly terms in watts of (a) temperature tendency, (b) zonal advection, (c) meridional advection, and (d) vertical advection plotted as a function of CHI longitude for El Niño.

Discussion of Errors

Model bias

The impact of model bias on the strength and location of El Niño and La Niña events can be verified by comparing SODA 2.2.0, the simulation and SODA 2.2.4. During periods of dense observations we expect that the assimilation will be less biased than the simulation. Figure 44a shows a comparison of CHI longitude from SODA 2.2.0 and CHI longitude from SODA 2.2.4 for periods of sparse observations (1871-1949) in red and for periods of dense observation (1950-2008) in blue. The location of El Niño in SODA 2.2.4 and SODA 2.2.0 are well correlated during both periods of sparse observations (0.75) and dense observations (0.86). There is a 5° westward bias in the location of warming in SODA 2.2.0 during 1950-2008. Figure 44b shows CHI amplitude for El Niño events from SODA 2.2.0 plotted as a function of those from SODA 2.2.4. The strengths of El Niño in SODA 2.2.0 and SODA 2.2.4 are highly correlated at 0.94 for both periods of sparse and dense observations. However, the CHI amplitude from SODA 2.2.0 shows a slightly warmer average SST anomaly than that from SODA 2.2.4 before 1950. The comparison of simulation and assimilation suggests that there is a tendency for the model to put El Niño slightly to the west of where it occurs in nature. However this bias is relatively weak. This bias does not appear to impact the modeled strength of El Niño.

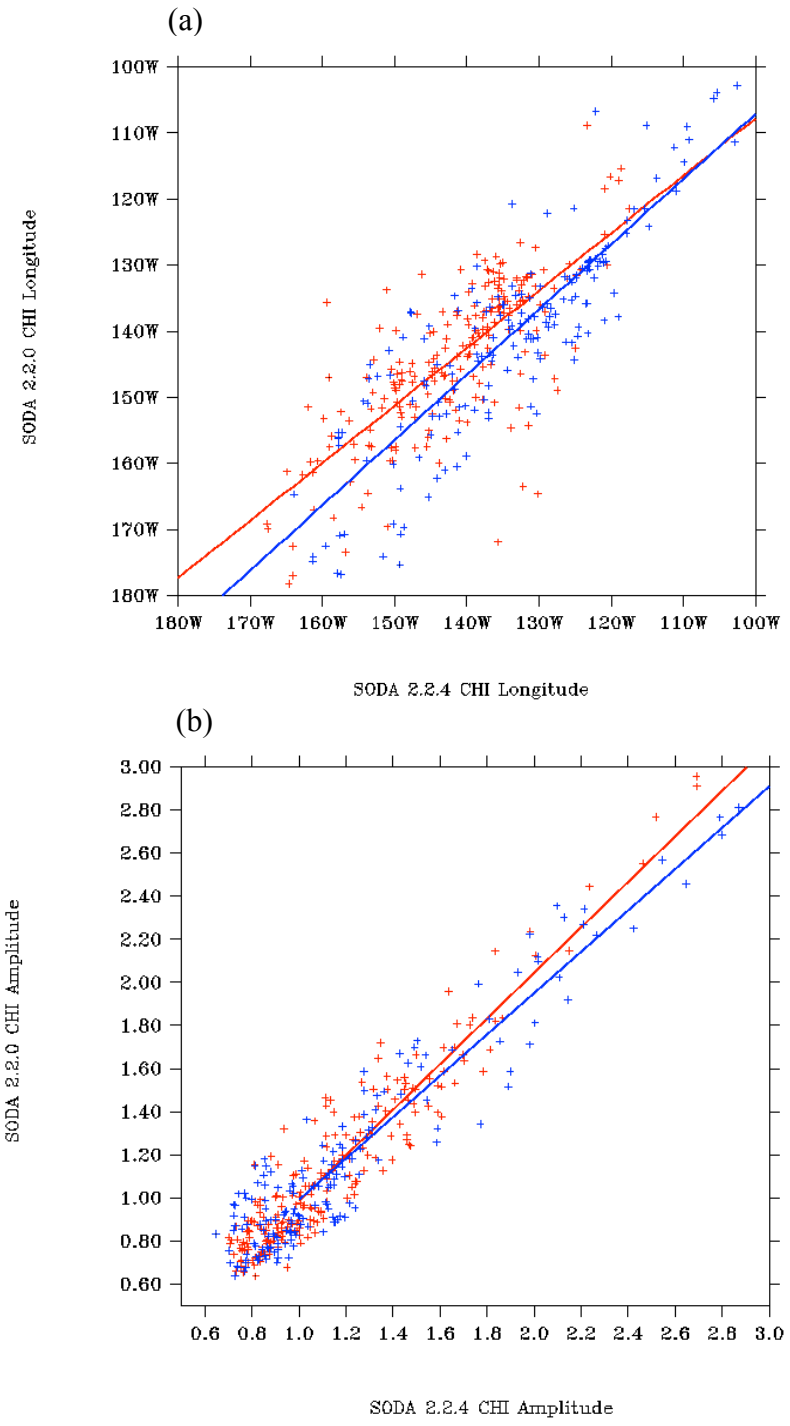

Figure 44. (a) CHI longitude from SODA 2.2.0 plotted as a function of CHI longitude from SODA 2.2.4. Values from 1871 through 1949 are shown in red and values from 1950 through 2008 are shown in blue. The least squares regression for both periods of time are shown as a solid line. (b) CHI amplitude from SODA 2.2.0 plotted as a function of CHI amplitude from SODA 2.2.4.

CHAPTER IV

SUMMARY AND CONCLUSIONS

An ocean reanalysis that spans the period from 1871-2008 is used to study El Niño and La Niña variations. SODA 2.2.4 is the first ocean reanalysis that starts from the late nineteenth century. This provides an opportunity to study the climate variability of the twentieth century through reanalysis. In this dissertation the variability in ENSO is addressed. A central question is whether ENSO has changed because of global warming.

To understand changes in El Niño strength, frequency, and duration a new metric called the Center of Heat Index (CHI) is used. CHI is the first moment of temperature anomaly, and can be used for warm events (El Niño) and cold events (La Niña) events. SODA 2.2.4 shows a centennial modulation in the strength of El Niño from late nineteenth century to late twentieth century. El Niño events in the late twentieth century (during periods of global warming) are as strong as the events in the late nineteenth century and early twentieth century (periods of little global warming). The mid-twentieth century is dominated by weak El Niño events. A closer look indicates that the strong El Niños undergo distinct modulation in strength compared to weak El Niños. Weak events occur consistently throughout the record but strong warm events show strengthening in the early and late part of the record. The strength of El Niños from 1970 onward increases but taking into consideration the entire period of study (1871-2008), this trend is negligible. A similar behavior does not occur for La Niña. In contrast with El Niño the strength of La Niña events does not show a centennial variation. The strength of La Niña events shows remarkable consistency throughout the record with little decadal variation

or trend. The asymmetry between El Niño and La Niña events is prominent when comparing their strength. El Niño events are generally stronger than La Niña events. The El Niño events have comparatively broad distribution of its strength than La Niña events. The variability in El Niño and La Niña strength do not show changes due to anthropogenic global warming. However, there exists decadal modulation in El Niño strength, which could be part of its internal variability.

Recent literatures suggest that the location of El Niño has changed, possibly in response to global warming [*Yeh et al.,* 2009; *Lee and McPhaden,* 2010]. *Newman et al*. [2011] propose multiple flavors of El Niño can occur as part of its internal variability. *Yeh et al*. [2011] suggests the possibility of increased occurrence of central Pacific type El Niño being part of natural variability of ENSO rather than being anthropogenically forced. The CHI longitude metric is used to identify the location of El Niño. The hypothesis that there are different types of El Niño and that the location of El Niño is shifting to the west Pacific is investigated. An analysis using CHI longitude shows that the location of warming does not change in the record. The location of El Niño can be described by a normal distribution centered at 139°W. This does not support the hypothesis that there are two flavors of El Niño, one in the east and one in the central Pacific. The location of El Niño warming varies between the dateline and 100°W in the eastern Pacific along the equator. Strong El Niños generally occur in the eastern Pacific. The mean location of CHI longitude in subsurface is 3° east to the mean location on surface. The location of subsurface warming follows the mean position of 20°C isotherm depth shoaling eastward. The distribution of the location of La Niña is not Gaussian

hence the possibility of different locations of La Niña cannot be rejected. The proposed change in location of El Niño in future climate change scenario is not obvious from this study. Rather the random distribution in the location of El Niño rejects the suggestion of distinct types of El Niño.

Another feature of El Niño that is proposed to have changed due to global warming is the period of El Niño. This study shows that the frequency of El Niño varies considerably over the record, with periods of time when ENSO occurs every other year to a period of almost ten years for which there is no El Niño event. Frequent El Niño characterizes the early twenty-first century. The period between 1930-1940 is distinct due to lack of El Niño. Both periods before 1930 and after 1940 show regular occurrence of El Niño events. However, the mean frequency of El Niño does not change during the period of study. A statistical test is used to demonstrate that a population of 34 El Niño is too few to determine a change in the mean frequency of the events. Rather hundreds of events are required to determine a change in the mean frequency of El Niño. In case of La Niña the frequency of occurrence also varies widely in the record. The distribution of the frequency of La Niña is broader than that of El Niño. Thus the study shows that the period of El Niño and La Niña remains unaffected during anthropogenic climate change.

There is a change in the duration of El Niño events from before 1931 to after 1941. Before 1931 El Niño events were both long (~20 months) and short (~10 months), but after 1941 the duration of El Niño events seems to have shortened (less than 15 months). La Niña events generally last longer than El Niño events throughout the record. Recent cold events are long persisting and relatively few compared to warm events. It is

possible that due to frequently occurring warm events it takes longer time for the tropical Pacific to return back to its normal conditions and produce conditions conducive for La Niña events. An asymmetry in the durations of El Niño and La Niña is observed. The asymmetry could be due to differences in the dynamics of evolution of the two events. A second cooling in the eastern Pacific during the end of year 1 of La Niña events of 1980-2008 is significant. This calls for a closer look into conditions favoring such an evolution of the cold anomaly.

The direction of propagation of El Niño or La Niña anomalies does not show significant changes in the record. Small propagations are found in anomalies warmer than 0.5°C during El Niño. The direction of propagation of these anomalies does not change much between the composites of El Niños during 1950-1976 and that during 1980-2008. The composite of the 1980-2008 El Niños is distinct due to the appearance of small warm anomalies around the dateline in the beginning of the warm event. The direction of propagation of La Niña anomalies does not show any changes during 1871-2008. The composite of the 1980-2008 La Niñas shows cold anomalies reappearing at the end of year 1 and further prolonging the cold event.

Overall, there is no evidence that there are changes in the strength, frequency, duration, location or propagation of El Niño and La Niña anomalies caused by global warming during the period from 1871-2008. In a recent paper *Stevenson et al.* [2011, submitted] suggest that changes in ENSO characteristics might not occur concurrent to changes in the climate. Instead, impact of changing climate may cause ENSO to change more than a century after the change in the climate first occurs. *Yeh et al.* [2009], *Lee*

and McPhaden [2010] suggest change in location of ENSO in future climate change scenario with central Pacific type of El Niño warming predicted to occur more than in the eastern Pacific type warming. But *McPhaden et al.* [2011] find that the current background conditions do not match to the projected changes in background conditions of climate models and is not conducive for increased occurrence of central Pacific warming. Thus they suggest that the current increase in central Pacific warming is part of ENSO's natural variability instead of being externally forced. In our study we show that a central Pacific warming cannot be distinguished from an eastern Pacific type warming in a record of 138 years of El Niño. As *Newman et al.* [2011] points out that although anthropogenic forcing might drive changes in ENSO [*Yeh et al*., 2009] but the changes are so small compared to the short datasets and comparatively small model ensembles [*Deser et al.,* 2011] that it is hard to separate the anthropogenic from the natural variability. Thus, decadal changes in the strength of El Niño could well be part of its natural variability.

The cause of decadal changes in El Niño could be complex and involve a wide range of timescales. A change in the mean state of the wind and thermocline depth can determine which state the evolution of El Niño would follow [*Fedorov and Philander* 2000; *Philander and Fedorov* 2003]. A deep thermocline with strong winds in the east favors the delayed oscillator mode in which the sea surface temperature variations occur in response to the vertical movement of the thermocline. A shallow thermocline favors a local mode in which the SST variation is affected by cold water entrained across the thermocline. Recent studies emphasize the importance of the tropical Pacific Ocean

circulation and, in particular, the role of subtropical cells as a mechanism linking wind stress variations and tropical Pacific SST [*Nonaka et al.,* 2002; *Capotondi et al.,* 2005]. In addition to changes in the tropical Pacific, other remote forcing, such as midlatitude changes [*Kleeman et al.,* 1999] and weakened Atlantic thermohaline circulation [*Timmerman et al.,* 2005], have been cited as possible reasons for decadal changes in El Niño. Studies suggest that during the mid-Holocene period (~6,000 years ago), when northern hemisphere ice sheets melted and the earth was slowly approaching the current warm Holocene, ENSO activity was suppressed [*Chiang* 2009; *Clement et al.,* 2000]. Various hypotheses explain this ENSO suppression using proxy records and coupled model studies, which could be further explored to explain ENSO changes in more recent years. Accordingly, an increase in the boreal summer Asian monsoon played a dominant role in modulating the amplitude of El Niño in the mid-Holocene [*Liu et al.*, 2000]. On the basis of a fully coupled model *Liu et al.* [2000] suggested that an increase in the subduction of warm subtropical waters into the equatorial thermocline reduced the strength of coupling between upwelling and SST changes thereby affecting El Niño dynamics during the period. However, *Clement et al.* [2000] proposed a different hypothesis for the suppressed ENSO activity of the mid-Holocene. They suggested that due to increased tropical insolation during the time both the eastern and western equatorial Pacific warmed, but as the SST in the eastern Pacific is mainly determined through upwelling and SST in the western Pacific is determined by the intensity of solar radiation, the response to changes of insolation was a warmer western Pacific compared to the eastern Pacific. This east-west contrast was further amplified through the

Bjerkness hypothesis, which leads to damping of El Niño activity [*Chiang* 2009]. A different approach to explain the decadal to centennial variations in El Niño amplitude was proposed by *Wittenberg* [2009]. In his study, *Wittenberg* [2009] argued that the slow modulation in El Niño amplitude can be calculated from Poisson statistics applied to El Niño's seasonal phase-locking and interannual memory instead of applying it to the decadal variation of tropical climate conditions. The slow modulation of El Niño amplitude could occur even without orbital or anthropogenic forcing.

Climate change is an ongoing process that is projected to continue in future, but how El Niño and La Niña variability will react to this change is yet an unresolved question. Both an increase and decrease in the intensity of El Niño activity has been argued in a future climate change scenario through climate model studies. In this study we show that changes in ENSO are so far not due to changes in anthropogenic climate. Of course it is possible that global warming might influence ENSO teleconnections instead of affecting the ENSO variation itself. Some studies suggest that under future global warming scenario the mid-latitude drought areas and the tropical cyclones will increase. This could alter the response to El Niño. In such case future changes in El Niño might follow its intrinsic variability. That El Niño is not affected by global warming could be taken as a hypothesis and tested through longer reanalysis. On the other hand, since global warming accelerated over the last 50-60 years its impact on El Niño variability could be in a transient stage. Studies of longer period could demonstrate whether changes in ENSO could be seen in future.

REFERENCES

Alexander, M. A., I. Bladé, M. Newman, J. R. Lazante, N-C. Lau, and J. D. Scott (2002), The atmospheric bridge: the influence of ENSO teleconnections on air-sea interaction over the global oceans, *J. Clim., 15,* 2205-2231.

An, S.-I., and F.-F. Jin (2004), Nonlinearity and asymmetry of ENSO, *J. Clim., 17*, 2399-2412.

An, S.-I., J.-S. Kug, Y.-G. Ham, I.-S. Kang (2008), Successive modulation of ENSO to the future greenhouse warming, *J. Clim., 21,* 3-21.

An, S-I and B. Wang (2000), Interdecadal change of the structure of the ENSO mode and its impact on the ENSO frequency, *J.Clim*., *13*, 2044-2055.

Ashok, K., S.K.Behera, S.A.Rao, H.Weng, and T.Yamagata (2007), El Niño Modoki and its possible teleconnection. *J.Geophys.Res*., *112*, C11007, doi:10.1029/2006JC003798.

Battisti, D. S., and A. C. Hirst (1989), Interannual variability in a tropical atmosphere-ocean model: influence of the basic state, ocean geometry and nonlinearity, *J.Atmos.Sc., 46,* 12, 1687-1712.

Bloom, S. C., L. L. Takacs, A. M. da Silva, and D. Ledvina (1996), Data assimilation using incremental analysis updates, *Mon. Wea. Rev., 124,* 1256-1271.

Boyer, T. P., J. I. Antonov, O. K. Baranova, H. E. Garcia, D. R. Johnson, R. A. Locarnini, A. V. Mishonov, T. D. O'Brien, D. Seidov, I. V. Smolyar, and M. M.

Zweng (2009), *World Ocean Database* 2009, S. Levitus, Ed., *NOAA Atlas NESDIS 66*, U.S. Government Printing Office, Washington, D.C., 216 pp., DVDs.

Brandt, P., A. Funk, V. Hormann, M. Dengler, R. J. Greatbatch, and J. M. Toole (2011), Interannual atmospheric variability forced by the deep equatorial atlantic ocean, *Nature, 473,* 497-501.

Bronnimann, S. (2007), Impact of El Niño-Southern Oscillation on european climate, *Rev. of Geophys., 45,* RG3003.

Cane, M.A., 2005: The evolution of El Niño, past and future, *Earth and Planetary Sc. Letts, 230*, 227-240, doi:10.1016/j.epsl.2004.12.003.

Cane, M. A., A. Clement, A. Kaplan, Y. Kushnir, D. Pozdnyakov, R. Seager, S. E. Zebiak, and R. Murtugudde (1997), Twentieth-century sea surface temperature trends, *Science, 275,* 957-960.

Cane, M. A., and S. E. Zebiak (1985), A theory for El Niño and the southern oscillation, *Science, 228,* 4703, 1085-1087.

Capotondi, A., M. A. Alexander, C. Deser, and M. J. McPhaden (2005), Anatomy and decadal evolution of the pacific subtropical cells (STCs), *J. Clim., 18,* 3739-3758.

Carton, J.A., G. Chepurin, X. Cao, and B.S. Giese (2000a), A simple ocean data assimilation analysis of the global upper ocean 1950-1995, Part 1: methodology, *J. Phys. Oceanogr., 30,* 294-309.

Carton, J.A., G. Chepurin, and X. Cao (2000b), A simple ocean data assimilation analysis of the global upper ocean 1950-1995 Part 2: results, *J. Phys. Oceanogr., 30,* 311-326.

Carton, J.A., and B.S. Giese (2008), A reanalysis of ocean climate using simple ocean data assimilation (SODA). *Mon. Weather Rev., 136,* 2999-3017.

Carton, J. A., H.F. Seidel, and B.S. Giese (2011), Detecting historical ocean climate variability, *J. Geophys. Res.,* submitted.

Chang, P. (1994), A study of the seasonal cycle of sea surface temperature in the tropical Pacific Ocean using reduced gravity models, *J. Geophys. Res., 99(C4),* 7725-7741.

Chang, P., Y. Fang, R. Saravanan, L. Ji, and H. Seidel (2006), The cause of the fragile relationship between the pacific El Niño an the atlantic niño, *Nature, 443,* 324-328.

Chang, P., L. Ji, B. Wang, and T. Li (1995), Interactions between the seasonal cycle and El Niño-Southern Oscillation in and intermediate coupled ocean-atmosphere model. *J.Atmos.Sci., 52,* 2353-2372.

Chelliah, M., and G. D. Bell (2004), Tropical multidecadal and interannual climate variability in the NCEP-NCAR Reanalysis, *J.Clim., 17*, 1777-1803.

Chen, J., B. E. Carlson, A. D. Del Genio (2002), Evidence for strengthening of the tropical general circulation in the 1990s, *Science, 295,* 838-841.

Chiang, J. C. H. (2009), The tropics in paleoclimate. *Ann. Rev. Earth Planet. Sci., 37*, 263-297.

Clement, A. C., R. Seager, and M. A. Cane (2000), Suppression of El Niño during the mid-Holocene by changes in the earth's orbit. *Paleoceanography, 15*, 731-737.

Clement, A. C., R. Seager, M. A. Cane, and S. E. Zebiak (1996), An ocean dynamical thermostat, *J. Clim., 9,* 2190-2196.

Cobb, K.M., C.D. Charles, H.Cheng, and R.L. Edwards (2003), El Niño/Southern Oscillation and tropical pacific climate during the last millennium, *Nature,424,* 271-276.

Cole, J. E., R. G. Fairbanks, and G. T. Shen (1993), Recent variability in the Southern Oscillation: isotopic results from a Tarawa Atoll coral, *Science*, 260, 1790-1793

Collins, M. The CMIP Modelling Groups (2005), El Niño- or La Niña-like climate change?, *Clim.Dyn.,24,* 89-104, doi:10.1007/s00382-004-0478-x.

Collins, M., S-I. An, W. Cai, A.Ganachaud, E. Guilyardi, F-F. Jin, M. Jochum, M. Lengaigne, S. Power, A. Timmermann, G. Vecchi and A. Wittenberg (2010), The impact of global warming on the tropical pacific ocean and El Niño, *Nat Geosci, 3,* 391-397, doi: 10.1038/NGEO868.

Compo, G. P., J. S. Whitaker, and P. D. Sardeshmukh (2006), Feasibility of a 100-year reanalysis using only surface pressure data. *Bull. Am. Met. Soc., 87*, 175-190, doi: 10.1175/BAMS-87-2-175.

Compo, G.P., J.S. Whitaker, and P.D. Sardeshmukh (2008), The 20th century reanalysis project, paper presented at third WCRP international conference on reanalysis, The University of Tokyo, Tokyo, 28 Jan to 1 Feb. (Available online at http://wcrp.ipsl.jussieu.fr/Workshops/Reanalysis2008/Documents/V5-511_ea.pdf).

Compo, G. P., J. S. Whitaker, P. D. Sardeshmukh, N. Matsui, R. J. Allan, X. Yin, B. E. Geason Jr, R. S. Vose, G. Rutledge, P. Bessemoulin, S Brönnimann, M. Brunet, R. I. Crouthamel, A. N. Grant, P. Y. Groisman, P. D. Jones, M.C. Cruk, A. C. Kruger, G. J. Marshall, M. Maugeri, H. Y. Mok, Ø. Nordli, T. F. Ross, R. M. Trigo, X. L.

Wang, S. D. Woodruff, S. J. Worley (2011), The twentieth century reanalysis project, *Q. J. R. Meteorol. Soc.,* 137, 1-28.

Cook, E. R., and P. J. Krusic (2004), *North American Drought Atlas*, Lamont-Doherty Earth Observatory and the National Science Foundation.

D'Arrigo, R., E.R.Cook, R.J.Wilson, R.. Allan, and E. Mann (2005), On the variability of ENSO over the past six centuries, *Geophys. Res. Lett., 32,* L03711.

Deser, C., A. Phillips, V. Bourdette, and H. Tang (2011), Uncertainity in climate change projections: the role of internal variability, *Clim. Dyn.,* doi: 10.1007/s00382-010-0977-x.

DiNezio, P. N., A. C. Clement, G. A. Vecchi, B. J. Soden, B. P. Kirtman, S.-K. Lee (2009), Climate response of the equatorial Pacific to global warming, *J. Clim., 22,* 4873-4892.

Enfield, D. B., and D. A. Mayer (1997), Tropical atlantic sea surface temperature variability and its relation to El Niño-Southern Oscillation, *J. Geophys. Res., 102,* C1, 929-945.

Evans M. N., R. G. Fairbanks, and J. L. Rubenstone (1999), The thermal oceanographic signal of El Niño reconstructed from a Kiritimati Island coral, *J.Geophys.Res.,* 104, C6, 13409-13421.

Fedorov, A.V., and S.G.Philander (2000), Is El Niño changing?, *Science*, *288,* 1997-2002.

Fedorov, A. V., and S. G. Philander (2001), Stability analysis of tropical ocean-atmosphere interactions: bridging measurements and theory for El Niño, *J. Clim., 14*, 3086-3101.

Garreaud, R., and D. S. Battisti (1999), Interannual (ENSO) and interdecadal (ENSO-like) variability in the southern hemisphere tropospheric Circulation, *J. Clim., 12,* 2113-2123.

Gastineau, G., L.Li, and H. Le Treut (2009), The hadley and walker circulation changes in global warming conditions described by idealized atmospheric simulations, *J.Clim, 22,* 3993-4013.

Giese, B. S., G. A. Chepurin, J. A. Carton, T. P. Boyer, and H. F. Seidel (2011), Impact of bathythermograph temperature bias models on an ocean reanalysis, *J. Clim., 24,* 84-93, doi: 10.1175/2010JCLI3534.1.

Giese, B.S., G.P.Compo, N.C.Slowey, P.D.Sardeshmukh, J.A.Carton, S.Ray and J.S.Whittaker (2010), The 1918/19 El Niño, *Bull.Amer.Meteo.Soc*. *91,*2 177-183

Giese, B. S., and S. Ray (2011), ENSO variability in simple ocean data assimilation (SODA), 1871-2008, *J. Geophys. Res., 116,* C02024.

Goddard, L., and S.G.Philander (2000), The energetics of El Niño and La Niña, *J.Clim*, *13,* 1496-1516.

Graham, N. E., and W. B. White (1988), The El Niño cycle: a natural oscillator of the pacific ocean-atmosphere system, *Science, 24,* 1293-1304.

Gu, D., and S. G. H. Philander (1995), Secular changes of annual and interannual variability in the tropics during the past century. *J.Clim, 8,* 864-876.

Harrison, D. E., and N. K. Larkin (1997), Darwin sea level pressure, 1876-1996: evidence for climate change, *Geophys. Res. Lett., 24,* 14, 1779-1782.

Held, I. M., and B. J. Soden (2006), Robust response of the hydrological cycle to global warming, *J. Clim., 19,* 5686-5699.

Horel, J. D., and J. M. Wallace (1981), Planetary scale atmospheric phenomena associated with the Southern Oscillation, *Mon. Weather Rev., 109,* 813-829.

Houghton, J. T., et al. (1995), Eds., *Climate Change 1995-The Science of Climate Change,* Cambridge Univ. Press, Cambridge.

Jin, F.-F. (1997), An equatorial ocean recharge paradigm for ENSO. Part I: conceptual model, *J. Atmos. Sc., 54,* 811-829.

Jin, F.-F., S.-I. An, A. Timmermann, and J. Zhao (2003), Strong El Niño events and nonlinear dynamical heating, *Geophys. Res. Lett., 30*, 3, 1120, doi:10.1029/2002GL016356.

Jin, F.-F., D. Neelin, and M. Ghil (1994), El Niño on the devil's staircase: annual subharmonic steps to chaos, *Science, 264*, 70-72.

Jones, P.W. (1999), First- and second-order conservative remapping schemes for grids in spherical coordinates, *Mon. Weather Rev*., *127,* 2204-2210.

Kalnay, E., M. Kanamitsu, R. Kistler, W. Collins, D. Deaven, L. Gandin, M. Iredell, S. Saha, G. White, J. Woollen, Y. Zhu, A. Leetmaa, B. Reynolds, M. Chelliah, W. Ebisuzaki, W. Higgins, J. Janowiak, K. Mo, C. Ropelewski, J. Wang, R. Jenne, and D. Joseph (1996), The NCEP/NCAR 40-Year reanalysis project, *Bull. Amer. Meteor. Soc., 77,* 437–471.

Kao, H.Y. and J.Y.Yu (2009), Contrasting eastern-pacific and central-pacific types of ENSO, *J.Clim*., *12,* 615-632, doi: 10.1175/2008JCLI2309.1.

Kaplan, A., M. Cane, Y. Kushnir, A. Clement, M. Blumenthal, and B. Rajagopalan (1998), Analyses of global sea surface temperature 1856-1991, *J.Geo.Res*., *103,* C9, 18,567-18,589.

Karnauskas, K. B., R. Seager, A. Kaplan, Y. Kushnir, and M. A. Cane (2009), Observed strengthening of the zonal sea surface temperature gradient across the equatorial Pacific ocean, *J. Clim., 22,* 4316-4321.

Kessler, W.S., L. M. Rothstein, and D. Chen (1998), The annual cycle of SST in the eastern tropical Pacific, diagnosed in an ocean GCM, *J. Clim., 11,* 777-799.

Kirtman, B. P., and J. Shukla (2000), On the influence of Indian summer monsoon on ENSO., *Quart. J. Roy. Meteor. Soc., 126*, 213-239.

Knapp K. R., M. C. Kruk, D. H. Levinson, H. J. Diamond, and C. J. Neumann (2010), The international best track archive for climate stewardship (IBTrACS): Unifying tropical cyclone best track data, *Bull. Ameri. Meteorol. Soc.,* 91, 363-376.

Koshlyakov, M. N., A. A. Romanov, and Y. A. Romanov (1998), El Niño-Southern Oscillation and the iceberg distribution in the pacific sector of the Antarctic, *Oceanology, 38,* 437-446.

Krishnamurthy, V., and B.N.Goswami (2000), Indian monsoon-ENSO relationship on interdecadal timescale, *J. Clim., 13,* 579-595.

Kucharski, F., A. Bracco, J. H. Yoo, and F. Molteni (2007), Low-frequency variability of the Indian monsoon-ENSO relationship and the tropical Atlantic: The 'weakening' of the 1980s and 1990s. *J. Clim., 20,* 4255-4266.

Kug J-S, S-l. An, Y. G. Ham, and I-S. Kang (2010), Changes in El Niño and La Niña teleconnections over north pacific-America in the global warming simulations, *Theor. Appl. Climatol. 100,* 275-282.

Kug, J-S., F. F. Jin, and S-I. An (2009), Two types of El Niño events; cold tongue El Niño and warm pool El Niño, *J.Clim., 22*, 1499-1515, doi: 10.1175/2008JCLI2624.1.

Kuleshov, Y., L. Qi, R. Fawcet, and D. Jones (2008), On tropical cyclone activity in the Southern Hemisphere: trends and the ENSO connection. *Geophys. Res. Lett., 35,* L14S08.

Kumar, K. K., B. Rajagopalan, and M. A. Cane (1999), On the weakening relationship between the Indian monsoon and ENSO, *Science, 284,* 2156-2159.

Kumar, K. K., B. Rajagopalan, M. Hoerling, G. Bates, and M. Cane (2006), Unraveling the mystery of Indian monsoon failure during El Niño, Science, 314, 115-119, doi:10.1126/science.1131152.

Larkin, N.K. and D.E.Harrison (2005), On the definition of El Niño and associated seasonal average U.S. weather anomalies, *Geophys. Res. Lett., 32,* L13705, doi: 10.1029/2005GL022738.

Lee, T., and M. J. McPhaden (2010), Increasing intensity of El Niño in the central-equatorial pacific. *Geophys. Res. Lett.,* **37**, L14603, doi:10.1029/2010GL044007.

Levitus, S., J. I. Antonov, T. P. Boyer, R. A. Locarnini, H. E. Garcia, and A. V. Mishonov (2009), Global ocean heat content 1955-2008 in light of recently revealed instrumentation problems, *Geophys. Res. Lett.*, *36,* L07608, doi:10.1029/2008GL037155.

Li, J., S-P Xie, E. R. Cook, G. Huang, R. D'Arrigo, F. Liu, J. Ma, and X-T. Zheng (2011), Interdecadal modulation of El Niño amplitude during the past millennium, *Nature Climate Change, 1,* 114-118.

Liu, Z., and M. Alexander (2007), Atmospheric bridge, oceanic tunnel, and global climatic teleconnections, *Rev. geophys., 45,* RG2005, doi: 10.1029/2005RG000172.

Liu, Z., J. Kutzbach, and L. Wu (2000), Modeling climate shift of El Niño variability in the Holocene, *Geophys. Res. Lett., 27,* 15, 2265-2268.

Liu, Z., S. Vavrus, F. He, N. Wen, and Y. Zhong (2005), Rethinking tropical ocean response to global warming: the enhanced equatorial warming, *J. Clim., 18*, 4684-4700.

Lu, R., W. Chen, and B. Dong (2008), How does a weakened Atlantic thermohaline circulation lead to an intensification of the ENSO-south Asian summer monsoon interaction, *Geophys. Res. Lett., 35,* L08706.

Luterbacher, J., D. Dietrich, E. Xoplaki, M. Grosjean, and H. Wanner (2004), European seasonal and annual temperature variability, trends, and extremes since 1500, *Science, 303,* 1499-1503.

McPhaden, M. J., T. Lee, and D. McClurg (2011), El Niño and its relationship to changing background conditions in the tropical Pacific Ocean, *Geophys. Res. Lett., 38,* L15709, doi:10.1029/2011GL048275.

McPhaden, M. J., and X. Zhang (2009), Asymmetry in zonal phase propagation of ENSO sea surface temperature anomalies, *Geophysic. Res. Lett., 36,* L13703, doi: 10.1029/2009GL038774.

Meehl, G. A., H. Teng (2007), Multi-model changes in El Niño teleconnections over North America in a future warmer climate, *Climate Dyn 29*, 779–790.

Meinen, C. S., and M. J. McPhaden (2000), Observations of warm water volume changes in the equatorial pacific and their relationship to El Niño and La Niña, *J.Clim., 13,* 3551-3559.

Merryfield, W.J. (2006), Changes to ENSO under CO_2 doubling in a multimodel ensemble, *J.Clim., 19(16),* 4009-4027.

Mitchell, T.P., and J.P.Wallace (1996), ENSO seasonality: 1950-78 versus 1979-92, *J.Clim. 9,* 3149-3161.

Moron, M., and I. Gouirand (2003), Seasonal modulations of the ENSO relationship with sea level pressure anomalies over the north atlantic in October-March 1873-1996, *Int. J. Climatol., 23,* 143-155.

Newman, M, S-I Shin, and M. A. Alexander (2011), Natural variation in ENSO flavors, *Geophys. Res. Lett., 38*, L14705, doi: 10.1029/2011GL047658.

Nicholls, N. (2008), Recent trends in the seasonal and temporal behavior of the El Niño-Southern Oscillation, *Geophys. Res. Lett., 35,* L19703, doi: 10.1029/2008GL034499.

Nonaka, M., S.-P. Xie, and J. P. McCreary (2002), Decadal variations in the subtropical cells and equatorial Pacific SST, *Geophys. Res. Lett., 29*(7), 1116.

Nurhati, I. S., K. M. Cobb, C. D. Charles, and R. B. Dunbar (2009), Late 20th century warming and freshening in the central tropical Pacific, *Geophys. Res. Lett, 36*, L21606, doi:10.1029/2009GL040270.

Okumura, Y. M., and C. Deser (2010), Asymmetry in the duration of El Niño and La Niña, *J.Clim., 23,* 5826-5843.

Okumura, Y. M., M. Ohba, C. Deser, and H. Ueda (2011), A proposed mechanism for the asymmetric duration of El Niño and La Niña, *J. Clim., 24,* 3822-3829.

Pan, A. J., Q. Y. Liu, Z. Y. Liu (2005), Periodic forcing and ENSO suppression in the Cane-Zebiak model. *J. Oceanography, 61,* 109-113.

Penland, C., and P. D. Sardeshmukh (1995), The optimal growth of tropical sea surface temperature anomalies. *J. Clim., 8,* 1999-2024.

Philander, S. G., and A. Fedorov (2003), Is El Niño sporadic or cyclic?, *Annu. Rev. Earth Planet. Sci., 31,* 579-594, doi:10.1146/annurev.earth.31.100901.141255.

Philip, S., and G. J. van Oldenborgh (2006), Shifts in ENSO coupling processes under global warming, *Geophys. Res. Lett., 33,* L11704, doi: 10.1029/2006GL026196.

Picaut, J., F. Masia, and Y. d-Penhoat (1997), An advective-reflective conceptual model for the oscillatory nature of the ENSO, *Science, 277,* 663-666.

Power, S., T.Casey, C.Folland, A.Colman and V.Mehta (1999), Inter-decadal modulation of the impact of ENSO on Australia, *Clim Dyn*., *15*, 319-324, doi:10.1007/s003820050284

Power, S.B. and I.N.Smith (2007), Weakening of the Walker Circulation and apparent dominance of El Niño both reach record levels, but has ENSO really changed?, *Geophys. Res. Lett*., *34*, L18702, doi:10.1029/2007GL030854.

Rao, V. B., C. E. Santo, and S. H. Franchito (2002) A D\diagnosis of rainfall over South America during the 1997/98 El Niño event. Part I: validation of NCEP-NCAR reanalysis rainfall data, *J. Clim., 15,* 502-211.

Rasmusson, E.M., and T.H. Carpenter (1982), Variations in tropical sea surface temperature and surface wind fields associated with the Southern Oscillation/El Niño, *Mon. Wea. Rev., 110*, 354-384.

Rasmusson, E. M., and T.H. Carpenter (1983), The relationship between eastern equatorial pacific sea surface temperatures and rainfall over India and Sri Lanka*, Mon. Wea. Rev., 111,* 517-528.

Rasmusson, E. M., X. Wang, and C. F. Ropelewski (1990), The biennial component of ENSO variability, *J. Marine Sc., 1,* 71-96.

Rayner, N.A., D.E. Parker, E.B. Horton, C.K. Folland, L.V. Alexander, D.P. Rowell, E.C. Kent, and A. Kaplan (2003), Global analyses of sea surface temperature, sea ice, and night marine air temperature since the late nineteenth century. *J. Geophys. Res*., *108*, doi:10.1029/2002JD002670.

Ren, H-L, and F. F. Jin (2011), Niño indices for two types of ENSO, *Geophys. Res.*

Lett., 38, L04704, doi: 10.1029/2010GL046031.

Reynolds, R. W., N. A. Rayner, T. M. Smith, D. C. Stokes, and W. Wang (2002), An improved in situ and satellite SST analysis for climate, *J. Clim., 15,* 1609-1625.

Romanov, Y. A., N. A. Romanova, and P. Romanov (2008), Distribution of icebergs in the Atlantic and Indian ocean sectors of the Antarctic region and its possible links with ENSO, *Geophys. Res. Lett., 35,* L02506.

Saravanan, R., and P. Chang (2000), Interaction between Tropical Atlantic variability and El Niño-Southern Oscillation, *J.Clim., 13,* 2177-2194.

Schneider, E. K., B. Huang, and J. Shukla (1995), Ocean wave dynamics and El Niño, *J.Clim, 8,* 2415-2439

Schopf, P. S., and M. J. Suarez (1988), Vacillations in a coupled ocean-atmosphere model, *J.Atmos.Sci., 45*, 680-702.

Schubert, S. D., M. J. Suarez, P. J. Pegion, R. D. Koster, and J. T. Bacmeister (2004), On the cause of the 1930s Dust Bowl, *Science, 19,* 303, 5665, 1855-1858.

Smith, R.D., J.K. Dukowicz and R.C. Malone (1992), Parallel ocean general circulation modeling. *Physica D, 60,* 38-61.

Smith, T.M., and R. W. Reynolds (2005), A global merged land air and sea surface temperature reconstruction based on historical observations (1880-1997), *J. Clim., 18,* 2021-2036.

Smith, T. M., R. W. Reynolds, T. C. Peterson and J. Lawrimore (2008), Improvements to NOAA's historical merged land-ocean surface temperature analysis (1880-2006), *J. Clim., 21,* 2283-2296.

Takahashi, K, A. Montecinos, K. Goubanova, and B. Dewitte (2011), ENSO regimes: reinterpreting the canonical and Modoki El Niño, *Geophys. Res. Lett., 38,* L10704, doi:10.1029/2011GL047364.

Timmermann, A., F.-F. Jin, and M. Collins (2004), Intensification of the annual cycle in the tropical Pacific due to greenhouse warming, Geophys. Res. Lett., 31, L12208, doi:10.1029/2004GL019442.

Timmermann, A., J. Oberhuber, A. Bacher, M.Esch, M. Latif and E. Roeckner (1999), Increased El Niño frequency in a climate model forced by future greenhouse warming, *Nature, 398*, 694-697.

Torrence, C., and P. J. Webster (1999), Interdecadal changes in the ENSO-Monsoon system, *J. Clim., 12,* 2679-2690.

Trenberth, K. E., G. W. Branstator, D. Karoly, A. Kumar, N-C. Lau, and C. Ropelewski (1998), Progress during TOGA in understanding and modeling global teleconnections associated with tropical sea surface temperatures, *J. Geophys. Res., 103,* 14291-14324.

Trenberth, K. E., and T. J. Hoar (1996), The 1990-1995 El Niño-Southern Oscillation event: longest on record, *Geophys. Res. Lett., 23*, 1, 57-60.

Trenberth, K. E., and T. J. Hoar (1997), El Niño and climate change, *Geophys. Res. Lett*., *24*, 23, 3057-3060.

Trenberth, K.E., and D. P. Stepaniak (2001), Indices of El Niño evolution, *J.Clim*., *14*, 1697-1701.

Trenberth, K. E., D. P. Stepniak, and J. M. Caron (2002), Interannual variations in the atmospheric heat budget, *J. Geophys. Res., 107*(D8), 4066, doi:10.1029/2000JD000297.

Tudhope, A. W., C.P. Chilcott, M.T. McCulloch, E. R. Cook, J. Chappell, R. M. Ellam, D. W. Lea, J. M. Lough, and G. B. Shimmield (2001), Variability in the El Niño-Southern Oscillation through a glacial-interglacial cycle, *Science, 291,* 1511-1517, doi: 10.1126/science.1057969.

Tziperman, E., L. Stone, M. Cane, and H. Jarosh (1994), El Niño chaos: overlapping of resonances between the seasonal cycle and the pacific ocean-atmosphere oscillator. *Science, 264*, 72-74.

Urban, F.E., J.E.Cole, and J.T.Overpeck (2000), Influence of mean climate change on climate variability from a 155-year tropical Pacific coral record, *Nature, 407,* 4316-4340.

Van Oldenborgh, G. J., S. Y. Philip, and M. Collins (2005), El Niño is a changing climate: a multi-model study, *Ocean Science, 1,* 81-95.

Vecchi, G. A., and B. J. Soden (2007), Global warming and weakening of the tropical circulation, *J. Clim., 20,* 4316-4340.

Vecchi, G. A., A. Clement, B. J. Soden (2008), Examining the tropical pacific's response to global warming, *EOS, 89,* 9.

Vecchi, G. A., B. J. Soden, A. T. Wittenberg, I. M. Held, A. Leetma and M. J. Harrison (2006), Weakening of tropical Pacific atmospheric circulation due to anthropogenic forcing, *Nature, 441,* 73-76, doi:10.1038/nature/04744.

Vecchi, G. A., and A. T. Wittenberg (2010), El Niño and our future climate: where do we stand?, *WIREs Clim Change, 1*, 260-270, doi:10.1002/wcc.33.

Walker, G. T. (1923), Correlation in seasonal variation of weather VIII: a preliminary study of world weather, *Mem. Indian Meteorol. Dep., 24,* 75-131.

Walker, G. T. (1924), Correlation in seasonal variation of weather IX: a preliminary study of world weather, *Mem. Indian Meteorol. Dep., 24,* 225-232.

Walker, G. T., and E. W. Bliss (1932), World weather V, *Mem. Indian Meteorol. Dep., 4,* 53-84.

Wallace, J. M., and D. S. Gutzler (1981), Teleconnections in the geopotential height field during the northern hemisphere winter, *Mon. Weather Rev., 109,* 784-812.

Wang B. (1995), Interdecadal changes in El Niño onset in the last four decades, *J.Clim*, *8,* 267-285.

Wang, B., and S-I An (2002), A mechanism for decadal changes of ENSO behavior: roles of background wind changes, *Clim. Dyn., 18,* 475-486.

Wang, C., S.-P. Xie, and J. A. Carton (2004), A global survey of ocean atmosphere interaction and climate variability, in *Earth's Climate: The Ocean-Atmosphere Interaction, Geophys. Monogr. Ser., 147,* edited by C. Wang et al., 1-19, AGU, Washington, D. C.

Weisberg, R. H. amd C. Wang (1997), A western Pacific oscillator paradigm for the El Niño-Southern Oscillation, *Geophys. Res. Lett., 24,* 779-782.

Weng, H., K. Ashok, S. K. Behera, S. A. Rao, and T. Yamagata (2007), Impacts of recent El Niño Modoki on dry/wet conditions in the pacific rim during boreal summer, *Clim. Dyn. 29,* 113-129.

Whitaker, J.S., G.P. Compo, X. Wei, and T.M. Hamill (2004), Reanalysis without radiosondes using ensemble data assimilation, *Mon. Wea. Rev., 132,* 1190–1200.

Whitaker, J.S., and T.M. Hamill (2002), Ensemble data assimilation without perturbed observations. *Mon. Wea. Rev*., *130,* 1913–1924.

Woodruff, S. D., S. J. Worley, S. J. Lubker, Z. Ji, J. E. Freeman, D. I., Berry, P. Brohan, E. C. Kent, R. W. Reynolds, S. R. Smith, and C. Wilkinson (2010), ICOADS release 2.5: extensions and enhancements to the surface marine meteorological archive, *Int.J.Climatol.,* doi:10.1002/joc.2103.

Xie, S.P. C.Deser, G.A.Vecchi, J.Ma, H.Teng, and A.T.Wittenberg (2010), Global warming pattern formation: sea surface temperature and rainfall, *J.Clim, 23,* 966-986.

Yang, H., and Q. Zhang (2008), Anatomizing the ocean's role in ENSO changes under global warming, *J.Clim*, *21*, 6539-6555, doi:10.1175/2008JCLI2324.1.

Ye, Z., and W. W. Hseih (2008), Changes in ENSO and associated overturning circulations from enhanced greenhouse gases by the end of the twentieth century, *J.Clim*, *21*, 5745-5763, doi:10.1175/2008JCLI1580.1.

Yeh, S.-W., B. P. Kirtman, J.-S. Kug, W. Park, and M. Latif (2011), Natural variability of the central pacific El Niño event on multi-centennial timescales, *Geophys. Res. Lett., 38*, L02704, doi:10.1029/2010GL045886.

Yeh, S.-W., J.-S. Kug, B. Dewitte, M-H. Kwon, B. P. Kirtman and F. F. Jin (2009), El Niño in a changing climate, *Nature, 461,* 511-674, doi:10.1038/nature08316.

Zhang, Q., Y. Guan, and H. Yang (2008), ENSO amplitude change in observation and coupled models, *Adv. Atmos. Sci., 25,* 361-366.

Zhang, M., and H. Song (2006), Evidence of deceleration of atmospheric vertical overturning circulation over the tropical Pacific, *Geophys. Res. Lett., 33,* L12701.

VITA

Name:	Sulagna Ray
Address:	Department of Oceanography, MS 3146, Texas A&M University, College Station, Texas 77843-3146
Email Address:	sulagna.ray@gmail.com
Education:	B.S., mathematics, University of Calcutta, Kolkata, 2001
	M.S., applied mathematics, University of Calcutta, Kolkata, 2003
	Ph.D., oceanography, Texas A&M University, 2011